

**The Efficiency of Enzymatic L-Cysteine Oxidation in Mammalian Systems Derives from
the Optimal Organization of the Active Site of Cysteine Dioxygenase**

by

Catherine Wangui Njeri

A dissertation submitted to the Graduate Faculty of
Auburn University
in partial fulfillment of the
requirements for the Degree of
Doctor of Philosophy

Auburn, Alabama
May 4, 2014

Copyright 2014 by Catherine Wangui Njeri

Approved by

Holly R. Ellis, Chair, Associate Professor of Chemistry and Biochemistry
Douglas C. Goodwin, Associate professor of Chemistry and Biochemistry
Evert E. Duin, Associate Professor of Chemistry and Biochemistry
Paul A. Cobine, Assistant Professor of Biological Sciences
Benson T. Akingbemi, Associate Professor of Anatomy

Abstract

Intracellular concentrations of free cysteine in mammalian organisms are maintained within a healthy equilibrium by the mononuclear iron-dependent enzyme, cysteine dioxygenase (CDO). CDO catalyzes the oxidation of L-cysteine to L-cysteine sulfinic acid (L-CSA), by incorporating both atoms of molecular oxygen into the thiol group of L-cysteine. The product of this reaction, L-cysteine sulfinic acid, lies at a metabolic branch-point that leads to the formation of pyruvate and sulfate or taurine. The available three-dimensional structures of CDO have revealed the presence of two very interesting features within the active site (1-3). First, in close proximity to the active site iron, is a covalent crosslink between Cys93 and Tyr157. The functions of this structure and the factors that lead to its biogenesis in CDO have been a subject of vigorous investigation.

Purified recombinant CDO exists as a mixture of the crosslinked and non crosslinked isoforms, and previous studies of CDO have involved a heterogenous mixture of the two. The current study presents a new method of expressing homogenously non crosslinked CDO using the cell permeative metal chelator, 1,10-phenanthroline. Electron paramagnetic resonance (EPR) analysis of purified non crosslinked CDO revealed that the iron was in the EPR silent Fe^{2+} form. Dioxygen utilization by non crosslinked CDO occurred in two distinct phases, which correlated with crosslink formation and enzymatic cysteine oxidation. Generation of homogenously crosslinked CDO resulted in a ~5 fold higher k_{cat}/K_m value compared to the enzyme with a heterogenous mixture of crosslinked and non crosslinked CDO isoforms. EPR analysis of

homogenously crosslinked CDO revealed that this isoform exists in the Fe^{3+} form. The current studies present a new perspective on the redox properties of the active site iron and the results demonstrate that a redox switch commits CDO towards either formation of the Cys93-Tyr157 crosslink or cysteine oxidation.

The second unusual structural feature in the active site of CDO involves the catalytic iron which is ligated by only 3-His residues. The 3-His metal coordination pattern is a deviation from the 3-His/1-Glu metal coordination pattern that is commonly observed in most cupin metalloproteins. A clear rationale behind this deviation is still lacking, but evidence is accumulating that indicate that the deviation might be a mechanistically driven strategy to optimize the dioxygenation reaction. The three-dimensional structure of CDO in complex with L-cysteine revealed a bidentate mode of substrate coordination via the thiol and amino groups. The current studies have evaluated the relevance of the functional groups of L-cysteine in catalysis and the results indicate a remarkable substrate specificity exhibited by CDO. In fact, kinetic analyses of wild-type CDO with structural analogs of L-cysteine revealed a ~30-fold decrease in the $k_{\text{cat}}/K_{\text{m}}$ value with either D-cysteine or with cysteamine, and there was no detectable activity with 3-mercaptopropionate. Additionally, the relevant enzyme-substrate interactions were evaluated using variants of Tyr58 and Arg60 residues which are in close proximity to the active site iron and have been proposed to play a role in substrate coordination (1-3). The protonation states of key functional groups that are relevant to the catalytic mechanism of CDO were evaluated through determination of the pH dependence of the kinetic parameters of wild-type CDO. Taken together, the results from the current studies have provided invaluable insights into the influence of second sphere interactions on catalysis, and the relevant protonation states of groups participating in catalysis.

Acknowledgements

I would like to express my heartfelt gratitude to my advisor, Dr. Holly R. Ellis. She has been a great mentor, and her hardworking nature and commitment to excellence impacted me in the most positive way possible. I am extremely grateful for all the support, encouragement, and guidance throughout my graduate career, and I will be forever indebted to her for equipping me with the skills to succeed in the research world.

I would also like to sincerely thank my committee members, Dr. Douglas Goodwin, Dr. Evert Duin, and Dr. Paul Cobine for their genuine contribution towards my academic progress. A special thanks to Dr. Goodwin for the insightful discussion on methodologies that proved very beneficial to my research. I would also like to thank Dr. Duin for assisting me with the EPR studies, and allowing me to use his anaerobic glove box. I would like to thank Dr. Cobine for assisting me with the metal analysis. I would like to express my sincere gratitude to Dr. Benson Akingbemi for accepting to serve the role of the University Reader.

I would like to thank my lab members Dr. Jingyuan Xiong, Dr. John Robbins, Paritosh Dayal, Jonathan Musila, and Dianna Forbes for providing a friendly working environment and engaging in meaningful scientific discussions. I would like to thank the Department of Chemistry and Biochemistry at Auburn University for providing me with the opportunity to pursue my graduate career. Last but not least, I would like to sincerely thank my dearest family and friends for their love and support throughout my studies. This work is dedicated to my dear niece, Alice Njeri, the source of my motivation.

Table of Contents

Abstract	ii
Acknowledgments.....	iv
Table of contents.....	v
List of tables	ix
List of figures.....	x
List of abbreviations.....	xiv
Chapter One: Literature Review	1
1.1. Cysteine metabolism	1
1.2. Biosynthesis of cysteine	2
1.3. Incorporation of cysteine into proteins.....	4
1.4. Incorporation of cysteine into biomolecules.....	10
1.4.1. Glutathione biosynthesis.....	10
1.4.2. Coenzyme A biosynthesis.....	12
1.5. Cysteine catabolism.....	14
1.5.1. Non oxidative catabolism of cysteine.....	14
1.5.2. Oxidative catabolism of cysteine	17
1.6. The cupin superfamily	21
1.6.1. Germin	22
1.6.2. Quercetin dioxygenase.....	24

1.6.3.	Acireductone dioxygenase	28
1.7.	Variations from the 3-His/1-Glu metal binding pattern	29
1.7.1.	β -Diketone cleaving enzyme.....	33
1.7.2.	Cysteine dioxygenase	35
1.8.	Protein derived cofactors	38
1.8.1.	Tryptophan tryptophylquinone (TTQ).....	40
1.8.2.	Cysteine tryptophanylquinone (CTQ)	43
1.8.3.	Met-Tyr-Trp covalent adduct in KatG.....	44
1.8.4.	Topaquinone (TPQ) in copper amine oxidase	47
1.8.5.	Cysteine-Tyrosine crosslink in galactose oxidase.....	50
1.8.6.	Cysteine-Tyrosine crosslink in cysteine dioxygenase	55
1.9.	Summary	57
Chapter Two: Shifting Redox States of the Iron Center Partitions CDO between Crosslink Formation or Cysteine oxidation		
		60
2.1.	Introduction.....	60
2.2.	Materials and methods.....	63
2.2.1.	Materials	63
2.2.2.	Expression and purification of C93S, Y157F, and wild-type CDO.....	63
2.2.3.	Expression and purification of non crosslinked CDO	64
2.2.4.	Quantitation of iron	65
2.2.5.	Correlating crosslink formation with non crosslinked CDO activity.....	65
2.2.6.	Generation of homogenously crosslinked form of CDO.....	66
2.2.7.	Steady-state kinetic analyses of homogenously crosslinked CDO	66
2.2.8.	Analysis of the cysteine sulfinic acid product	67

2.2.9. EPR spectroscopy.....	68
2.3. Results.....	69
2.3.1. Preparation of homogenously non crosslinked CDO	69
2.3.2. Activity of non crosslinked CDO.....	71
2.3.3. Steady-state kinetic parameters of crosslinked CDO	72
2.3.4. Contribution of Cys93 and Tyr157 residues to the activity of CDO.....	73
2.3.5. EPR analysis of non crosslinked and crosslinked CDO	73
2.4. Discussion	83
Chapter Three: Investigating the Enzyme-Substrate Interactions within the Active site of Cysteine Dioxygenase	
	91
3.1. Introduction.....	91
3.2. Materials and methods.....	94
3.2.1. Materials	94
3.2.2. Construction of expression vectors	94
3.2.3. Expression and purification of the variants and wild-type CDO	95
3.2.4. Quantitation of iron	96
3.2.5. Circular dichroism spectroscopy.....	96
3.2.6. Steady-state kinetic analyses of the variants and wild-type CDO	96
3.2.7. Dependence of kinetic parameters of wild-type CDO on pH.....	97
3.2.8. EPR spectroscopy.....	98
3.3. Results.....	99
3.3.1. Structural characterization of the CDO variants	99
3.3.2. Activity analyses of the CDO variants with L-cysteine.....	106
3.3.3. Activity analyses of the variants and wild-type CDO with substrate analogs	106

3.3.4. Probing the effect of L-cysteine and cysteine analogs on the metal coordination site of wild-type CDO	111
3.3.5. Evaluating the effect of L-cysteine and cysteine analogs on the metal coordination site of the CDO variants	112
3.3.6. Dependence of wild-type CDO kinetic parameters on pH	120
3.4. Discussion	124
Chapter Four: Summary	132
4.1. Analysis of non crosslinked and crosslinked CDO	134
4.2. Physiological relevance	135
4.3. Enzyme-substrate interactions within the active site of CDO	136
References	140

List of Tables

Table 2.1: Steady-state kinetic parameters of crosslinked and wild-type CDO	75
Table 2.2: Specific activity of dioxygen utilization and cysteine sulfinic acid production of crosslinked and wild-type CDO	76
Table 2.3: Steady-state kinetic parameters and percent iron content of wild-type, C93S and Y157F CDO	77
Table 3.1: Iron incorporation in wild-type, Y58A, Y58F, R60A, and R60K CDO	105
Table 3.2: Steady-state kinetic parameters of wild-type, Y58A, and Y58F CDO	109
Table 3.3: Steady-state kinetic parameters of wild-type, R60A, and R60K CDO	110

List of Figures

Figure 1.1: The transsulfuration pathway	3
Figure 1.2: Schematic representation of reactions catalyzed by thioredoxin and thioredoxin reductase	5
Figure 1.3: Schematic representation of reactions catalyzed by typical and atypical 2-Cys peroxiredoxins	7
Figure 1.4: Schematic representation of reactions catalyzed by 1-Cys peroxiredoxins	8
Figure 1.5: Schematic representation of reactions catalyzed by the glutaredoxin system	9
Figure 1.6: Schematic representation of reduction and oxidation of glutathione	10
Figure 1.7: Biosynthetic pathway of glutathione	11
Figure 1.8: Biosynthetic pathway of coenzyme A.....	13
Figure 1.9: Production of H ₂ S by cystathionine β-synthase.....	15
Figure 1.10: Reactions catalyzed by cystathionine γ-lyase in the formation of cysteine and H ₂ S.....	16
Figure 1.11A: The taurine biosynthetic pathway	19
Figure 1.11B: Cysteine toxicity; iron and cysteine mediated production of free radicals	19
Figure 1.12: Crystal structure of cysteine dioxygenase highlighting the β-barrel fold.....	21
Figure 1.13: Reaction catalyzed by oxalate oxidase	22
Figure 1.14: Active site of oxalate oxidase highlighting the 3-His/1-Glu metal binding site....	23
Figure 1.15: Reaction catalyzed by quercetin dioxygenase	24
Figure 1.16: Catalytic mechanism of quercetin dioxygenase.....	27

Figure 1.17: An outline of the reactions of Fe ²⁺ and Ni ²⁺ -containing acireductone dioxygenases.....	30
Figure 1.18: Proposed mechanisms of Fe ²⁺ and Ni ²⁺ -containing acireductone dioxygenases ...	31
Figure 1.19: Active site of cysteine dioxygenase highlighting the 3-His metal binding site	32
Figure 1.20: Proposed catalytic mechanism of Dke1	34
Figure 1.21: Reaction catalyzed by cysteine dioxygenase	35
Figure 1.22: Proposed catalytic mechanism of cysteine dioxygenase	37
Figure 1.23: The active site of cysteine dioxygenase highlighting the covalent crosslink involving Cys93 and Tyr157	39
Figure 1.24: Tryptophan tryptophylquinone	40
Figure 1.25: Catalytic mechanism of methylamine dehydrogenase (MADH) showing the reductive and oxidative reactions	42
Figure 1.26: Cysteine tryptophylquinone (CTQ).....	43
Figure 1.27: Reaction mechanisms showing the catalase and peroxidase mechanisms in KatG.....	44
Figure 1.28: The Met-Tyr-Trp crosslink in KatG.....	45
Figure 1.29: Proposed mechanism for the formation of the Met-Tyr-Trp crosslink in KatG	46
Figure 1.30: Reaction mechanisms of copper amine oxidases showing the reductive and oxidative reactions	47
Figure 1.31: 2,4,5-trihydroxyphenylalanine quinone (TPQ).....	48
Figure 1.32: Proposed mechanism for TPQ biogenesis	49
Figure 1.33: Reaction catalyzed by galactose oxidase.....	50
Figure 1.34: Oxidation states of galactose oxidase.....	51
Figure 1.35: Catalytic mechanism of galactose oxidase	52
Figure 1.36: Proposed mechanism for aerobic and anaerobic formation of the Cys-Tyr crosslink in galactose oxidase	54

Figure 1.37: SDS-PAGE analysis of wild-type CDO, C93S, and Y157F CDO	56
Figure 2.1: Analysis of non crosslinked and wild-type CDO by SDS-PAGE	70
Figure 2.2: Dioxygen utilization of non crosslinked CDO	78
Figure 2.3: Analysis of crosslink formation during catalysis by SDS-PAGE.....	79
Figure 2.4: Steady-state kinetic traces of crosslinked CDO enzyme	80
Figure 2.5: X-band EPR spectra of non crosslinked CDO	81
Figure 2.6: X-band EPR spectra of crosslinked CDO.....	82
Figure 2.7: Proposed mechanism for cysteine oxidation	90
Figure 3.1: Active site of cysteine dioxygenase with bound L-cysteine	101
Figure 3.1: SDS-PAGE analysis of wild-type CDO, Y58A, and R60A CDO	102
Figure 3.3: Circular dichroism spectra of wild-type, Y58A, and Y58F CDO	103
Figure 3.4: Circular dichroism spectra of wild-type, R60A, and R60K CDO	104
Figure 3.5: Substrates utilized in kinetic and spectroscopic investigations	108
Figure 3.6A: X-band EPR spectra of wild-type CDO showing the effects of various substrates on the metal coordination environment	114
Figure 3.6B: X-band EPR spectra of wild-type CDO showing the effects of S-methylcysteine and L-cysteine sulfinic acid on the metal coordination environment	115
Figure 3.7A: X-band EPR spectra of Y58F CDO showing the effects of various substrates on the metal coordination environment	116
Figure 3.7B: X-band EPR spectra of Y58A CDO showing the effects of various substrates on the metal coordination environment	117
Figure 3.8A: X-band EPR spectra of R60K CDO showing the effects of various substrates on the metal coordination environment	118
Figure 3.8B: X-band EPR spectra of R60A CDO showing the effects of various substrates on the metal coordination environment	119
Figure 3.9: Circular dichroism spectra showing stability of wild-type CDO with varying pH	121

Figure 3.10A: Dependence of k_{cat} values of wild-type CDO on pH.....	122
Figure 3.10B: Dependence of k_{cat}/K_m values of wild-type CDO on pH	123

List of Abbreviations

CDO	cysteine dioxygenase
CSA	cysteine sulfinic acid
IPTG	isopropyl- β -D-thiogalactoside
SDS-PAGE	sodium dodecyl sulfate polyacrylamide gel electrophoresis
EPR	electron paramagnetic resonance
ICP-AES	inductively coupled plasma-atomic emission spectroscopy
CD	circular dichroism
MCD	magnetic circular dichroism
XAS	X-ray absorption spectroscopy

Chapter One

Literature Review

1.1 Cysteine metabolism

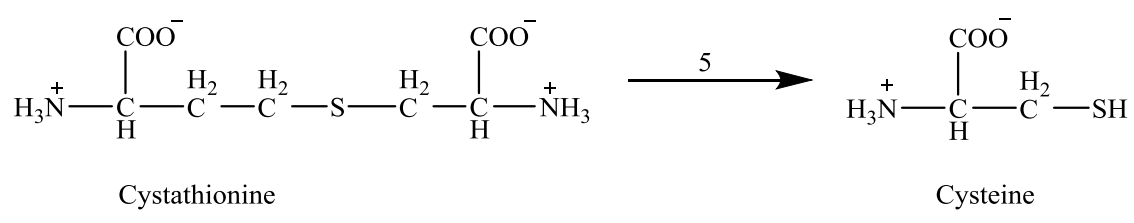
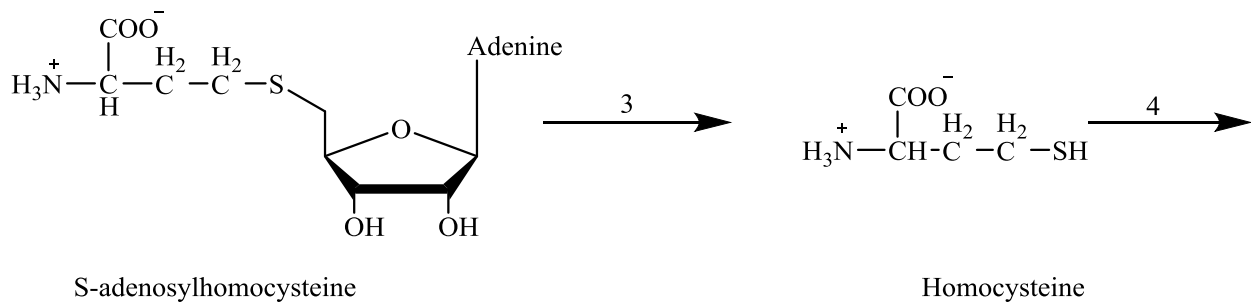
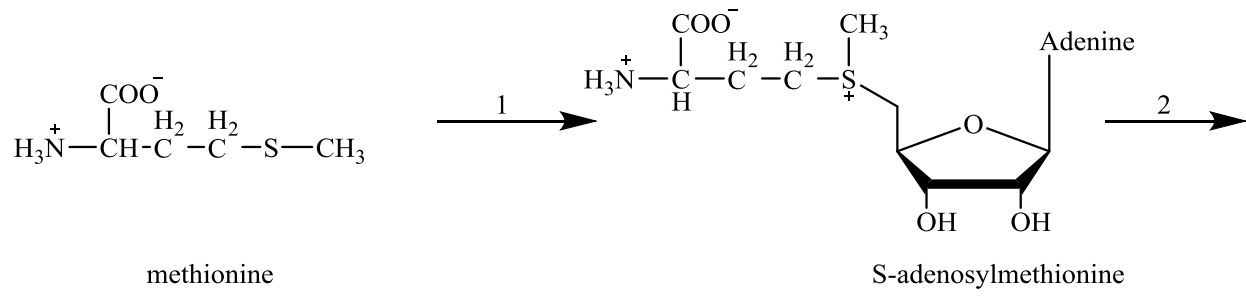
Cysteine is an indispensable amino acid with a broad range of metabolic functions. In addition to being incorporated into proteins, cysteine serves as a precursor for the biosynthesis of several essential biomolecules including glutathione (GSH), coenzyme A, taurine, and inorganic sulfur (4). Cysteine can either be obtained from the diet or it can be synthesized from methionine and serine via the transsulfuration pathway (5). Cellular cysteine concentrations in mammalian organisms are maintained within a very narrow range. In fact, experimentally determined plasma cysteine concentrations in rats range between 0.1-0.2 mM whether dietary protein or sulfur amino acid intake is varied below or above the required levels (6). Such a tight regulation of intracellular free cysteine is necessary because when present at high concentrations, cysteine may be toxic, and has been linked with several disease conditions which are associated with oxidative stress (6-7).

A proper balance in cellular cysteine concentrations is maintained by cysteine dioxygenase (CDO), which is an enzyme that adds molecular oxygen to the thiol group of cysteine to form cysteine sulfinic acid (CSA) (4, 6, 8). Cysteine sulfinic acid when formed is further catabolized either to hypotaurine and taurine or to pyruvate and sulfate. These end products of cysteine catabolism have essential physiological functions (6, 8). Therefore, CDO plays a pivotal role in facilitating the removal of excess intracellular free cysteine which could

otherwise be harmful to the cell, and the cysteine is converted to end products that are beneficial to the cell. The current study aims at unraveling some distinctive structural characteristics of CDO, that enhance its functionality, thereby enabling the enzyme to fulfill the obligation of maintaining healthy concentrations of cysteine within mammalian cells.

1.2 Biosynthesis of cysteine

Cysteine and methionine are interconnected metabolically through the transsulfuration pathway (5). The transsulfuration pathway which involves degradation of methionine, facilitates the transfer of methionine sulfur to serine to form cysteine (Fig. 1.1) (4). The initial step in methionine degradation involves activation of methionine by ATP to form S-adenosylmethionine (SAM), in a reaction catalyzed by methionine adenosyltransferase. SAM is then converted to S-adenosylhomocysteine in a reaction catalyzed by a methyltransferase. Hydrolysis of S-adenosylhomocysteine by adenosylhomocysteine hydrolase yields adenosine and homocysteine. The sulfur atom of methionine forms the thiol group of homocysteine. Condensation of homocysteine and serine to form cystathionine is catalyzed by the pyridoxal 5'-phosphate (PLP) dependent enzyme, cystathionine β -synthase. Cystathionine is then hydrolyzed by cystathionine γ -lyase to form cysteine, which now contains the sulfur atom of methionine. The other products of hydrolysis of cystathionine are α -ketobutyrate (further catabolized to propionyl-CoA) and ammonia (4-5). The synthesized cysteine combined with dietary cysteine forms the intracellular free cysteine pool which participates in various physiological processes.



- 1. Methionine adenosyltransferase
- 2. Methyl transferase
- 3. Adenosylhomocysteine hydrolase
- 4. Cystathionine β-synthase + serine
- 5. Cystathionine γ-lyase

Figure 1.1: The transsulfuration pathway for cysteine biosynthesis (4-5).

1.3 Incorporation of cysteine into proteins

Incorporation of cysteine into proteins is an essential process because cysteine plays a crucial role in maintaining the structural integrity of proteins due to its ability to form intra and interstrand disulfide linkages. Additionally, the reduced environment within cells is maintained by proteins with redox active thiols. These proteins which include thioredoxins, thioredoxin reductases, glutaredoxins, glutathione reductases, and peroxiredoxins play important roles in protecting the cell against oxidative stress (9). Oxidative stress is mainly associated with an increase in the level of oxidizing compounds such as free radicals, reactive oxygen species, and adventitious redox active metal ions within the cell (10). Thiol containing proteins function as effective antioxidants which protect cells from the damaging effects of oxidative stress. Thioredoxins are oxidoreductases present in both prokaryotic and eukaryotic organisms that catalyze the reduction of disulfide linkages in proteins. Formation of disulfide linkages in proteins is not always desirable and it can alter the function of proteins that contain catalytically important Cys residues. Therefore, thioredoxins play a major role in maintaining the functionally important Cys residues in their reduced state. Thioredoxins have two active site cysteine residues that are oxidized to disulfide upon reduction of a disulfide containing substrate (Fig. 1.2) (9). The formed disulfide in thioredoxin is subsequently reduced by thioredoxin reductase which is a NADPH-dependent oxidoreductase. Mammalian thioredoxin reductases contain a selenocysteine residue at the C-terminal active site, which has been shown to be essential for catalytic activity (11-12). Reduction of thioredoxin reductases involves the transfer of electrons from NADPH via the enzyme bound FAD to an active site disulfide linkage at the N-terminal active site forming a dithiol. The dithiol is subsequently oxidized by the selenenylsulfide linkage formed by the Cys-

Sec pair at the C-terminal active site of the dimeric protein. The reduced selenolthiol at the C-terminal active site can then be used to reduce thioredoxins and other protein disulfides (11).

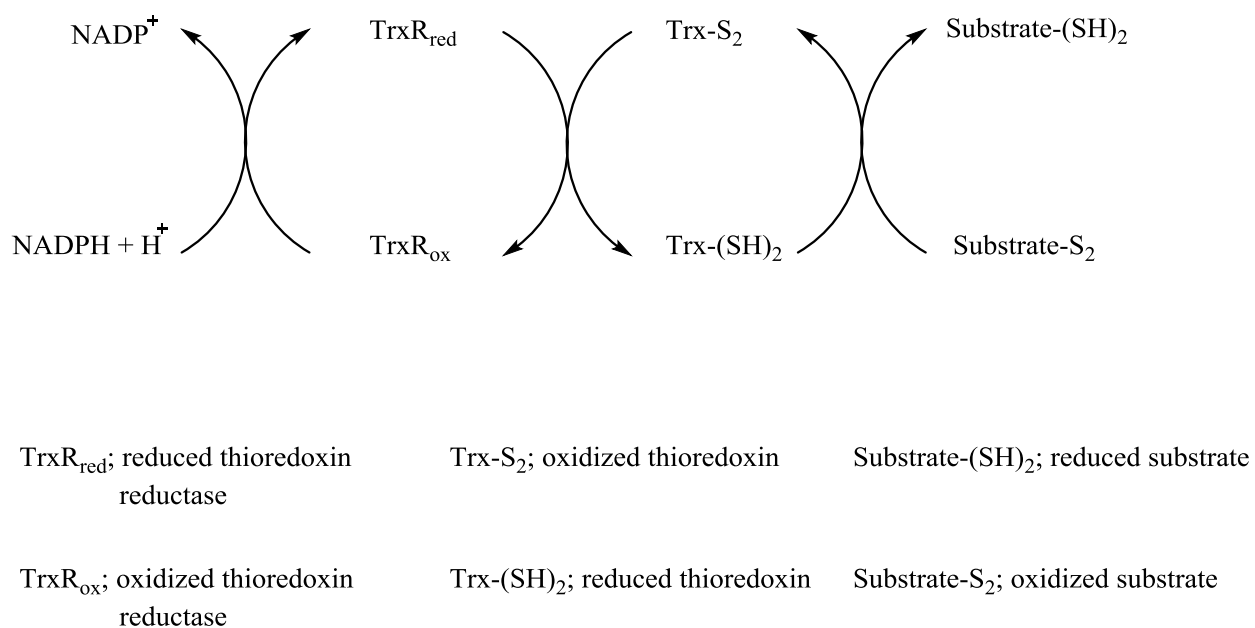


Figure 1.2: Schematic representation of reactions catalyzed by thioredoxin and thioredoxin reductase (9).

High concentrations of hydrogen peroxide within cells can result in cellular damage through Fenton chemical processes. In addition to catalases and peroxidases, the cell utilizes a group of enzymes known as peroxiredoxins (Prx), which contain redox active cysteine residues involved in the reduction of hydrogen peroxide. In all peroxiredoxins, the redox active cysteine residues are located at the N-terminal region which is the primary site where hydrogen peroxide reduction takes place (13). There are six isoforms of mammalian peroxiredoxins which have been identified, and they have been classified into three subgroups depending on the number of redox active cysteine residues (9). These subgroups include; typical 2-Cys proteins (include isoforms I, II, III, and IV), atypical 2-Cys proteins (include isoform V) and 1-Cys proteins (include isoform VI). The typical 2-Cys proteins are homodimers with two identical active sites and in addition to the cysteine residue at the N-terminal region of one subunit, these proteins have an additional cysteine residue at the C-terminal region of the other subunit (13). Peroxiredoxins catalyze reduction of hydrogen peroxide through oxidation of the sulfhydryl group of cysteine to cysteine sulfenic acid (14-16). The cysteine sulfenic acid moiety then reacts with the cysteine residue at the C-terminal region of the other subunit of typical 2-Cys peroxiredoxins, forming an intermolecular disulfide linkage. The disulfide is then reduced by thioredoxin (Fig. 1.3). In the atypical 2-Cys peroxiredoxins, cysteine sulfenic acid formed upon reduction of hydrogen peroxide reacts with a cysteine residue located within the same polypeptide chain forming an intramolecular disulfide which is consequently reduced by thioredoxin (Fig. 1.3). The cysteine sulfenic acid generated by the 1-Cys peroxiredoxins upon reduction of hydrogen peroxide is reduced by a thiol containing electron donor whose identity is unclear although there are speculations that glutathione may be involved (Fig. 1.4) (9, 13-14).

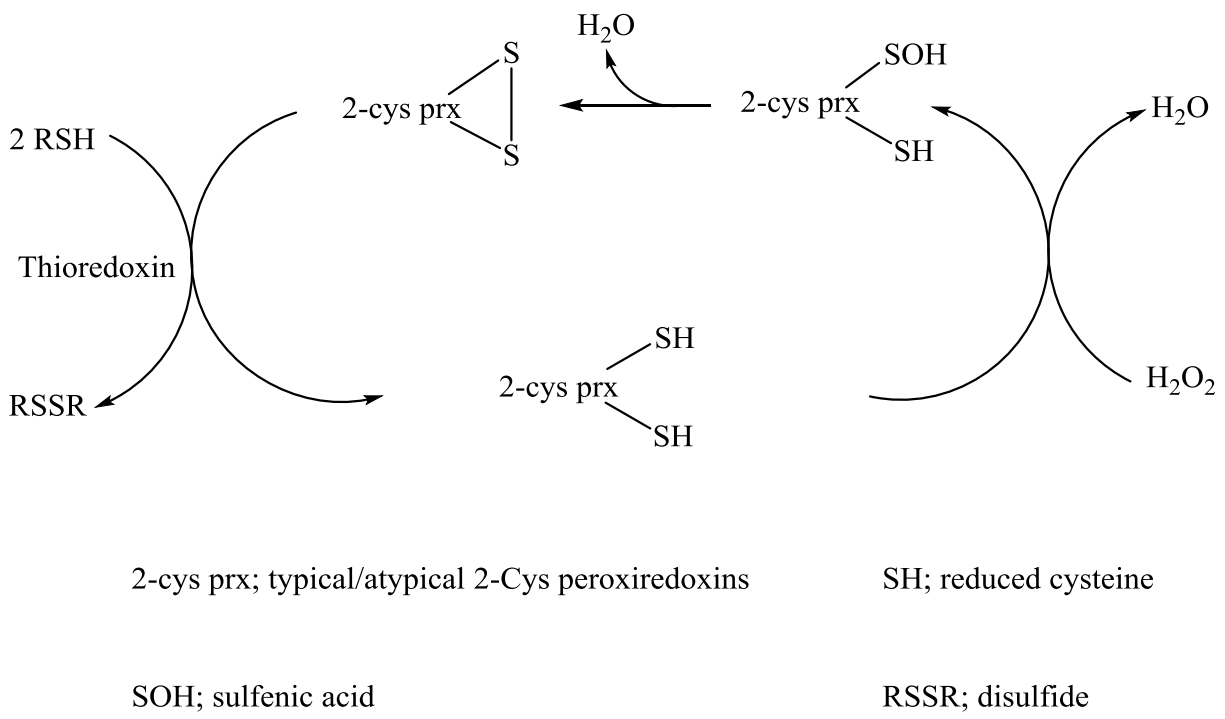


Figure 1.3: Schematic representation of reactions catalyzed by typical and atypical 2-Cys peroxiredoxins (14).

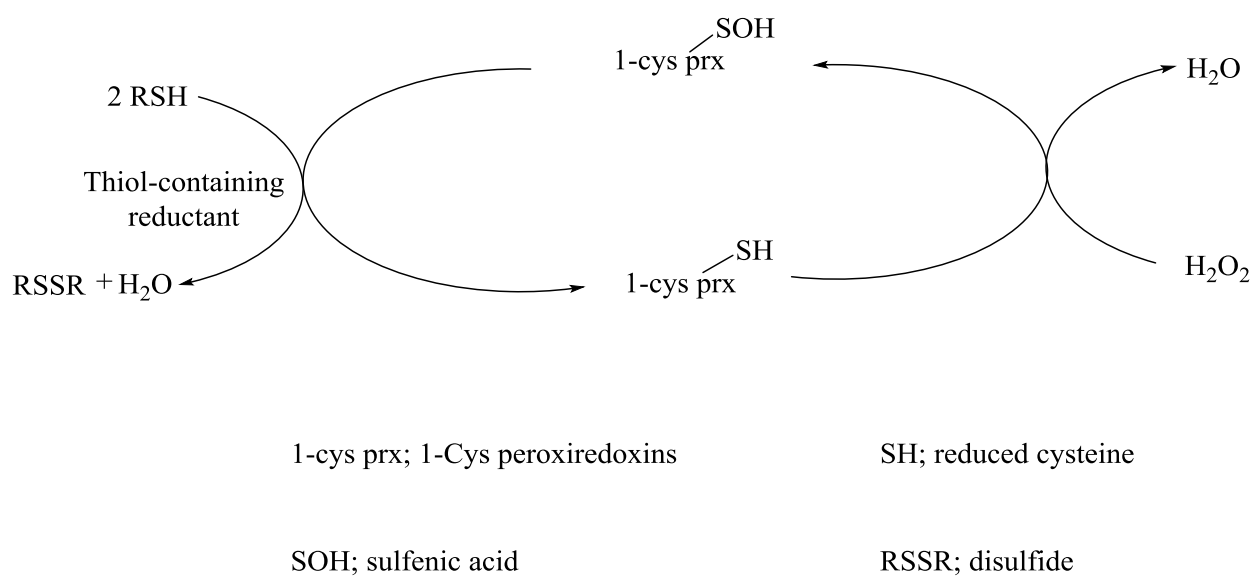


Figure 1.4: Schematic representation of reactions catalyzed by 1-Cys peroxiredoxins (14).

The intracellular redox environment is also maintained by the glutaredoxin system which is comprised of glutathione/glutathione disulfide (GSH/GSSG) redox couple, glutathione reductase and glutaredoxin. The glutaredoxin system facilitates the reduction of protein disulfides and mixed disulfides. Glutaredoxins can either utilize a monothiol type mechanism where only one redox active cysteine residue is involved in the reaction, or they can utilize a dithiol type mechanism which involves two cysteine residues at the active site (9). Regardless of the type of mechanism utilized, upon reduction of protein disulfides and mixed disulfides, oxidized glutaredoxins are reduced by glutathione (Fig. 1.5). Oxidized glutathione is subsequently reduced by NADPH-dependent glutathione reductase.

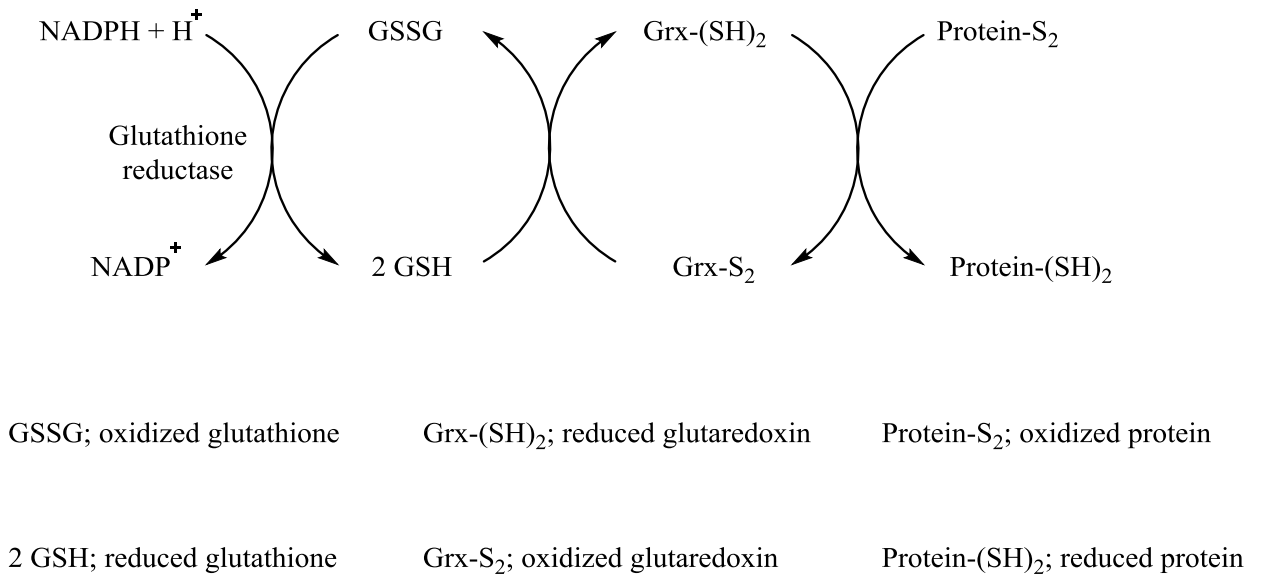


Figure 1.5: Schematic representation of reactions catalyzed by the glutaredoxin system (9).

1.4 Incorporation of cysteine in biomolecules

1.4.1 Glutathione biosynthesis

Glutathione or γ -L-glutamyl-L-cysteinyl-glycine is the most abundant intracellular low molecular weight thiol, with concentrations ranging between 0.5-10 mM (17). Glutathione plays a major role in protecting cells from reactive oxygen species due to its ability to scavenge free radicals, reduce peroxides, and react with electrophilic compounds. The reduced form of glutathione (GSH) is oxidized to glutathione disulfide (GSSG) by glutathione peroxidase and GSSG can be reduced back to GSH by glutathione reductase (Fig.1.6). The glutathione/glutathione disulfide (GSH/GSSG) redox couple helps to maintain the cellular redox environment and because it is the most abundant redox couple, it serves as an indicator of oxidative stress (18). The first step in the glutathione biosynthetic pathway involves formation of the dipeptide γ -GluCys in a reaction catalyzed by the ATP-dependent enzyme, glutamate-cysteine ligase (GCL) which is also known as γ -glutamylcysteine synthetase (Fig. 1.7). The γ -GluCys dipeptide then combines with glycine to form GSH in a reaction catalyzed by another ATP dependent enzyme, glutathione synthase (GS).

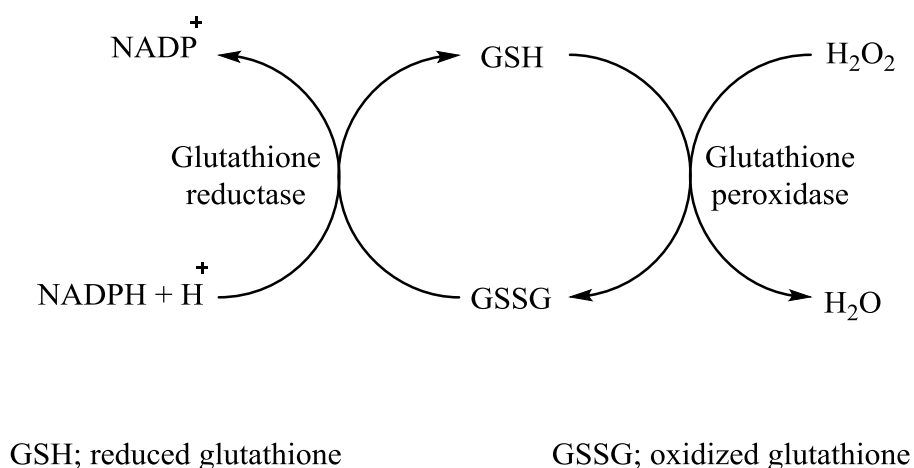


Figure 1.6: Schematic representation of reduction and oxidation of glutathione (17).

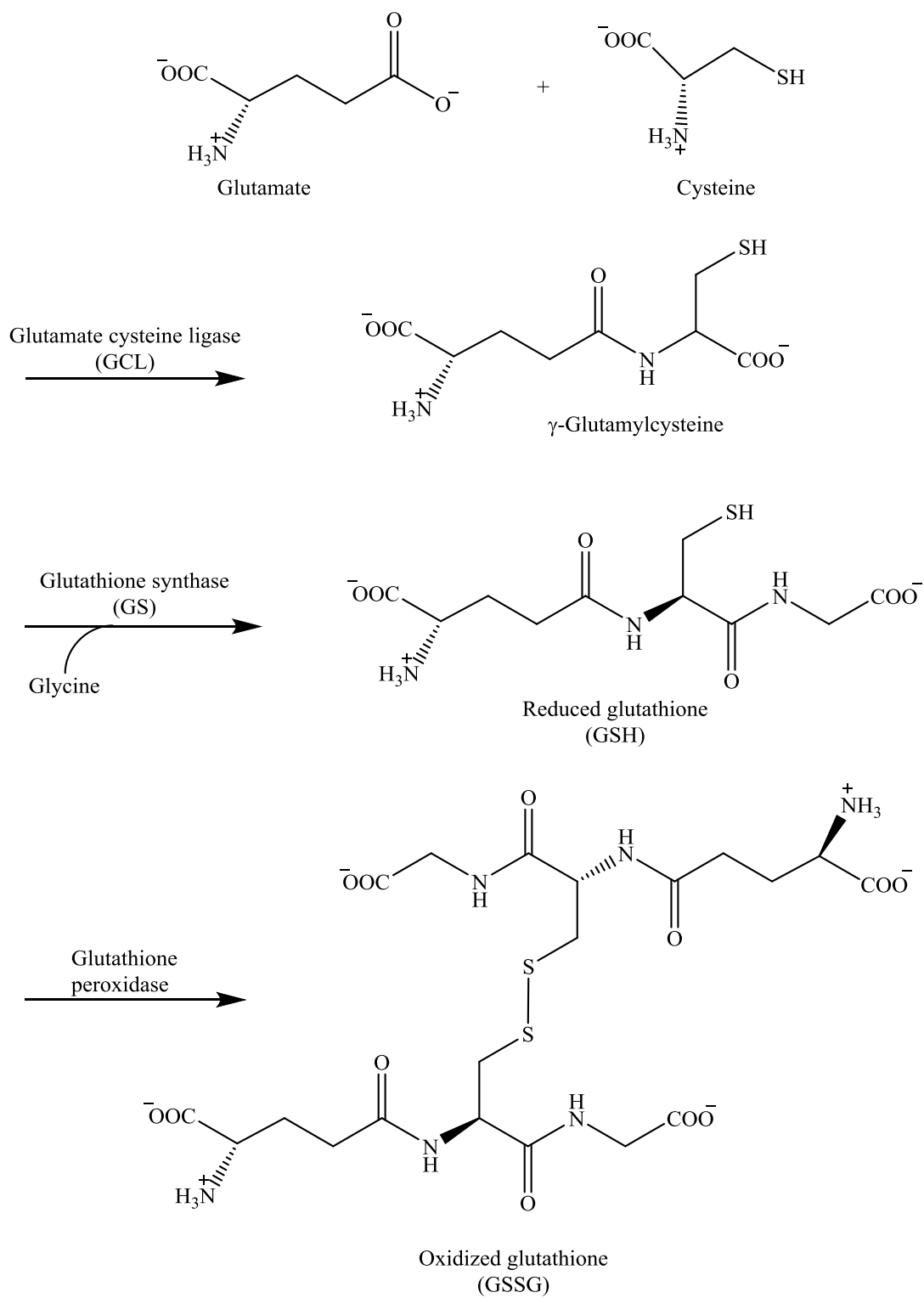
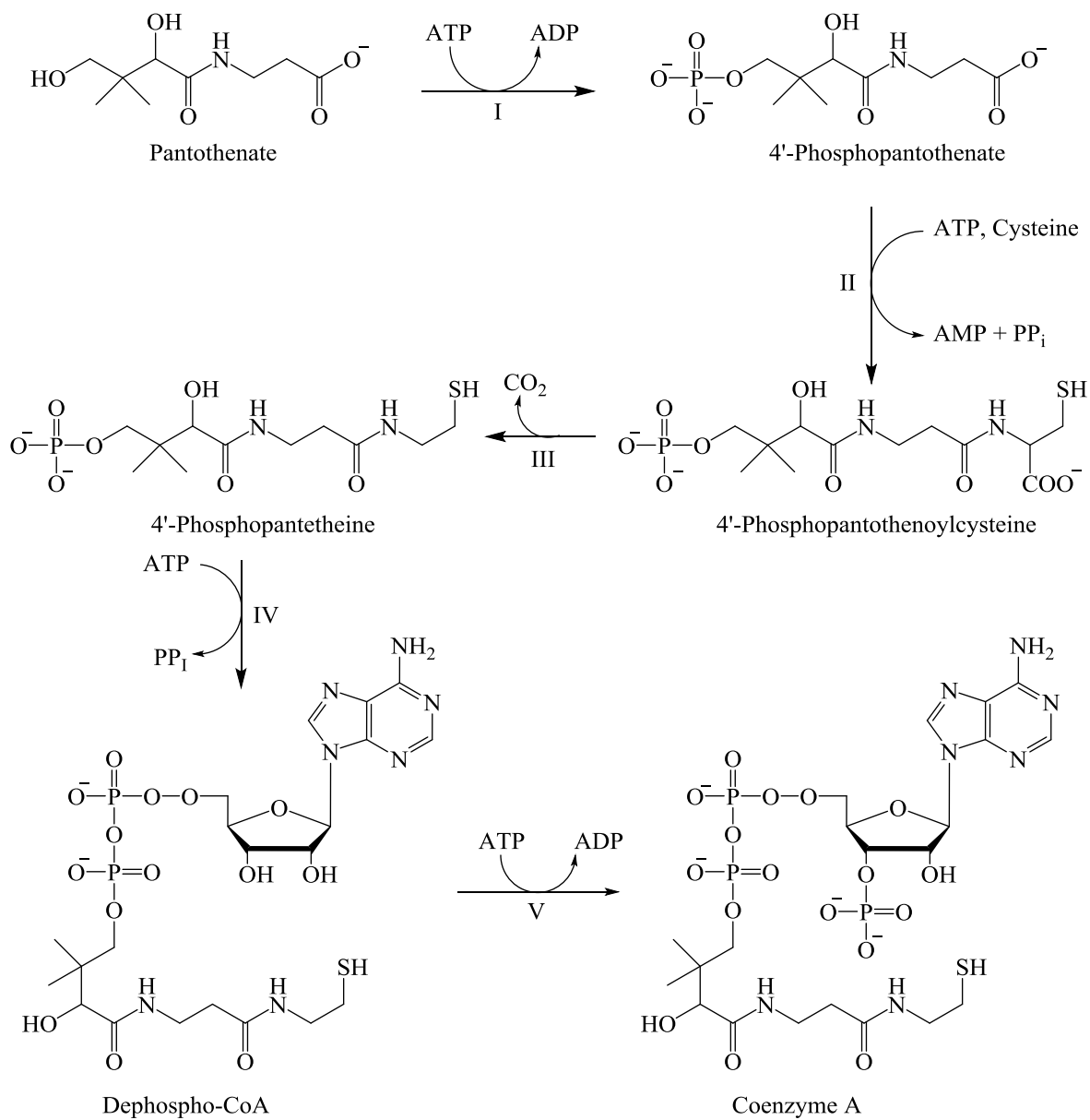


Figure 1.7: Biosynthetic pathway of glutathione (17).

1.4.2 Coenzyme A biosynthesis

Coenzyme A (CoA) is an important cofactor involved in many biochemical transformations including tricarboxylic acid cycle and fatty acid metabolism. The substrates required to synthesize CoA are pantothenic acid or vitamin B₅, ATP and cysteine. The first step in CoA biosynthetic pathway involves the phosphorylation of pantothenic acid to 4'-phosphopantothenate in a reaction catalyzed by pantothenate kinase (19) (Fig. 1.8). Cysteine is then condensed with 4'-phosphopantothenate to form 4'-phosphopantothenoylcysteine in a reaction catalyzed by 4'-phosphopantothenoylcysteine synthase. The condensation reaction was shown to be specific for cysteine because other sulfhydryl containing compounds like β -mercaptoethylamine could not replace cysteine (19). Cysteine is then decarboxylated by 4'-phosphopantothenoylcysteine decarboxylase to form 4'-phosphopantetheine. AMP is then added to 4'-phosphopantetheine to form dephospho-CoA in a reaction catalyzed by phosphopantetheine adenyltransferase. Dephospho-CoA is then phosphorylated at the 3'-OH of the ribose to form CoA in a reaction catalyzed by dephospho-CoA kinase (19-20).

The rate-limiting step in CoA biosynthesis is the pantothenate kinase reaction and is regulated by CoA and the thioesters of CoA (20). The various isoforms of mammalian pantothenate kinase (PanK) are encoded by four genes which include *PANK1*, *PANK2*, *PANK3*, and *PANK4*. Mutations in *PANK2* gene have been associated with the human pantothenate kinase associated neurodegeneration disorder (PKAN), which was formerly known as Hallervorden-Spatz syndrome (21). PKAN is associated with an accumulation of cysteine and iron in the brain as a result of impaired CoA biosynthesis (22). Cysteine in the presence of iron may undergo autooxidation resulting in the formation of free radicals, which consequently contribute to the pathogenesis of PKAN (21).



I. Pantothenate kinase

IV. Phosphopantetheine adenyltransferase

II. 4'-phosphopantothenoylcysteine synthase

V. Dephospho-CoA kinase

III. 4'-phosphopantothenoylcysteine decarboxylase

Figure 1.8: Biosynthetic pathway of Coenzyme A (15, 16).

1.5 Cysteine catabolism

So far, only the uses of the intact cysteine molecule have been considered. Cysteine can also be degraded to form molecules with important metabolic functions. Degradation of cysteine can either occur through oxidative or non oxidative pathways and the relative contribution of each pathway depends on the cellular concentrations of cysteine/sulfur containing amino acids and is also dependent on the respective tissue and type of cells being analyzed (5).

1.5.1 Non oxidative catabolism of cysteine

The non oxidative pathways include desulfuration of cysteine either by cystathionine β -synthase (CBS) or cystathionine γ -lyase (CSE). CBS catalyzes the condensation of homocysteine and serine to form cystathionine, as illustrated in the transsulfuration pathway for cysteine biosynthesis (Fig. 1.1). Under physiological conditions, serine can be replaced with cysteine such that the condensation of homocysteine and cysteine results in the formation of cystathionine and hydrogen sulfide (H_2S) (Fig. 1.9). The choice of substrate between serine and cysteine depends on the tissue concentrations of the respective molecules. The reported K_m value of mammalian CBS for serine is 1.9 mM while the K_m value for cysteine is 6.5 mM suggesting that under physiological conditions, serine is the preferred substrate for CBS (5). In addition to catalyzing the cleavage of cystathionine to form cysteine, α -ketobutyrate, and ammonia (Fig. 1.10, I), cystathionine γ -lyase (CSE) can also catalyze desulfuration of cysteine to form serine and H_2S (Fig. 1.10, II) (5). H_2S has been shown to be a potent inhibitor of the respiratory system and studies have shown that it can be quite toxic if not properly regulated (23). Fortunately, H_2S does not accumulate to levels that can be toxic to the cell under physiological conditions. Recent reports have shown that H_2S also plays important physiological roles. For example, in the cardiovascular system, H_2S relaxes the vascular smooth muscle, an effect that is caused by

opening the vascular smooth muscle cells (VSMC) K_{ATP} channels which consequently leads to hyperpolarization of the membrane (23). H_2S also relaxes the ileal smooth muscle and reduces gastric injury caused by nonsteroidal anti-inflammatory drugs (24). The non oxidative pathways of cysteine catabolism may also include transamination reaction with aspartate amino transferase to form 3-mercaptopyruvate. However, because the K_m value of aspartate amino transferase for cysteine is considerably higher (~22 mM) relative to the value for aspartate (0.06-0.5 mM), cysteine is not a preferred substrate for aspartate amino transferases (5).

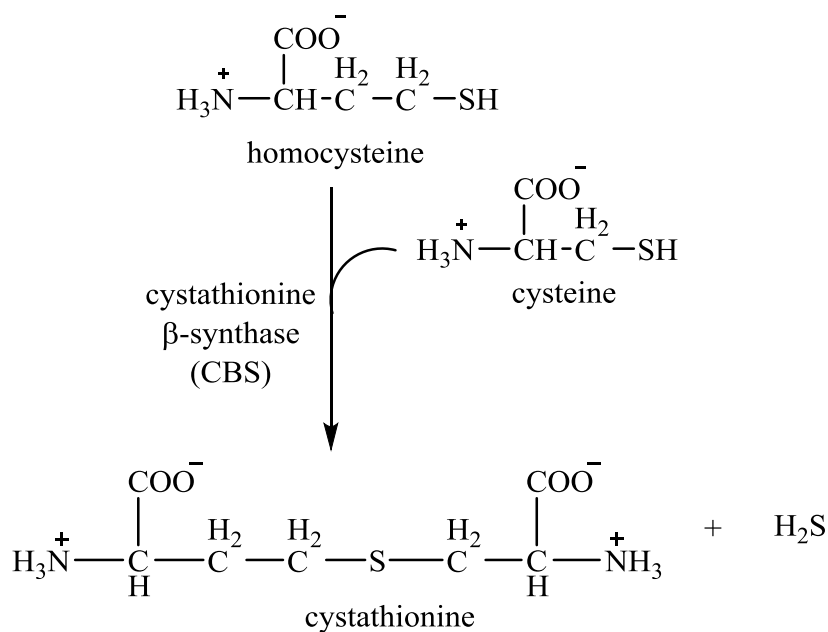


Figure 1.9: Production of H_2S by cystathionine β -synthase (5).

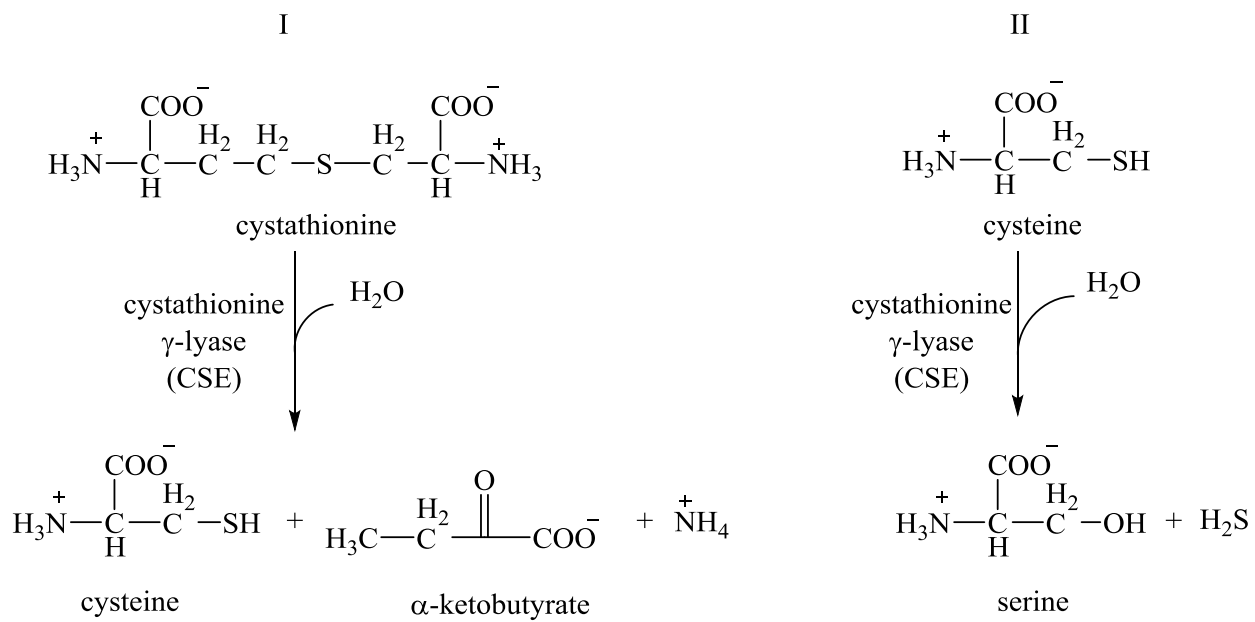


Figure 1.10: Reactions catalyzed by cystathionine γ -lyase in the formation of cysteine (I) and H_2S (II) (5).

1.5.2 Oxidative catabolism of cysteine

In addition to the several pathways of non oxidative cysteine catabolism, mammalian organisms also degrade cysteine oxidatively via the taurine biosynthetic pathway (Fig. 1.11A). Because the non oxidative pathways lead to the production of H₂S which may be potentially toxic at high concentrations, the taurine biosynthetic pathway is in fact the main pathway of cysteine catabolism in mammalian systems. In this pathway, cysteine is first oxidized to form cysteine sulfinic acid (CSA) in a reaction catalyzed by cysteine dioxygenase (CDO). The cysteine sulfinic acid formed is a branchpoint between two pathways. One pathway involves a decarboxylation reaction to form hypotaurine, in a reaction catalyzed by the pyridoxal 5'-phosphate (PLP) dependent enzyme, cysteine sulfinate decarboxylase (CSD). Hypotaurine is then oxidized to taurine, but whether this oxidation step is enzymatic or non enzymatic is currently unclear (5). Taurine is the most abundant free amino acid in mammalian cells (present in millimolar concentrations), and it is mainly found in the brain, heart, liver, and, kidney (25). Taurine has a wide range of biological functions including alleviation of cardiovascular risk factors, conjugation of bile acids, and it has been classified as a potent antioxidant. The involvement of taurine in cardiovascular health is demonstrated by its ability to prevent plaque formation in atherosclerosis by lowering the concentration of low density lipoproteins (LDL) which tend to accumulate in the arterial walls (26). Studies have shown that taurine reduces the concentration of LDL by upregulating the low density lipoprotein receptors (LDLR) and/or by improving the binding of LDL to LDLR (26). The hormone angiotensin II (Ang II) plays a key role in maintaining cardiovascular homeostasis. Taurine has been shown to decrease blood pressure through attenuation of angiotensin II signaling which causes vasoconstriction and consequently increases blood pressure. Increased taurine concentration allows blood vessels to

expand thereby lowering blood pressure (26). It has been suggested that taurine modulates the stress-related sympatho-adrenal responses and as such, may lower blood pressure by decreasing the levels of epinephrine (which increases heart rate) and norepinephrine (which causes vasoconstriction) (27). Taurine also plays a major role in cholesterol metabolism through conjugation of bile acids within the liver which are then secreted into the bile (26). Taurine has been described as an antioxidant due to its role in neutralizing hypochlorous acid, a powerful oxidant produced by neutrophils and monocytes during immune responses (28). Being one of the most abundant amine in the cell (>20 mM in neutrophils), taurine reacts with hypochlorous acid to form *N*-chlorotaurine which is less toxic than hypochlorous acid.

The second pathway of cysteine sulfinic acid metabolism involves a transamination reaction catalyzed by aspartate amino transferase to form β -sulfinylpyruvate which spontaneously dissociates to form pyruvate and sulfite. Sulfite may then be oxidized by sulfite oxidase to form sulfate (4). Partitioning of cysteine sulfinic acid between the decarboxylation and the transamination reactions depends on the relative affinities of cysteine sulfinic acid decarboxylase (CSD) and aspartate amino transferase for the substrate. CSD has a K_m of ~0.04-0.17 mM for cysteine sulfinic acid while aspartate amino transferase has a K_m of ~3-25 mM for the same substrate (29-30). This suggests that under physiological conditions, decarboxylation of cysteine sulfinic acid by CSD is favored over its transamination by aspartate amino transferase.

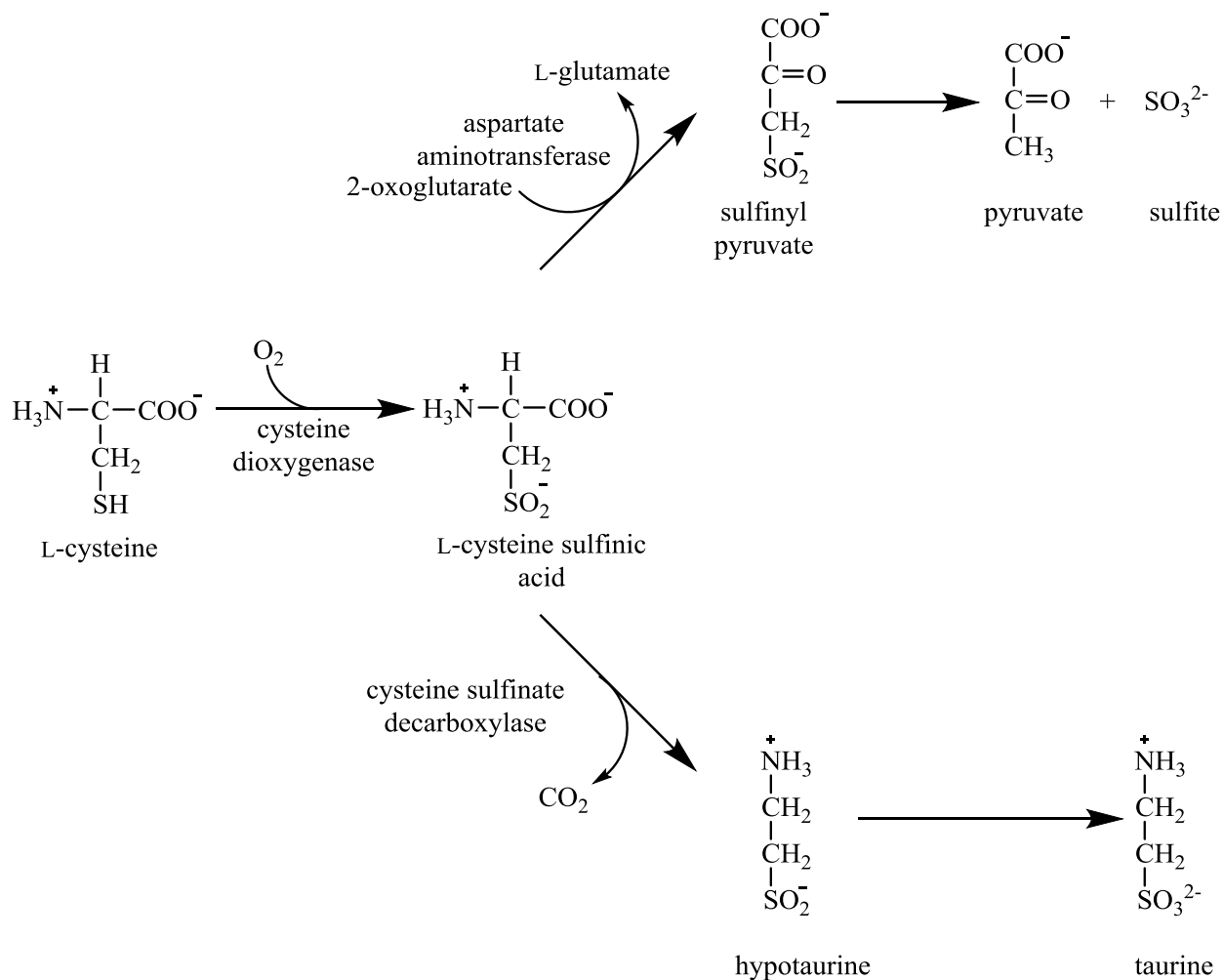


Figure 1.11A: The taurine biosynthetic pathway (31).

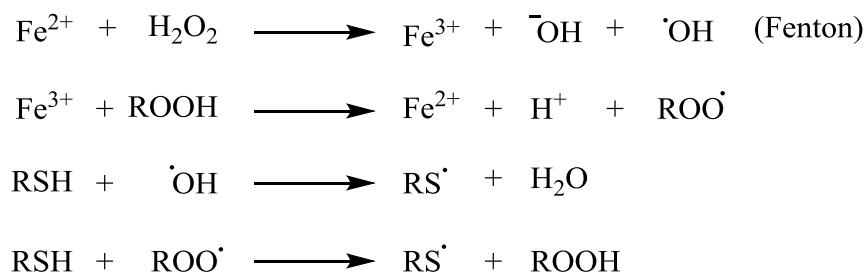


Figure 1.11B: Cysteine toxicity; iron and cysteine mediated production of free radicals (117).

The rate-limiting step in the taurine biosynthetic pathway is the oxidation of cysteine to cysteine sulfinic acid, catalyzed by cysteine dioxygenase, (CDO). CDO is a 23 kDa, iron containing enzyme which is mainly expressed in the liver but it has also been found in low concentrations in the kidney, lung, pancreas, and adipose tissue (32-33). The concentration of CDO within the cell corresponds with the concentration of cellular cysteine. For example, in animals fed with a low protein diet, the concentration of hepatic CDO was found to be very low, but when the diet was switched to a high protein diet, CDO concentration was found to rapidly increase (34-36). The regulation of CDO in response to the diet was found to be primarily post translational because the concentration of CDO mRNA was not affected by the diet (31, 36-37). CDO is regulated at the level of ubiquitination and degradation by the 26S proteasome (7). When animals were fed a low protein diet, CDO was found to be rapidly degraded by the 26S proteasome to minimize its activity so as to conserve the available cysteine. However, when animals were fed a high protein diet or a diet containing high levels of sulfur amino acids, increase in cellular cysteine concentration was shown to prevent CDO ubiquitination which lowered the rate of its degradation by the 26S proteasome, consequently allowing the enzyme to accumulate within the cell (37-38). Because high concentrations of cysteine can cause cellular damage through formation of free radicals in the presence of iron, maintaining proper concentrations of intracellular free cysteine is of critical importance (Fig.1.11B). The main mechanism by which mammalian systems maintain a proper balance of cellular cysteine is through CDO. Like most enzymes, CDO has adopted special structural properties that enhance its functionality. The current study will evaluate the correlation between the structural and functional characteristics of CDO that make the enzyme an optimal system for L-cysteine oxidation.

1.6 The cupin superfamily

Cysteine dioxygenase has a β -barrel fold that is characteristic of the cupin superfamily (1-3). Members of the cupin superfamily have relatively low overall sequence similarity, and they catalyze a diverse range of reactions. Cupin superfamily proteins have two partially conserved cupin sequence motifs, $G(X)_5HXH(X)_{3,6}E(X)_6G$ and $G(X)_{5,7}PXG(X)_2H(X)_3N$ which are separated by a less conserved intermotif region composed of 15-50 amino acids (39). The two cupin sequence motifs combined with the intermotif region form the characteristic β -barrel fold found in cupin superfamily proteins. In fact, the name cupin is derived from the Latin word ‘*cupa*’ which means a small barrel (40). Cupin superfamily proteins are generally metalloproteins and the active site of these proteins is located at the center of the β -barrel (39). The β -barrel fold (cupin fold) in CDO is highlighted in figure 1.12.

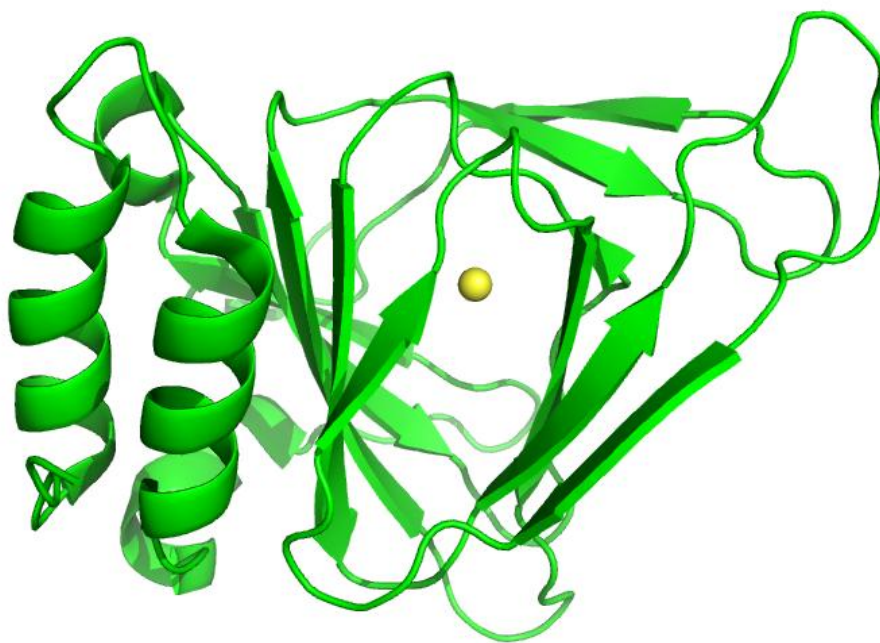


Figure 1.12: Crystal structure of cysteine dioxygenase highlighting the β -barrel fold (cupin fold). The structure was taken from PDB entry 2IC1.

1.6.1 Germin

Initial characterization of the cupin superfamily proteins was based on germin, a Mn^{2+} -containing oxalate oxidase that uses dioxygen to convert oxalate into two molecules of carbon dioxide and one molecule of hydrogen peroxide as illustrated in figure 1.13 (39, 41).

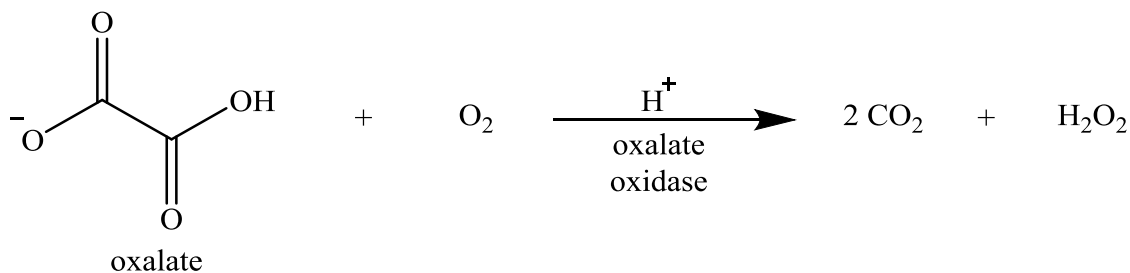


Figure 1.13: Reaction catalyzed by oxalate oxidase (40-41).

Structural characterization of germin showed that the protein is a homohexamer organized in a trimer of dimers with one manganese ion per subunit (42-43). Each monomer displays the characteristic β -barrel fold composed of the conserved cupin sequence motifs. The amino acid residues involved in coordinating the metal in cupin metalloproteins were first identified with the structure of germin in which the Mn^{2+} ion was found to be coordinated in a tetrad composed of 3-His and 1-Glu ligands (Fig. 1.14). The coordinating amino acid residues are derived from cupin motifs 1 and 2 and they include the two conserved His residues and the Glu residue in cupin motif 1 and a third His in cupin motif 2 (43-44). Subsequent three-dimensional structures of Mn^{2+} -containing oxalate decarboxylase and Cu^{2+} -containing quercetin dioxygenase revealed a similar coordination pattern which suggested that the 3-His/1-Glu metal coordination pattern may be a common feature among the cupin metalloproteins (45).

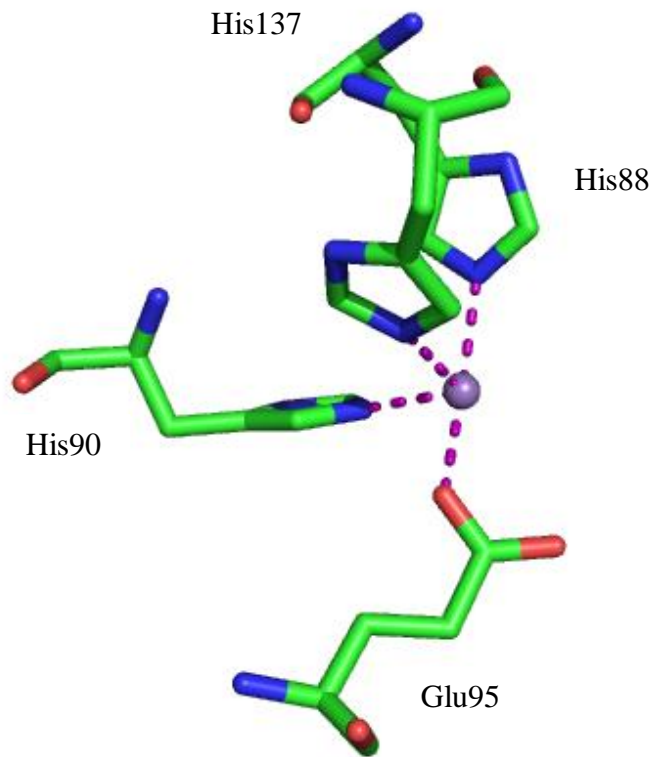


Figure 1.14: Active site of oxalate oxidase highlighting the 3-His/1-Glu metal binding site. The structure was taken from PDB entry 1FI2.

1.6.2 Quercetin dioxygenase

Quercetin is a plant flavonol commonly used in traditional medicine for its antioxidant and antimicrobial properties, and various strains of *Aspergillus* utilize quercetin as a source of carbon (46). The first step in the degradation of quercetin is catalyzed by quercetin dioxygenase (QDO) which catalyzes the oxidation of quercetin to 2-protocatechuoylphloroglucinolcarboxylic acid and carbon monoxide (Fig. 1.15).

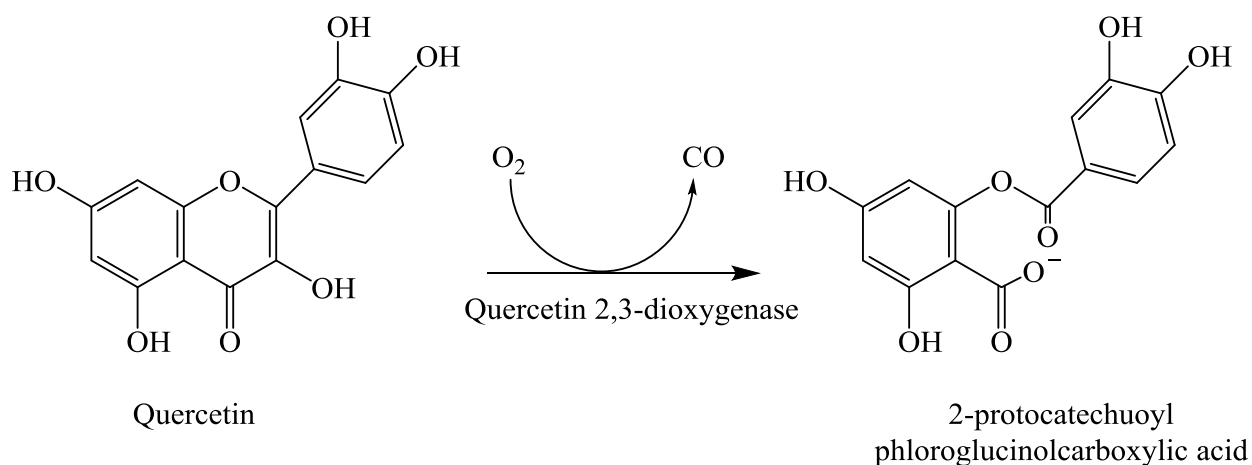


Figure 1.15: Reaction catalyzed by quercetin 2,3-dioxygenase (46).

Quercetin dioxygenase from *Aspergillus* strains was initially characterized as a Cu^{2+} -dependent enzyme but recent reports have illustrated that the QDO from *Bacillus subtilis* contains Fe^{2+} in the active site (47-48). Although the two enzymes seem to have different active site metal preferences, their overall three-dimensional structure is highly similar. The two enzymes are homodimers with two cupin domains in which the respective metals are bound by 3-His residues and 1-Glu residue (47-48). The striking similarity in the ligands that coordinate the active site metal in the two enzymes prompted further investigations into the effect of metal substitution on the activity of the respective enzymes. Interestingly, reconstitution of Fe^{2+} containing QDO from *B. subtilis* with Mn^{2+} , Co^{2+} , Ni^{2+} , and Cu^{2+} generated enzymes with comparable and even higher activities than the native enzyme. Since the catalytic activity of the Mn^{2+} -reconstituted QDO was higher than the native Fe^{2+} -containing enzyme, it was proposed that Mn^{2+} may be the preferred cofactor. It was suggested that the Fe^{2+} ion in QDO from *B. subtilis* may have been adventitiously bound as a result of expressing the enzyme in LB broth (46). Substituting the metal in the Cu^{2+} -dependent QDO from *Aspergillus* did not have significant effects on the activity of the enzyme, although Cu^{2+} was clearly the preferred cofactor in this enzyme (49). These studies demonstrate that QDO may not be very specific in the choice of active site metal, but instead is able to function with a number of different divalent metals.

Mechanistically, it has been proposed that QDO from *Aspergillus* strains uses a similar mechanism like the intradiol catechol dioxygenases, which utilize high-spin Fe^{3+} as the active site metal. The Cu^{2+} center is proposed to activate quercetin for a direct reaction with dioxygen (50). Electron paramagnetic resonance (EPR) analysis of the anaerobic enzyme-substrate complex supported the presence of Cu^{2+} and it was suggested that the Cu^{1+} species does not accumulate to appreciable amounts to be detected (50). The catalytic mechanism of the Fe^{2+} -

containing QDO from *B.subtilis* is proposed to be similar to that of the extradiol catechol dioxygenases which utilize high-spin Fe^{2+} as the catalytic metal cofactor (51). The Fe^{2+} center in *B.subtilis* QDO has been proposed to function as a conduit for the transfer of electron from the substrate to dioxygen (46). The starting viewpoints in the catalytic mechanisms between the two enzyme systems differ slightly, but the majority of the catalytic scheme is essentially similar as outlined in figure 1.17. The metal center is viewed as a site for bringing the reactants together for optimum interaction and not necessarily to activate dioxygen. This is supported by the relaxed metal specificity observed in QDO. After the formation of the quercetin radical-metal-superoxide complex (Fig. 1.16, II), the reaction may proceed by Criegee rearrangement as depicted in figure 1.16, route A. The breakdown of the rearrangement product, V, would lead to the formation of the final product. An alternative route (Fig. 1.16, route B) from intermediate II would be the formation of a dioxolane intermediate, IV', which consequently leads to formation of the final product, V', upon ring opening.

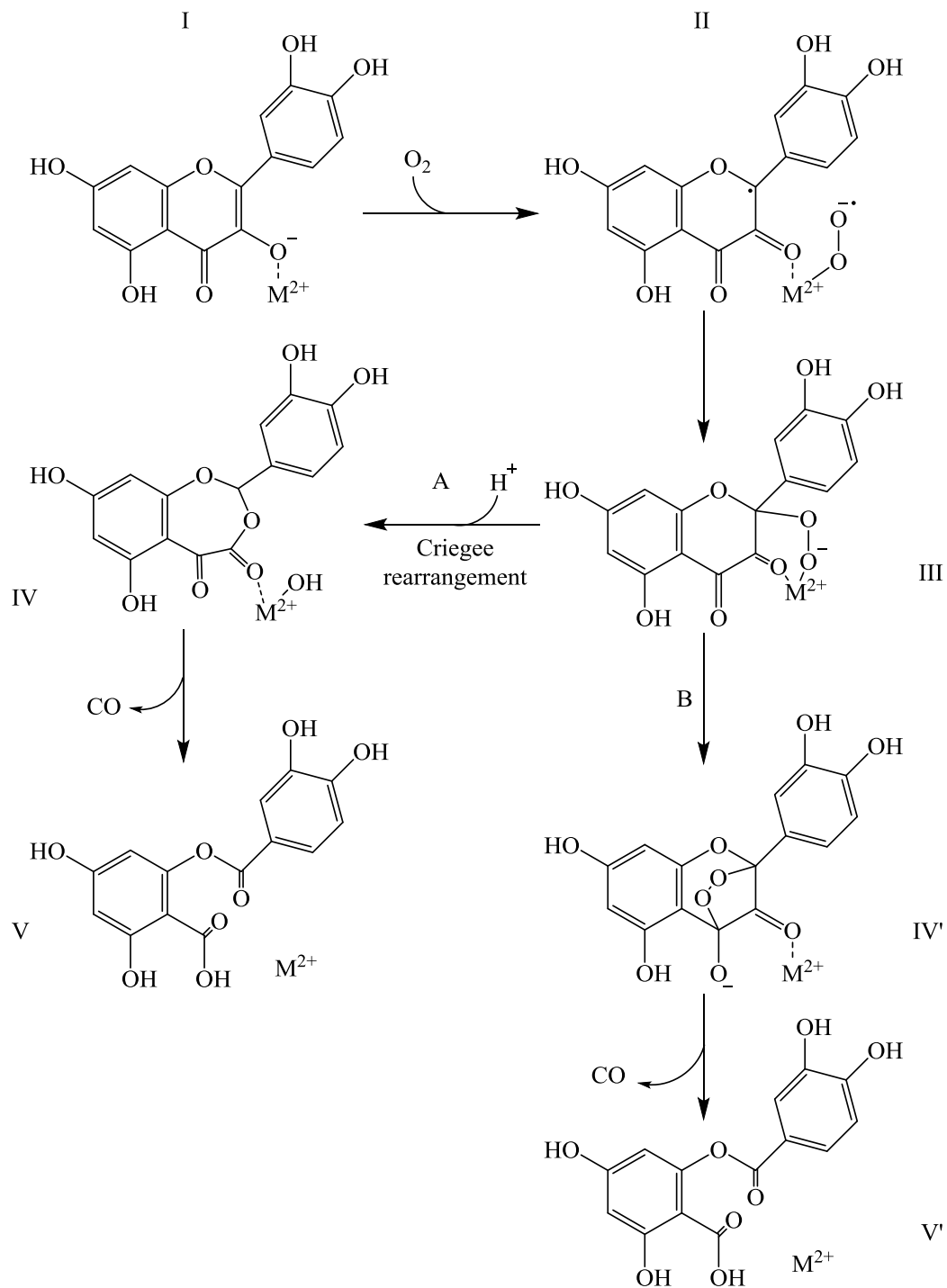


Figure 1.16: Catalytic mechanism of quercetin dioxygenase, (M^{2+} represents either Fe^{2+} , Mn^{2+} or Cu^{2+}) (46).

1.6.3 Acireductone dioxygenase

Acireductone or 1,2-dihydroxy-3-keto-5-(methylthio)pentene is an intermediate in the methionine salvage pathway. This pathway recycles methionine from 5'-methylthioadenosine (MTA) which is formed from S-adenosylmethionine (SAM) (52). The methionine salvage pathway has been intensively investigated in *Klebsiella pneumoniae* where two enzymes were identified that catalyze the oxidation of acireductone (53). Interestingly, the two enzymes which are both acireductone dioxygenases (ARD) have the same polypeptide sequence, the same molecular weight but they only differ in the identity of the metal bound in the active site. One enzyme contains Fe^{2+} ion in the active site while the other enzyme contains Ni^{2+} ion in the active site. Both enzymes utilize acireductone and dioxygen as substrate but they catalyze the formation of different products (52). The Fe^{2+} -containing enzyme (Fe^{2+} -Ard) converts acireductone to the α -ketoacid precursor of methionine and formate which are the expected intermediates of the methionine salvage pathway (Fig. 1.17 , route A) (41, 53). The Ni^{2+} -containing enzyme (Ni^{2+} -Ard) catalyzes an off-pathway oxidation of acireductone to form methylthiopropionate, carbon monoxide and formate, suggesting that this off-pathway reaction prevents recycling of methionine from MTA (Fig. 1.17, route B) (54). The functional properties of the Fe^{2+} -containing ARD and Ni^{2+} -containing ARD can be interconverted upon reconstitution of the respective enzymes with the appropriate metals (55). The two enzymes are separable by ion exchange and hydrophobic interaction chromatography suggesting they may have different structural properties (55). Acireductone dioxygenase has a monocupin structure in which the active site metals in the respective enzymes are coordinated by 3-His residues, (His96, His98, and His140) and 1-Glu, (Glu102) (54).

Mechanistically, an ordered binding of substrates was proposed for both enzymes in which acireductone was proposed to bind first as a dianion followed by dioxygen (52). Experiments with ^{18}O and ^{14}C established that the Ni^{2+} -containing ARD incorporates molecular oxygen into C_1 and C_3 positions of acireductone forming a cyclic 5-membered peroxide intermediate which may decompose into the final products upon C-C bond cleavage (Fig. 1.18). Conversely, Fe^{2+} -containing ARD incorporates molecular oxygen to the C_1 and C_2 positions of acireductone forming a cyclic 4-membered peroxide (dioxetane) intermediate which decomposes into the final products upon cleavage of the C-C bond, (Fig. 1.18). It is currently unclear how the two metals affect the points of addition of molecular oxygen to acireductone (52, 55).

1.7 Variations from the 3-His/1-Glu metal binding pattern

Although the 3-His/1-Glu metal coordination pattern is a common feature within the cupin superfamily proteins, some variations have been reported. For example, in mammalian cysteine dioxygenase, the conserved Glu residue from cupin motif 1 is replaced with a non-coordinating Cys residue. Therefore, the Fe^{2+} center in CDO is coordinated by a facial triad of 3-His residues (Fig. 1.19) (1-3). Such a variation from the canonical 3-His/1-Glu coordination pattern has been reported in only a few other enzymes including β -diketone cleaving enzyme (Dke1) but the rationale behind the variation is still unclear. Evaluation of a typical 3-His/1-Glu metal binding site and a typical 3-His metal binding site suggests that the two sites are well suited for their respective functions.

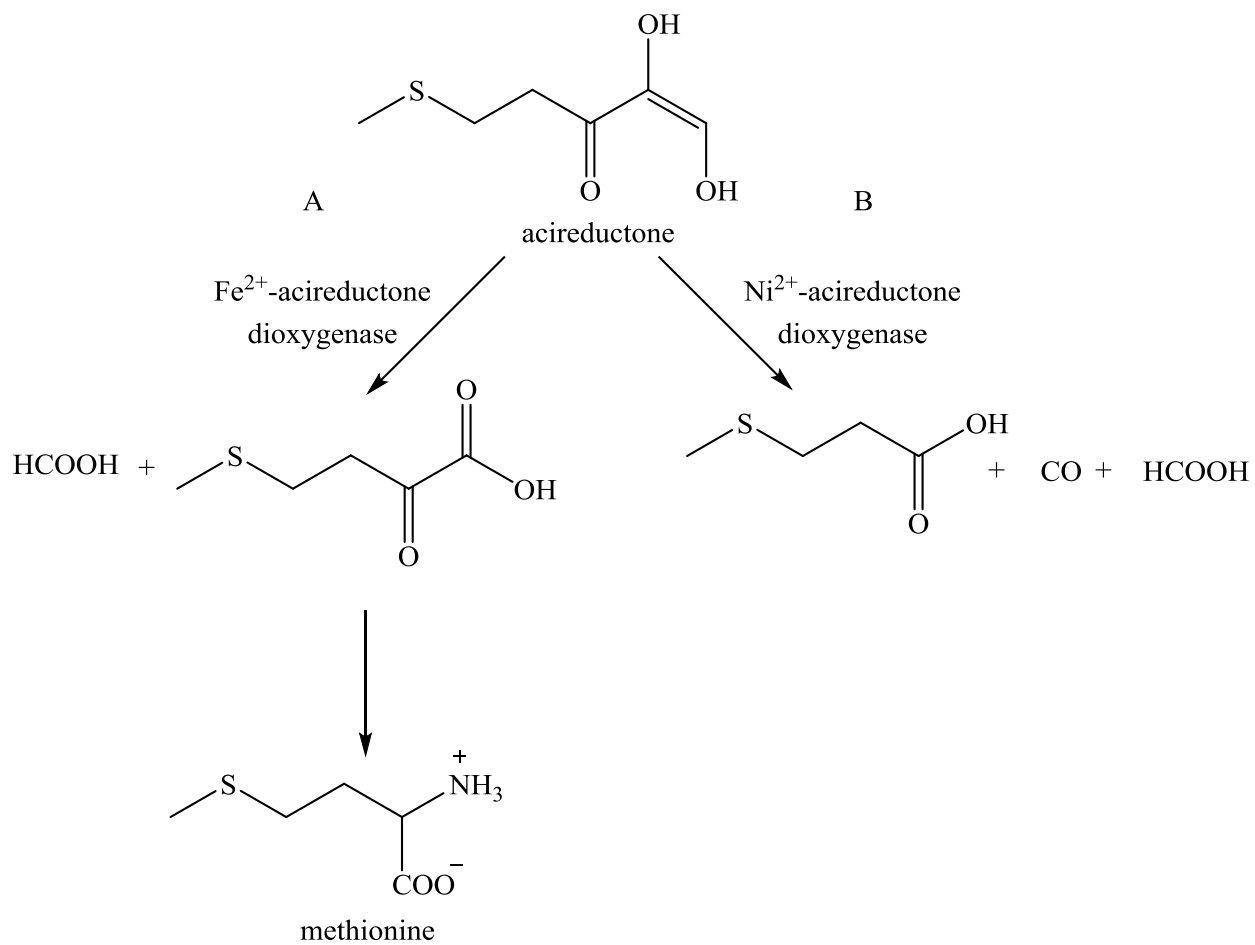


Figure 1.17: An outline of the reactions of Fe^{2+} and Ni^{2+} -containing acireductone dioxygenases (54).

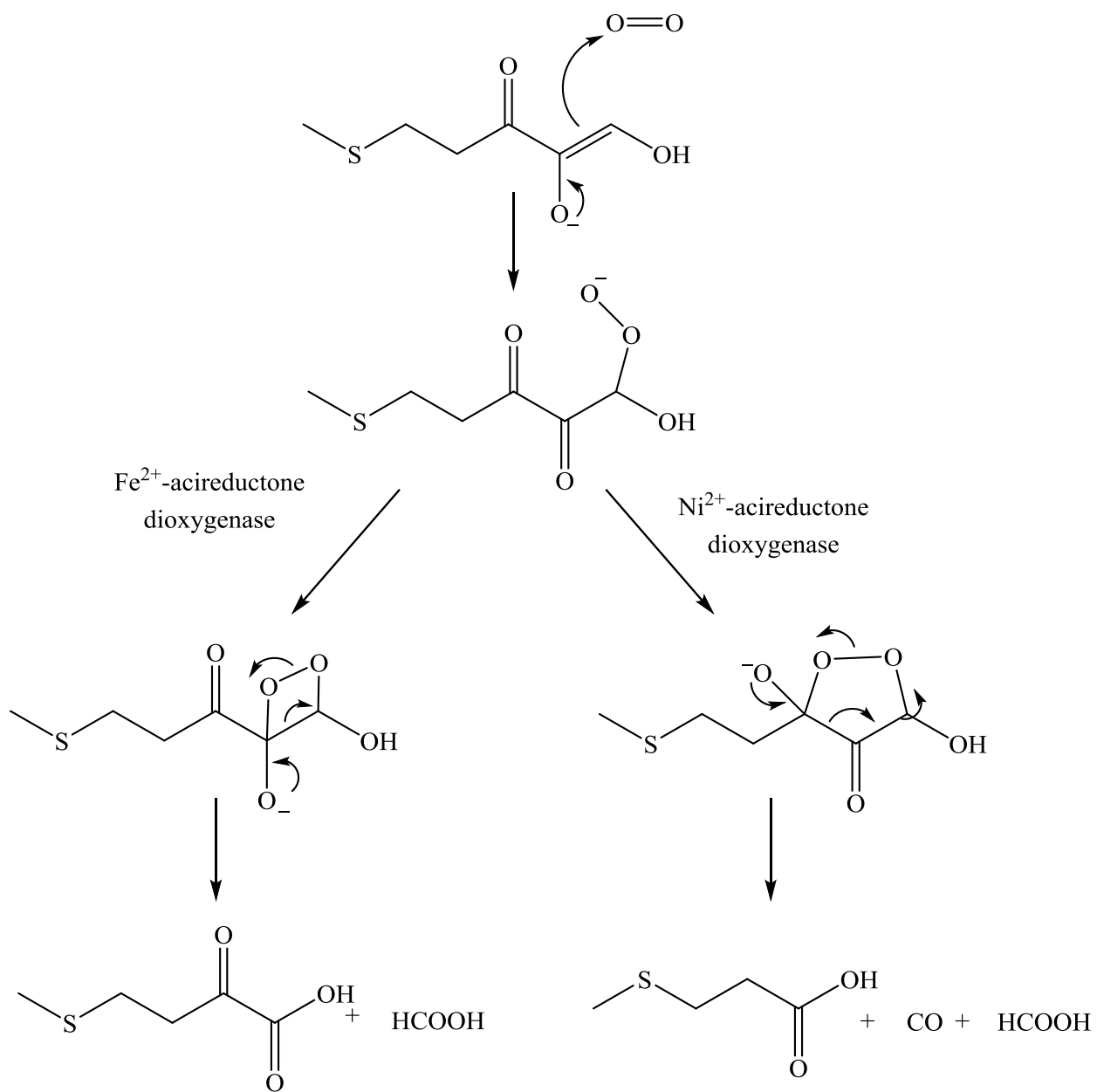


Figure 1.18: Proposed mechanisms of Fe^{2+} and Ni^{2+} -containing acireductone dioxygenases (55).

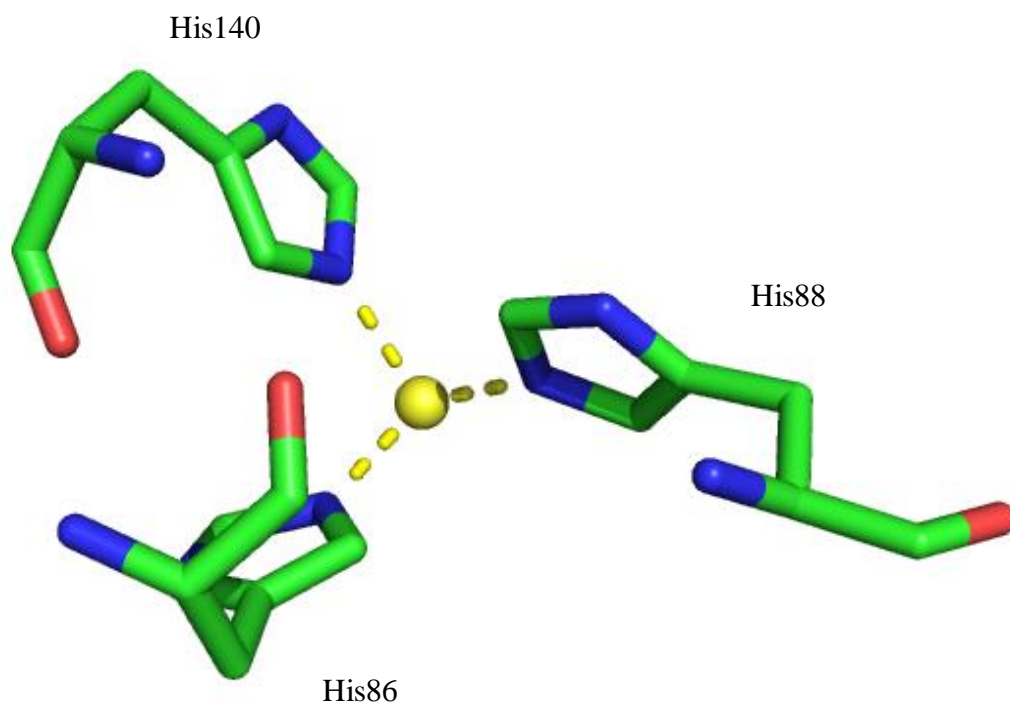


Figure 1.19: Active site of cysteine dioxygenase highlighting the 3-His metal binding site. The structure was taken from PDB entry 2B5H.

1.7.1 β -Diketone cleaving enzyme

Acetylacetone or 2,4-pentanedione is an industrial chemical that is widely used in various metal extraction procedures and it has been shown to be potentially toxic (56). The first step in the degradation of acetylacetone is catalyzed by β -diketone cleaving enzyme (Dke1), a homotetrameric non-heme Fe^{2+} -dependent enzyme which was initially isolated from a strain of *Acinetobacter johnsonii* which grew on acetylacetone as the sole source of carbon (57). Dke1 catalyzes the dioxygen dependent conversion of acetylacetone into methylglyoxal and acetate (58). The enzymatic breakdown of acetylacetone was observed to proceed with a stoichiometric consumption of molecular oxygen, as one μmol of dioxygen was consumed for every μmol of acetylacetone used (57). Results from ^{18}O labeling experiments revealed that one atom of ^{18}O was incorporated into each of the reaction products upon carbon-carbon bond fission (59). The crystal structure of an inactive form of Dke1 in which Fe^{2+} was substituted with Zn^{2+} revealed the β -barrel fold characteristic of the cupin superfamily proteins (59). The active site metal was found to be coordinated in a triad of His residues, His62, His64 and His104. Mutational analysis of the Fe^{2+} coordinating ligands was found to disrupt the metal binding affinity in the variants (58). Metal analysis studies revealed that the catalytic site of Dke1 was capable of binding other divalent metals like Cu^{2+} , Mn^{2+} , Ni^{2+} , and Zn^{2+} with similar binding constants with Fe^{2+} . However, the enzyme was only active when Fe^{2+} was bound. Additionally, it has been reported that the active site of Dke1 can distinguish between Fe^{2+} and Fe^{3+} . This suggestion was based on the observation that Dke1 exhibited low affinity for Fe^{3+} and oxidation of the bound Fe^{2+} ion to the Fe^{3+} form upon its exposure to H_2O_2 or excess dioxygen, led to its rapid release out of the active site (58). These observations clearly demonstrated that Dke1 strictly depends on ferrous iron for its catalytic activity (57-58).

The proposed mechanism in which acetylacetone is converted to methylglyoxal and acetate involves initial bidentate coordination of oxaloacetate to the Fe^{2+} active site of Dke1 as illustrated in figure 1.20 (41, 60-61). This is followed by dioxygen reduction to a superoxide coupled with the formation of C-O bond in steps II and III respectively. Nucleophilic attack of the peroxidate on an adjacent carbonyl carbon leads to the formation of a dioxetane intermediate, IV, which then decomposes into methylglyoxal and acetate products.

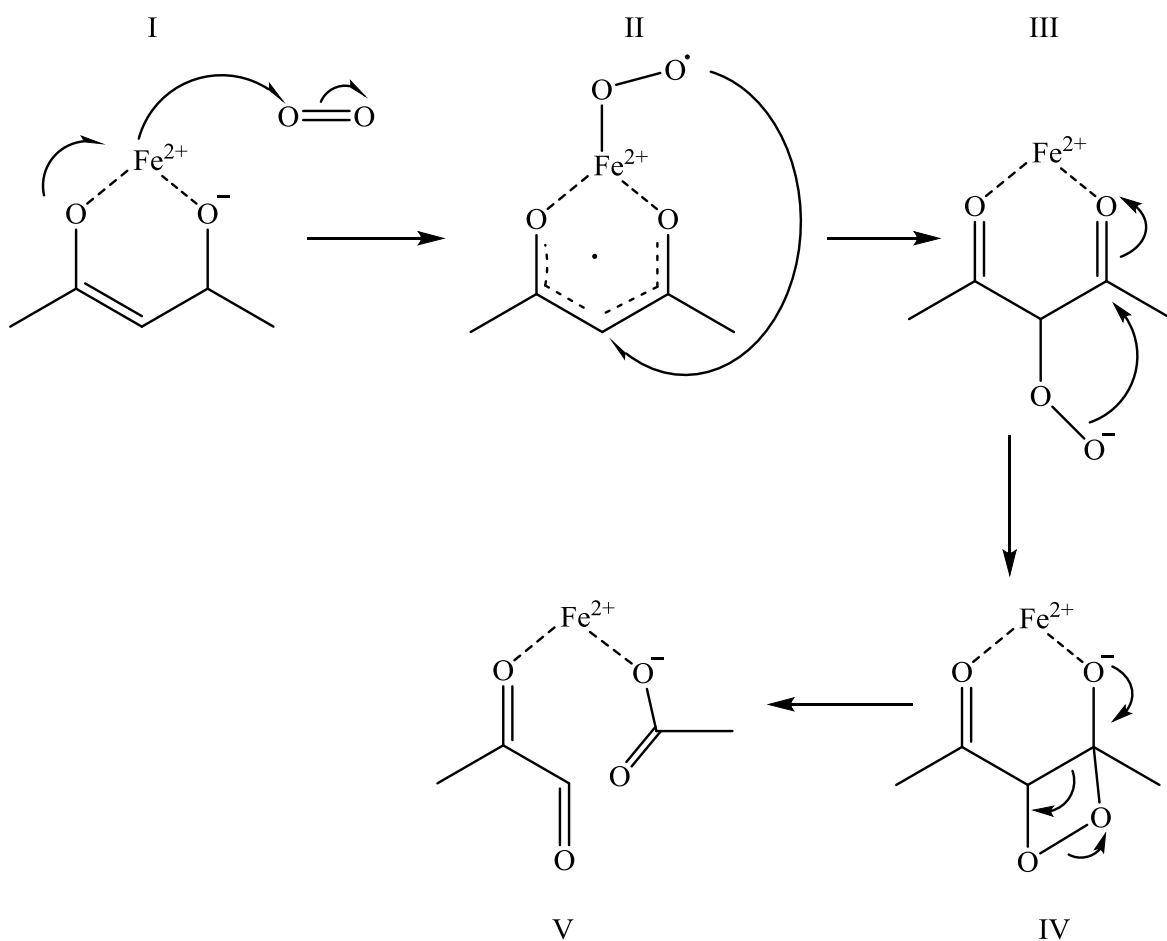


Figure 1.20: Proposed catalytic mechanism of Dke1 (60).

1.7.2 Cysteine dioxygenase

Cysteine dioxygenase (CDO) is a non heme mononuclear iron-dependent enzyme that catalyzes the oxidation of cysteine to cysteine sulfinic acid (Fig. 1.21).

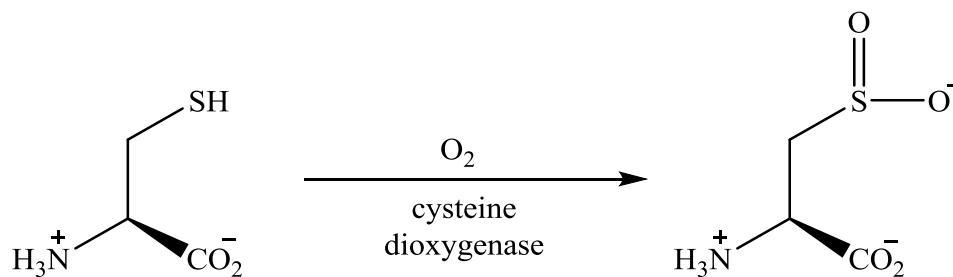


Figure 1.21: Reaction catalyzed by cysteine dioxygenase (62).

CDO was initially classified as a member of the cupin superfamily based on the sequence similarity with other cupin metalloproteins (40). The available three-dimensional structures of CDO have all confirmed the cupin fold (1-3). The first three-dimensional structure was of mouse CDO and it was solved as a Ni^{2+} -containing enzyme complex. The Ni^{2+} center was found to be hexa-coordinated with 3-His residues derived from cupin motif 1 (His86, His88) and cupin motif 2 (His140), and 3 additional water ligands. Studies of CDO involving active site metal requirement have shown that CDO strictly depends on iron for its catalytic activity (2, 63-64). Therefore, the Ni^{2+} -containing enzyme did not represent the active form of CDO, but it provided

useful structural information which was used as a guide for mechanistic proposals. Subsequent three-dimensional structures of rat and human CDO revealed an Fe^{2+} -containing active site in which the Fe^{2+} ion was coordinated by a facial triad consisting of the three conserved His residues and an additional solvent molecule.

The 3-His facial triad in CDO is rare and it seems to be well suited for the dioxygenation reaction. The three-dimensional structure of human CDO in complex with L-cysteine revealed that cysteine coordinates the Fe^{2+} center in a bidentate fashion via the thiol and amino groups (1). A similar mode of substrate coordination was also illustrated in MCD studies where it was shown that cysteine binds Fe^{2+} -CDO via the S atom in a similar manner as it binds Fe^{3+} -CDO (65). This mode of substrate binding creates an ideal coordination site for the dioxygen cosubstrate to bind. An obligate reactant binding order was recently reported using NO as a surrogate for dioxygen. In that study, the iron center in CDO was found to be essentially unreactive to NO unless cysteine was bound first (66). These studies demonstrated that cysteine binds to the active site iron first and consequently creates a favorable environment for dioxygen to bind (66). There are several mechanistic proposals on how CDO catalyzes the oxidation of cysteine to cysteine sulfinic acid. In all the proposed mechanisms, the unifying theme is the presence of Fe^{2+} center in the resting enzyme. Based on the structural evidence available, cysteine binds the active site ferrous iron via the thiol and amino groups (Fig. 1.22, II) (2). Binding of dioxygen would lead to formation of the Fe^{3+} superoxo intermediate (III). The coordinated S atom may reduce the oxidized Fe^{3+} center generating a sulfur radical cation which consequently recombines with the superoxo species to form a cyclic peroxo intermediate (IV). Homolytic bond cleavage of the O-O bond would generate a sulfoxy cation and an activated oxygen atom which would recombine to generate the final product upon hydrolysis (2).

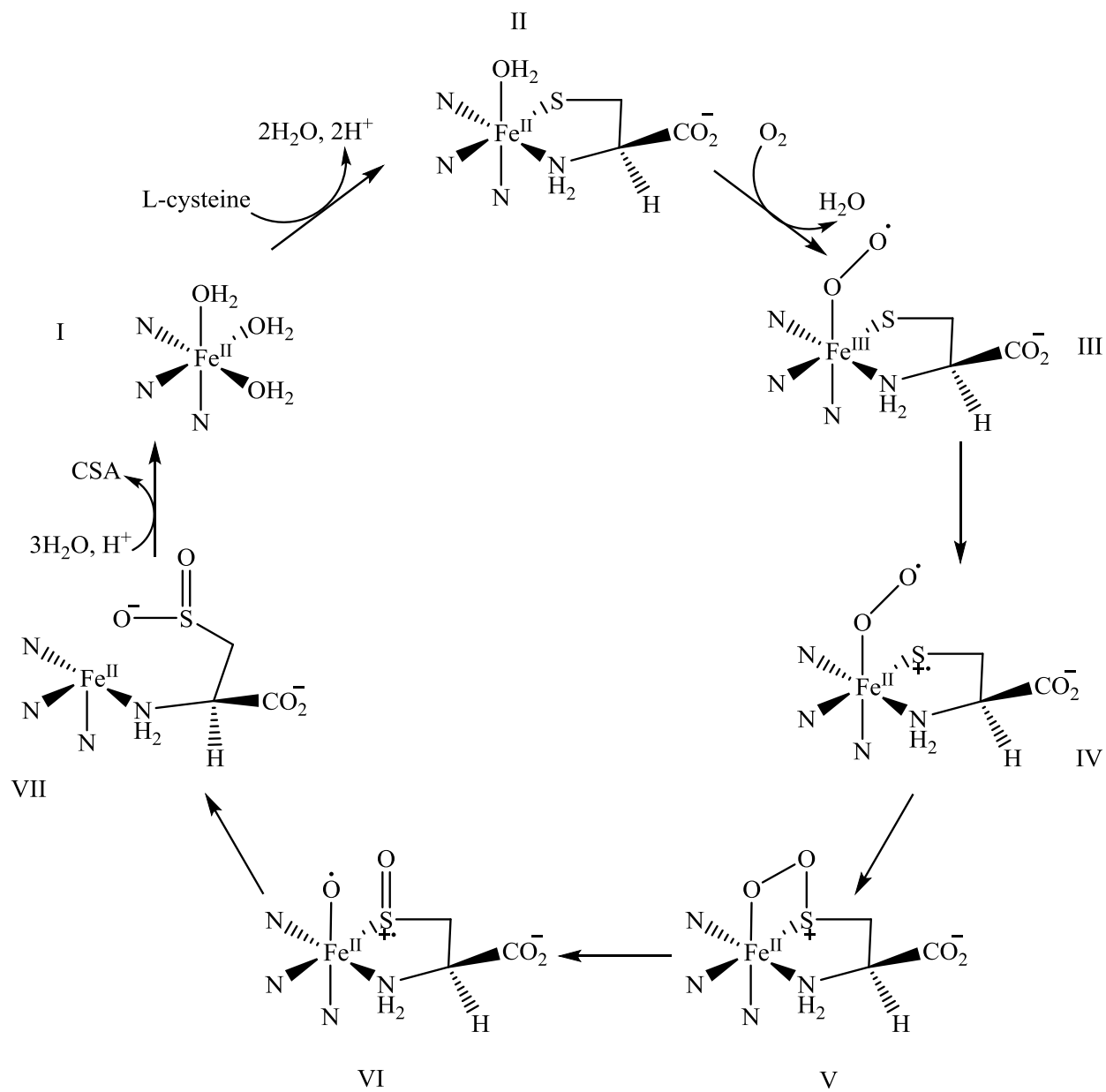


Figure 1.22: Proposed catalytic mechanism of cysteine dioxygenase (2).

In summary, the comparative analysis of a 3-His/1-Glu binding site and a 3-His binding site demonstrates that the enzymes that utilize a 3-His/1-Glu binding site have relaxed active site metal specificities, while the enzymes that utilize a 3-His binding site have specific metal preferences. The Fe²⁺-containing QDO for example is still active even when reconstituted with other divalent metals. ARD displays two different functionalities depending on the nature of the metal that is bound in the active site. The relaxed metal specificities in QDO and ARD suggests that changing the redox state of the active site metal during catalysis may not be a strict requirement in these enzyme systems (41). On the contrary, CDO and Dke1 are strictly dependent on iron for their catalytic activity, suggesting that the bound metal in these enzyme systems may function as a redox center facilitating either activation of dioxygen or activation of the substrate. Therefore, the deviation in metal coordination pattern observed in CDO may not be an accident, but a strategic move to optimize its functionality.

1.8 Protein derived cofactors

In addition to the unique metal binding site, cysteine dioxygenase also possesses a rare crosslink between Cys93 and Tyr157 close to the active site (Fig. 1.23) (1-3). The presence of this crosslink has triggered intense research involving the circumstances that lead to its biosynthesis and its function in the active site of CDO. Post translationally modified amino acid residues which are commonly referred to as protein derived cofactors, have been observed in other enzymes where they occur either by a self processing pathway, or their biogenesis is facilitated by accessory proteins (67). In most cases, these post translationally modified amino acids have been shown to provide additional advantages which the unmodified amino acid residues do not possess (67). The amino acid residues that are frequently involved in post translational modifications are tryptophan, tyrosine, cysteine, histidine, and methionine.

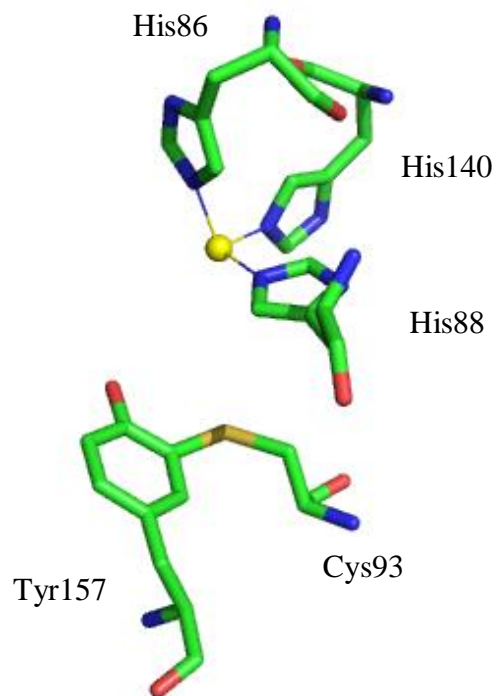


Figure 1.23: The active site of cysteine dioxygenase highlighting the covalent crosslink involving Cys93 and Tyr157. The structure was taken from PDB entry 2IC1.

1.8.1 Tryptophan tryptophylquinone (TTQ)

Tryptophan tryptophylquinone (TTQ) or 2,4-bistryptophan-6,7-dione is formed by post translational modification of two tryptophan residues in which two atoms of oxygen are incorporated into the indole ring of one of the tryptophan residues, and a covalent bond is formed between the two indole rings of the two tryptophan residues (Fig. 1.24) (68).

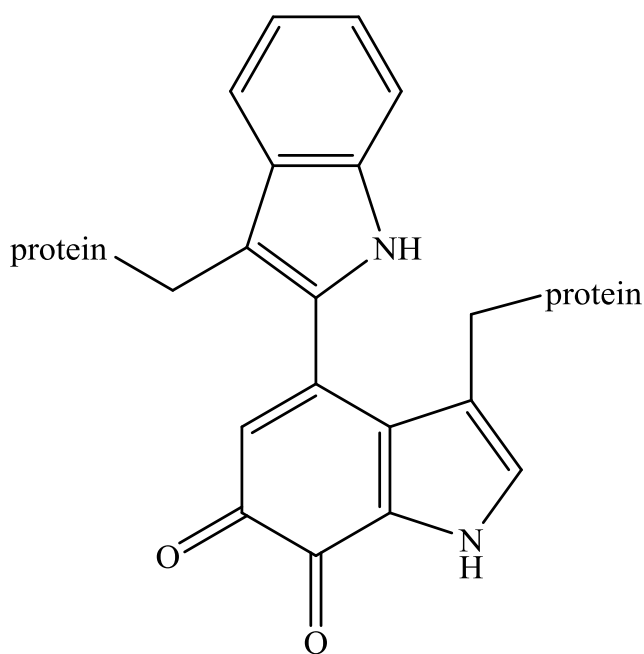


Figure 1.24: Tryptophan tryptophylquinone (TPQ) (69).

TTQ functions as a prosthetic group in methylamine dehydrogenase (MADH) and aromatic amine dehydrogenase (AADH). These enzymes catalyze the conversion of primary amines to their corresponding aldehydes and ammonia (70). The overall catalytic mechanism of MADH and AADH consists of a reductive and an oxidative reaction. The reductive reaction involves formation of a covalent adduct between the amine substrate and TTQ in which TTQ is reduced to an aminoquinol and the substrate is oxidized to an aldehyde (Fig. 1.25, I). The oxidative process involves two one-electron transfers to type 1 copper proteins, which are amicyanin for MADH and azurin for AADH. In the first electron transfer, an aminosemiquinone intermediate is formed, (Fig. 1.25, II) and in the second electron transfer, an aminoquinone is formed which is hydrolyzed to yield ammonia and regenerate oxidized TTQ (Fig. 1.25, III). Although the mechanism of TTQ biosynthesis has not been completely elucidated, studies have shown that its formation requires the participation of an accessory protein. In MADH, the accessory protein involved in TTQ biogenesis has been identified to be MauG. The gene that encodes for MauG is located within the methylamine utilization (*mau*) gene cluster of *Paracoccus denitrificans* together with the genes that encode the α and β subunits of MADH and eight other genes that have been shown to be necessary for MADH expression and function (69, 71). The role of MauG in TTQ biosynthesis was investigated using inactive variants of MauG that had been generated by site directed mutagenesis (71). Characterization of the MADH enzyme that was expressed with an inactive MauG, revealed the presence of an intermediate of MADH in which TTQ was incompletely synthesized, with only one of the Trp residues (Trp57) being monohydroxylated, and there was no covalent crosslink between Trp57 and Trp108. The MADH enzyme that contained the intermediate was inactive and exhibited weak subunit-subunit interactions (72). Incubation of the inactive MADH intermediate with purified active MauG

resulted in the incorporation of the second oxygen atom in Trp57 and formation of the covalent crosslink between Trp57 and Trp108. The activated MADH enzyme also exhibited normal subunit-subunit interactions as was shown by native polyacrylamide gel electrophoresis (PAGE). These studies demonstrated that active MauG is required for the biosynthesis of TTQ in MADH (69, 71-72).

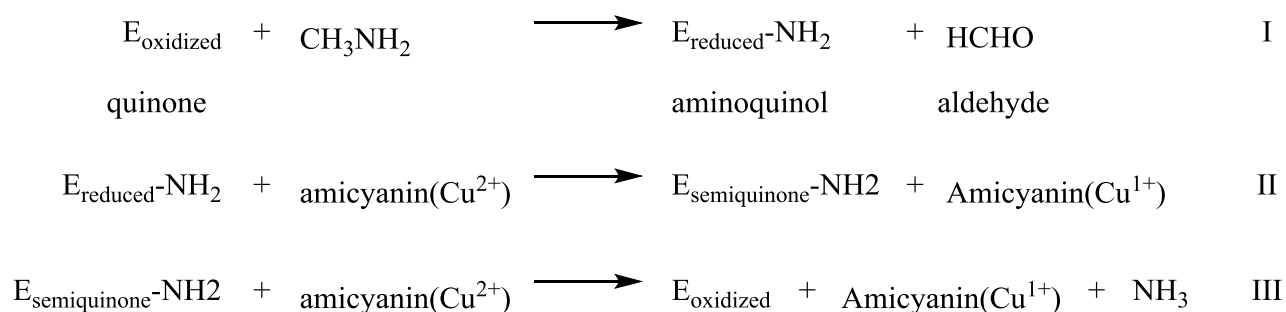


Figure 1.25: Catalytic mechanism of methylamine dehydrogenase (MADH) showing the reductive and the oxidative reactions (69).

1.8.2 Cysteine tryptophanylquinone (CTQ)

Cysteine tryptophanylquinone (CTQ) which is shown in figure 1.26 is formed by modification of a tryptophan residue in which two oxygen atoms are incorporated into the indole ring of the tryptophan and a covalent bond is formed between the modified tryptophan and the sulfur atom of cysteine. CTQ is the protein derived cofactor of quinohemoprotein amine dehydrogenase (QHNDH), an enzyme that catalyzes a similar reaction as the TTQ-dependent dehydrogenases (MADH and AADH), which is conversion of primary amines to their corresponding aldehyde products with the release of ammonia. QHNDH is a heterotrimeric protein composed of α , β and γ subunits (73). The active site of this enzyme which contains CTQ is in the γ subunit. The catalytic cycle of QHNDH is similar to that of TTQ-dependent dehydrogenases except that the electron acceptor from reduced CTQ is the heme in the α subunit of QHNDH (74). The mechanism of CTQ biogenesis has not been elucidated although there are speculations that the diheme protein subunit, α , may be involved in CTQ biogenesis and may serve in a similar capacity as MauG in TTQ biogenesis (69-70).

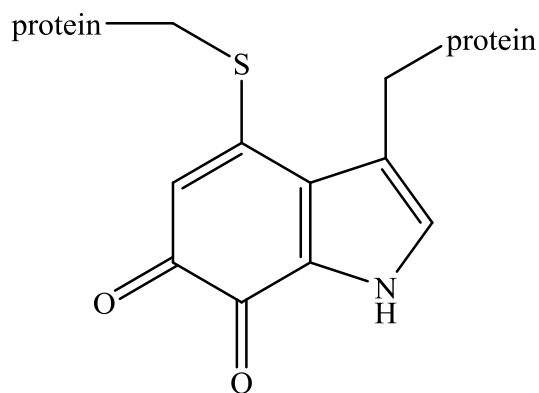


Figure 1.26: Cysteine tryptophanylquinone (CTQ) (70).

1.8.3 Met-Trp-Tyr covalent adduct in KatG

Catalase peroxidases (KatGs) are unique enzymes that display two functionalities in the same active site. These enzymes catalyze the decomposition of H_2O_2 via the catalase mechanism, which is illustrated in figure 1.27, I and peroxidase mechanism shown in figure 1.27, II (75-76).

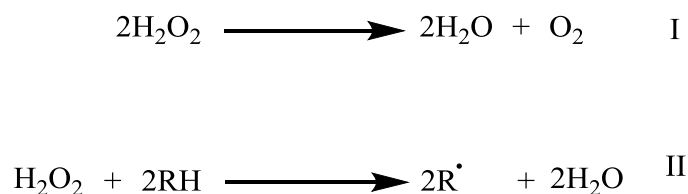


Figure 1.27: Reaction mechanisms showing the catalase mechanism (I) and the peroxidase mechanism (II) in KatG. RH represents the electron donor in the peroxidatic cycle and R^\cdot represents the donor radical (75, 77).

Structurally, KatG resembles monofunctional peroxidases. The three-dimensional structures of KatG from different organisms have revealed the presence of a unique Met-Tyr-Trp crosslink located on the distal side of the heme active site, shown in figure 1.28 (78-79). This crosslink is a common feature among all KatG enzymes but it is not found in monofunctional peroxidases (80). Substitution of any of the residues involved in the crosslink generated a catalase inactive enzyme but the peroxidase activity was retained (80-81). These observations

demonstrated that the Met-Tyr-Trp crosslink in KatG is required for the catalase activity but not for the peroxidase activity.

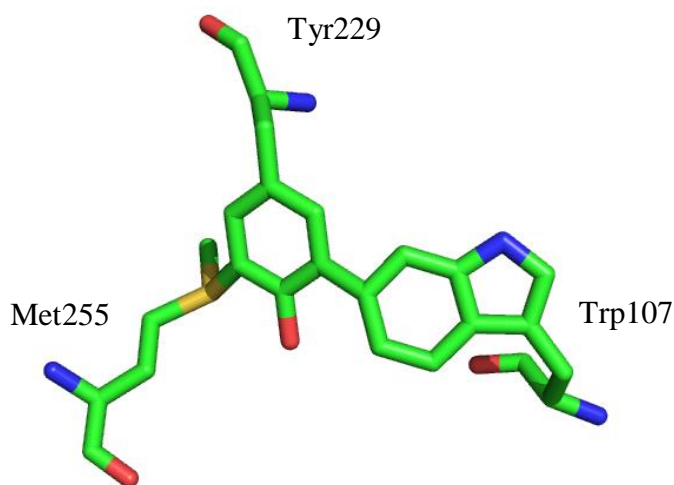


Figure 1.28: The Met-Tyr-Trp crosslink in KatG. The structure was taken from PDB entry 1SJ2.

The mechanism proposed for the formation of the crosslink in KatG was shown to require the presence of the heme and an additional oxidant, peracetic acid *in vitro*, but *in vivo* the oxidant would be hydrogen peroxide (76-77). In the proposed mechanism, peracetic acid/hydrogen peroxide reacts with the Fe^{3+} form of the resting enzyme generating the ferryl porphyrin π cation radical, commonly known as compound 1, shown in figure 1.29, II. This is followed by the oxidation of Trp and Tyr residues that are involved in the crosslink to their corresponding radical forms, complex III. Coupling of the two radicals results in the formation of the Trp-Tyr crosslink

intermediate IV. A second oxidation step of the Trp-Tyr crosslink via a second compound 1 intermediate, V, generates an electrophilic quinone-like intermediate VII. Nucleophilic attack of the methionine sulfur on this intermediate leads to complete formation of the Met-Tyr-Trp crosslink in KatG (76-77, 80).

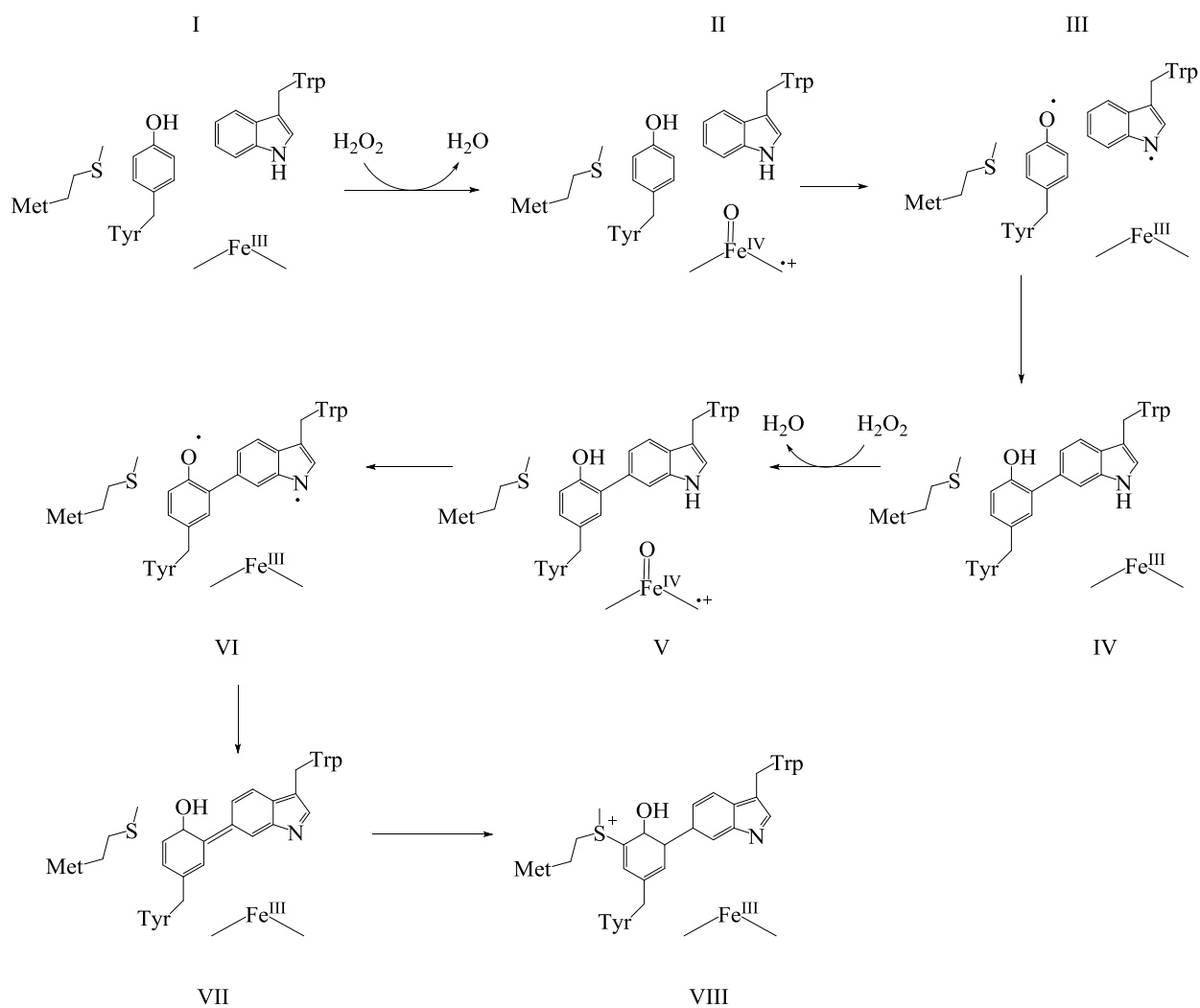


Figure 1.29: Proposed mechanism for the formation of the Met-Tyr-Trp crosslink in KatG (76-77, 80).

1.8.4 Topaquinone (TPQ) in copper amine oxidases

Copper amine oxidases are a group of enzymes that catalyze the two electron oxidation of primary amines to their corresponding aldehydes. These enzymes are widespread in nature and utilize a broad range of substrates including methylamine, ethylamine, benzylamine, phenylethylamine, and histamine (82). Because of the diverse nature of the substrates utilized by these enzymes, the biological functions associated with copper amine oxidases are also diverse (82). In humans for example, diamine oxidase is used in the detoxification of histamine, and in microorganisms, copper amine oxidases have been shown to catalyze the degradation of primary amines, which are used as a source of carbon and nitrogen for growth (70, 83). Copper amine oxidases utilize a mononuclear copper center and an amino acid derived cofactor, 2,4,5-trihydroxyphenylalanine quinone (TPQ) to catalyze the deamination reactions (84). The catalytic cycle consists of a reductive half reaction, in which the amine substrate is oxidized to an aldehyde and the TPQ cofactor is reduced to the aminoquinol form as illustrated in figure 1.30, I. In the oxidative half reaction, the aminoquinol is re-oxidized by dioxygen to TPQ with the release of NH₃ and H₂O₂ (Figure 1.30, II) (70).

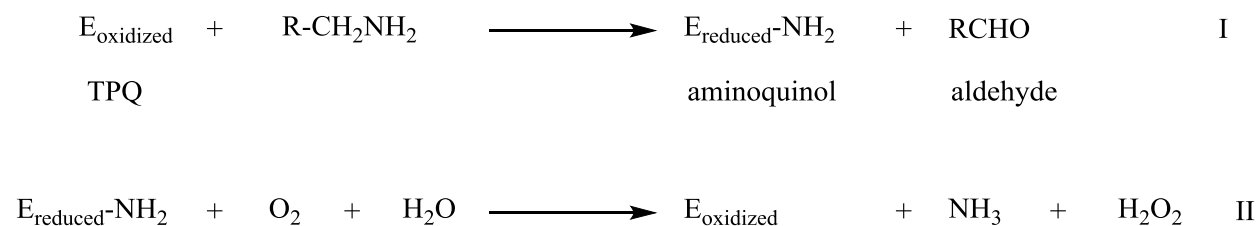


Figure 1.30: Reaction mechanisms of copper amine oxidases showing the reductive (I) and the oxidative (II) reactions (69).

TPQ which is shown in figure 1.31, is synthesized via the post-translational modification of a conserved tyrosine residue in the active site in a process that requires copper and dioxygen (84). In the mechanism for TPQ biogenesis, the catalytic copper is coordinated by three conserved His residues (Fig. 1.32, I) (82). Presence of dioxygen within the active site induces a conformational change in the tyrosine residue to be modified such that the hydroxyl group of that tyrosine becomes oriented towards the copper ion. Deprotonation of this tyrosine followed by electron transfer from the tyrosinate to Cu^{2+} would generate complex II. Activation of dioxygen to superoxide followed by a reaction of the superoxide with the tyrosyl radical would result in the formation of the peroxide intermediate III. Cleavage of the O-O bond would generate the orthoquinone and a hydroxide bound to the Cu^{2+} ion (complex IV). Rotation of the side chain of the modified tyrosine, 180° , would form complex V, in which the hydroxo group is in close proximity and in the proper orientation to be added to the tyrosyl ring forming the reduced form of TPQ, complex VI. This is then oxidized by a second molecule of oxygen to form mature TPQ and H_2O_2 (70).

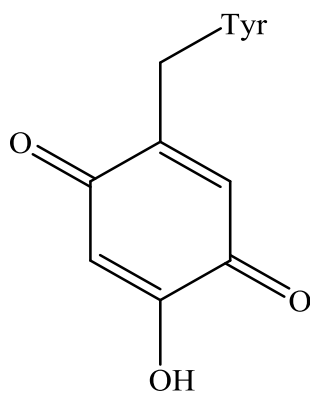


Figure 1.31: 2,4,5-trihydroxyphenylalanine quinone (TPQ) (69).

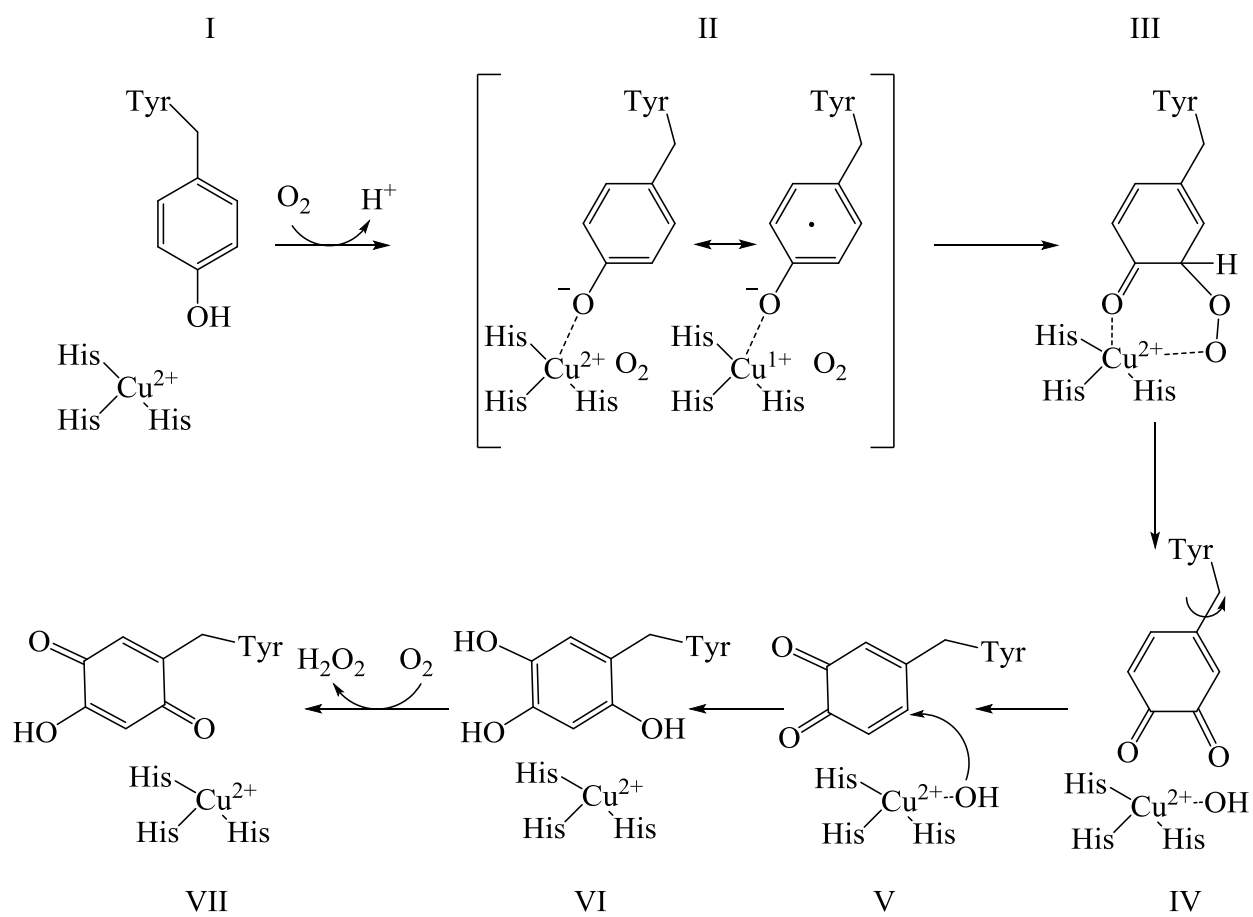


Figure 1.32: Proposed mechanism for TPQ biogenesis (69, 82).

1.8.5 Cysteine-Tyrosine crosslink in galactose oxidase

Galactose oxidase is a copper dependent metalloenzyme that catalyzes the oxidation of primary alcohols to their corresponding aldehydes, coupled with the two electron reduction of dioxygen to hydrogen peroxide, figure 1.33 (85-86).

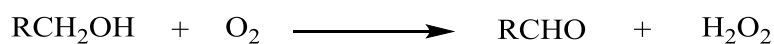


Figure 1.33: Reaction catalyzed by galactose oxidase (86).

The Cu^{2+} ion in the active site of galactose oxidase is in a five-coordinate environment consisting of two His residues (His496 and His581), two Tyr residues (Tyr495 and Tyr272) and an additional water molecule (87-88). An interesting feature about the active site of galactose oxidase is that one of the Cu^{2+} ligands (Tyr272) is covalently linked with the sulfur atom of Cys228. It has been proposed that the crosslink may function in a similar capacity as a disulfide bond in contributing to the overall rigidity of the active site (88). Galactose oxidase exists in three oxidation states; fully oxidized state (Fig. 1.34, I), semireduced state (Fig. 1.34, II), and fully reduced state (Fig. 1.34, III). In its active form, galactose oxidase exists in the fully oxidized form consisting of an oxidized Cu^{2+} center with a tyrosyl radical on the crosslinked tyrosine. The tyrosyl-radical- Cu^{2+} complex has been shown to be considerably stable in the

absence of reductants (89). However, in the presence of a reductant, oxidized galactose oxidase may undergo a single electron reduction to the semi-reduced state which is catalytically inactive. Further reduction would generate the fully reduced form which may potentially react with dioxygen and presents a catalytic intermediate in the catalytic mechanism (88).

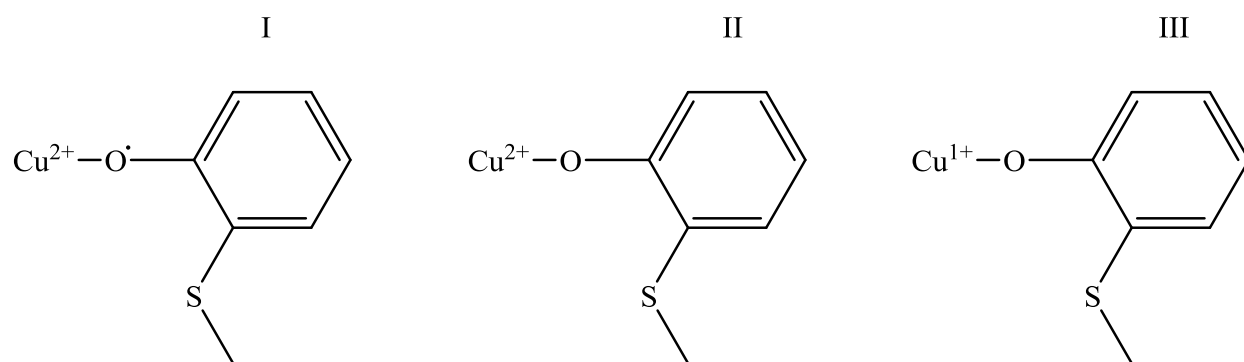


Figure 1.34: Oxidation states of galactose oxidase; fully oxidized (I), semi-reduced (II), and fully reduced (III) forms (88).

The oxidation of an alcohol to an aldehyde and the reduction of dioxygen to hydrogen peroxide is a two electron process that is often facilitated by the presence of redox active cofactors such as flavins and quinones in some enzyme systems. Because galactose oxidase does not contain any organic redox cofactor, the free radical-coupled Cu^{2+} center functions as the redox center. On this basis, the catalytic mechanism of galactose oxidase can be envisioned as two separate oxidation and reduction processes as depicted in figure 1.35. In the first oxidation reaction, the free radical- Cu^{2+} enzyme complex reacts with the primary alcohol to form the two electron reduced enzyme complex and the oxidized aldehyde product. In the second reduction reaction, the reduced Cu^{1+} enzyme complex reacts with dioxygen to form the oxidized free radical- Cu^{2+} enzyme complex and hydrogen peroxide (Fig. 1.35) (86, 88).

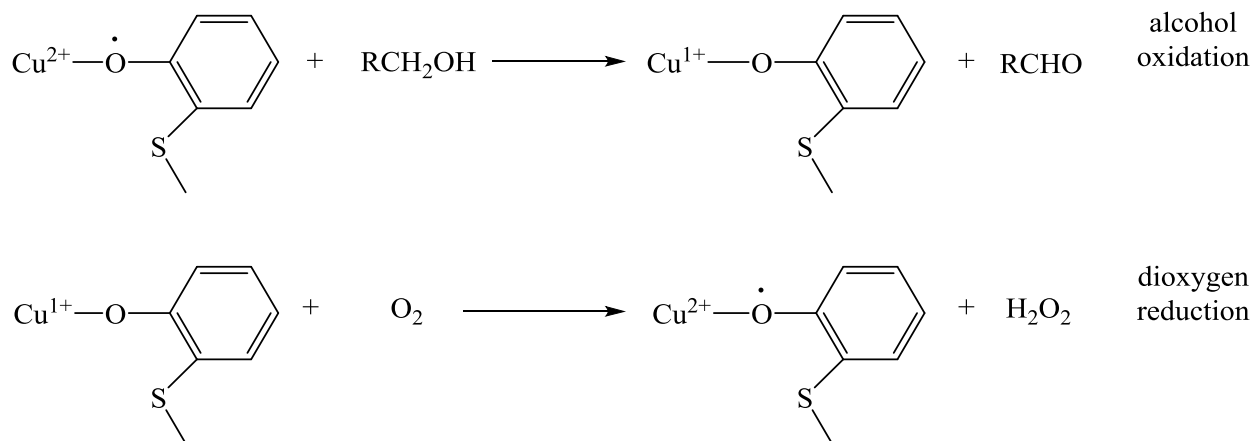


Figure 1.35: Catalytic mechanism of galactose oxidase (88).

Formation of the Cys-Tyr crosslink in galactose requires the presence of copper and dioxygen. However, a recent report has demonstrated that dioxygen may not be strictly required for crosslink formation in galactose oxidase (67, 88). A mechanism that has been proposed for the formation of the Cys-Tyr crosslink in galactose oxidase either under aerobic or anaerobic conditions is illustrated in figure 1.36 (67). This mechanism involves initial deprotonation of Cys228 generating a thiolate which consequently coordinates the active site Cu^{2+} ion (Fig. 1.36 II). This is followed by an electron transfer from the cysteine thiolate to Cu^{2+} forming a thiyl radical and Cu^{1+} (Fig. 1.36, III). Reaction of the thiyl radical with the aromatic ring of Tyr272 results in the formation of a crosslinked radical intermediate, IV. If the reaction takes place under aerobic conditions, two electron reduction of dioxygen to H_2O_2 would convert compound IV to the final crosslinked product complex V' with the oxidation of Cu^{1+} to Cu^{2+} . Under anaerobic conditions, conversion of compound IV to compound V requires the loss of one electron; it is however currently unclear what the final electron acceptor would be under these conditions. Deprotonation of intermediate V would lead to the formation of the Cys-Tyr crosslinked product, VI (67).

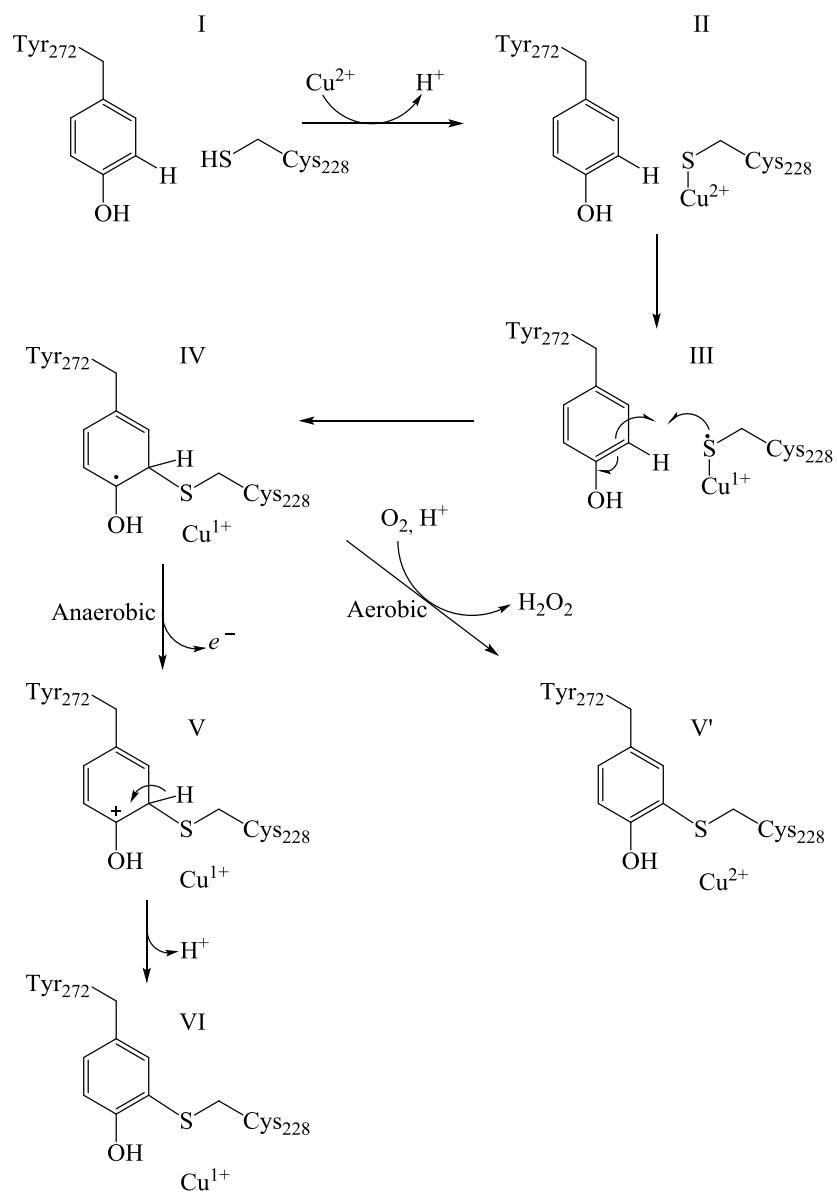


Figure 1.36: Proposed mechanism for aerobic and anaerobic formation of the Cys-Tyr crosslink in galactose oxidase (67).

1.8.6 Cysteine-Tyrosine crosslink in cysteine dioxygenase

As mentioned, cysteine dioxygenase (CDO) is an iron dependent enzyme that catalyzes the oxidation of L-cysteine to form L-cysteine sulfinic acid. The active site of CDO is characterized by an iron center coordinated by three conserved His residues (His86, His88, and His140). In addition to the iron coordinating ligands, CDO also contains several highly conserved amino acid residues within the active site, which include Cys93, Tyr157, Tyr58, Arg60, Ser153, and His155 (2-3). The three-dimensional structures of mammalian CDO have revealed an interesting structural feature within the active site involving a covalent linkage between Cys93 and Tyr157. Such an amino acid crosslink is analogous to the Cys-Tyr crosslink observed in the active site of galactose oxidase. Purified recombinant CDO from mammalian organisms migrates as two bands on SDS-PAGE (Fig. 1.37). To investigate the cause of this unusual migration pattern, Cys93 and Tyr157 (the residues involved in the crosslink) were subjected to mutational analysis. Substitution of Cys93 with Ser (C93S) resulted in a single protein band that corresponded to the slower migrating isoform (upper band) of wild-type CDO. Similarly, substitution of Tyr157 with Phe (Y157F) yielded a variant that migrated as a single band that corresponded to the upper band of wild-type CDO. These studies demonstrated that the slower migrating isoform represents the enzyme population that lacks the Cys-Tyr crosslink, while the faster migrating isoform (lower band) represents the enzyme population that contains the Cys-Tyr crosslink (90). The presence of this crosslink in the active site of CDO has triggered intense research as to why and how it is formed. Some reports have suggested that the Cys-Tyr crosslink increases the catalytic efficiency of CDO but the increased efficiency was compared to variants of CDO lacking the crosslink (90). The involvement of either Cys93 or Tyr157 in the catalytic mechanism was not considered in that study. There have been suggestions that the

Cys93-Tyr157 crosslink may not be catalytically essential as the catalytic activity of the C93S and Y157F CDO variants is not abolished although it is reduced compared to the wild-type enzyme (91). Nonetheless, the function of the Cys-Tyr crosslink within the active site of CDO still remains unclear.

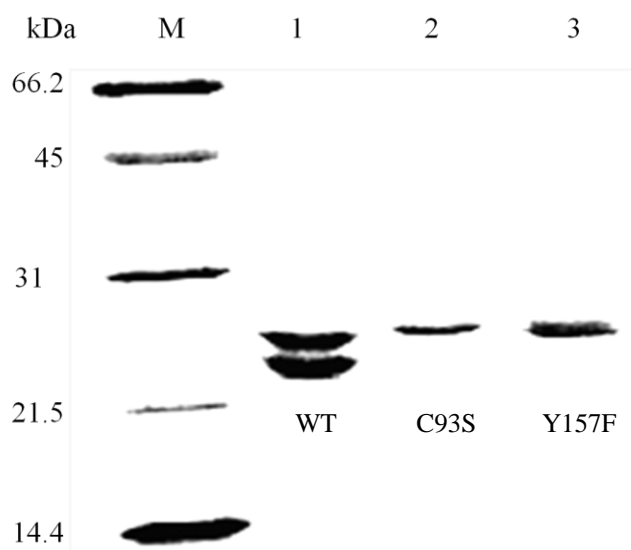


Figure 1.37: SDS-PAGE analysis showing the double band migration pattern of wild-type CDO (Lane 1) and the single upper bands of C93S (Lane 2) and Y157F (Lane 3). M represents the molecular weight marker.

1.9: Summary

Cysteine is one of the primary sulfur containing amino acids with diverse metabolic functions. When incorporated into proteins, cysteine contributes to the overall structural stability of the proteins due to its ability to form disulfide linkages. Because imbalances in the intracellular redox equilibrium arising from oxidative stress can lead to cellular damage, thiol containing proteins form one of the main antioxidant defense mechanisms utilized by cells in protection against the destructive effects caused by oxidative stress. Cysteine is also a major precursor in the biosynthesis of some small molecules such as glutathione and coenzyme A which play important metabolic functions. Glutathione plays a major role in cellular protection against oxidative stress, while coenzyme A (CoA) plays key roles as an acyl group carrier and a carbonyl activating molecule in major biochemical transformations including fatty acid metabolism and tricarboxylic acid cycle (17, 20). Like most other redox active molecules, the concentrations of cysteine are tightly regulated because in the presence of metal ions or when exposed to oxidizing conditions, cysteine can participate in undesirable redox transformations that may be deleterious to the cell. Cysteine dioxygenase (CDO) is the main mechanism utilized by mammalian systems in the regulation of cellular cysteine concentrations.

Sequence and structural analysis classifies CDO as a member of the cupin superfamily. Members of the cupin superfamily have a characteristic β -barrel fold (cupin fold) composed of two conserved cupin sequence motifs and a less conserved intermotif region. The cupin superfamily proteins are metalloproteins and the metal binding site is located at the center of the β -barrel fold. The metal binding ligands in most cupin metalloproteins are comprised of 3-His residues and 1-Glu that derive from the conserved cupin sequence motifs. CDO has two interesting structural features that facilitate its functionality. First, the active site iron is

coordinated by 3-His residues which is a deviation from the 3-His/1-Glu coordination pattern observed in most cupin metalloproteins. The comparative analysis of a typical 3-His/1-Glu active site and a typical 3-His binding site suggests that the two metal binding sites are mechanistically well suited for their respective reactions. The 3-His metal binding site in CDO may actually be an evolutionary advantage to optimize the dioxygenation reaction.

The second structural feature conspicuous within the active site of CDO is a covalent crosslink between Cys93 and Tyr157. This crosslink is not homogenous because a mixture of both the crosslinked and non crosslinked isoforms are present following purification of the enzyme. The crosslinked and the non crosslinked isoforms of CDO have similar physical properties which make it difficult to separate them by chromatographic methods. Previous characterization of CDO has involved a heterogenous mixture of both the crosslinked and non crosslinked isoforms and efforts to separate the two isoforms have not been successful. One of the main focuses of the current study is to evaluate the role played by the Cys-Tyr crosslink in CDO and to evaluate the factors that lead to its biosynthesis. In order to assign function to this crosslink, the two isoforms need to be evaluated independently. The studies presented in this dissertation will initially focus on the separation of the two isoforms. The detailed characterization of the individual isoforms has allowed us to make kinetic and spectroscopic distinctions between the non crosslinked and the crosslinked isoforms and our studies demonstrate the beneficial involvement of the Cys-Tyr crosslink in cysteine oxidation.

The available three-dimensional structures of CDO have revealed the presence of several highly conserved amino acid residues in close proximity to the active site iron. These residues, which include Tyr58 and Arg60, have been proposed from a structural point of view to interact with the bound cysteine substrate. However, adequate experimental evidence that supports the

participation of Tyr58 and Arg60 in catalysis is still lacking. The detailed evaluation of the relevant enzyme-substrate interactions within the active site of CDO during catalysis is presented in the third chapter of this dissertation and it has provided useful insights into how the active site geometry is optimized for its function.

Chapter Two

Shifting Redox States of the Iron Center Partitions CDO between Crosslink Formation or Cysteine Oxidation

2.1 Introduction

Enzymatic oxidation of L-cysteine to L-cysteine sulfinic acid (CSA) is catalyzed by the mononuclear iron-dependent enzyme, cysteine dioxygenase (CDO) (62, 64, 92-93). Both atoms of dioxygen are incorporated in the thiol group of cysteine to generate the cysteine sulfinic acid product (94). The product of this reaction is a branchpoint in the biosynthesis of pyruvate and sulfate or taurine (5).

Cysteine dioxygenase is a member of the cupin superfamily. Proteins within the cupin superfamily have a low overall sequence similarity, but they share a common β -barrel fold known as the cupin fold. Members of the cupin superfamily also share two partially conserved cupin motifs, GX₅HXHX₃₋₆EX₆G (motif 1) and GX₅₋₇PXGX₂HX₃N (motif 2) (39). The two His and Glu residues from motif 1 and His from motif 2 coordinate the active site metal in most proteins within the cupin superfamily. For CDO, the conserved Glu residue in motif 1 has been replaced with a cysteine leaving only 3-His residues to coordinate the active site iron. In addition to the unique metal coordination environment, CDO also possesses a rare crosslink involving Cys93 and Tyr157 (residues numbered according to mammalian CDO enzymes) (1-3, 95).

Several studies have been conducted to evaluate the role of the crosslink in cysteine oxidation. Purified recombinant CDO from mammalian systems migrates as two bands when

resolved on SDS-PAGE. This anomalous migration pattern has been observed in several other proteins including galactose oxidase, glyoxal oxidase, and *Mycobacterium tuberculosis* sulfite reductase (NirA), all of which contain a Cys-Tyr crosslink (67, 96-97). Mutational studies and mass spectrometric analysis have identified the faster migrating species as the isoform that contains the Cys-Tyr crosslink and the slower migrating species as the isoform that lacks the crosslink (90, 98). The kinetic and spectroscopic properties of CDO that have been reported so far have involved a heterogenous mixture of the crosslinked and non crosslinked CDO isoforms. In an effort to generate the homogenously crosslinked isoform, the heterogenous mixture of crosslinked and non crosslinked CDO isoforms was incubated with cysteine and ferrous iron under aerobic conditions (90). Crosslinked CDO once formed was shown to possess increased activity several fold over variants of CDO lacking the Cys93-Tyr157 crosslink; however, the crosslink was not absolutely required for activity (90). In a separate study, a 1:3 ratio of crosslinked to non crosslinked CDO was generated through anaerobic protein expression and separation by column chromatography (99). The activity assays showed a slow phase associated with the generation of the crosslink followed by a faster phase that correlated with increased activity due to the accumulation of crosslink. The biphasic trace was thought to be associated with an uncharacterized intermediate generated during crosslink formation and enzyme activation (99). Results from recent spectroscopic and computational studies support a role for the crosslink in stabilizing the substrate-bound enzyme (100). Attempts to obtain the fully non crosslinked isoform of CDO have been unsuccessful; all of the previous studies to evaluate the role of crosslink formation have been performed with recombinant enzyme that contains a significant amount of the crosslinked isoform (90, 99). Therefore, the non crosslinked and the crosslinked CDO isoforms have been difficult to evaluate independently as both species are

present following purification of the recombinant enzyme. The current study presents a protocol for expressing the homogenously non crosslinked form of CDO using a cell permeable metal chelator. The ability to obtain homogenously non crosslinked CDO provides a more thorough investigation of the role of the crosslink in catalysis. Kinetic and spectroscopic comparisons of the non crosslinked and crosslinked isoforms of CDO demonstrate a distinct mechanistic role for the Cys93-Tyr157 crosslink in the active site of CDO. Herein, we propose a substrate activation mechanism in which CDO utilizes the ferric iron to activate cysteine for reaction with dioxygen. These studies provide a new perspective on the redox state of the active site iron in Cys-Tyr crosslink formation and the mechanism of cysteine oxidation.

2.2 Materials and methods

2.2.1 Materials

4-(2-Hydroxyethyl)piperazine-1-ethanesulfonic acid (HEPES), L-cysteine, L-ascorbate, 1,10-phenanthroline, ammonium sulfate, ampicillin, streptomycin sulfate, lysozyme, sodium dithionite, potassium chloride (KCl), isopropyl- β -D-thiogalactoside (IPTG), and brilliant blue R were purchased from Sigma (St. Louis, MO). Sodium dodecyl sulfate (SDS) was purchased from Biorad (Hercules, CA). Glycerol and sodium chloride were purchased from Macron Fine Chemicals (Center valley, PA). Pfu Turbo DNA polymerase was purchased from Agilent (La Jolla, CA). Oligonucleotide primers were purchased from Invitrogen (Carlsbad, CA). Phenyl SepharoseTM 6 Fast Flow (high sub) was purchased from GE Healthcare Biosciences, (Uppsala, Sweden). Amicon Ultrafree-MC Centrifugal Filter Devices (10 kDa MWCO) and Amicon Ultra-4 Centrifugal Filter Devices (10 kDa MWCO) were purchased from Millipore (Billerica, MA). Difco-brand Luria-Bertani (LB) media was purchased from Becton, Dickinson and company (Sparks, MD).

2.2.2 Expression and purification of C93S, Y157F, and wild-type CDO

The cDNA gene for rat CDO was cloned into the pET21a expression vector, and used to generate C93S CDO as previously described (101). Primers for the Y157F CDO variant were designed as 29 base oligonucleotides replacing the wild-type Tyr codon with TTT. The Tyr to Phe substitution was confirmed by DNA sequence analysis. The respective plasmid was transformed into *E. coli* BL21 (DE3) competent cells for protein expression and stored as glycerol stocks at -80°C. Expression and purification of the wild-type and variants of CDO were carried out as previously described with minor modifications (101). The cell pellet was resuspended with 25 mM HEPES, pH 7.5, and 10% glycerol (v/v) supplemented with 2 μ g/mL

lysozyme. The supernatant following the nucleic acid precipitation step was supplemented with 20% ammonium sulfate (w/v) and applied onto a Phenyl SepharoseTM 6 Fast Flow column. Protein was eluted using a linear gradient from 20-15% ammonium sulfate in 25 mM HEPES buffer, pH 7.5 and 10% glycerol. Pure protein fractions were pooled and concentrated by precipitation in 70% ammonium sulfate. The protein pellet was resuspended in the desired volume of 25 mM HEPES buffer, pH 7.5, 100 mM NaCl, and 10% glycerol. The iron loading and dialysis steps were carried out as previously reported (101). Protein samples were divided into 500 μ L aliquots, flash frozen in liquid nitrogen and stored at -80°C.

2.2.3 Expression and purification of non crosslinked CDO

E. coli strain BL21 (DE3) containing the wild-type CDO plasmid were grown in Luria-Bertani broth containing 0.1 mg/mL ampicillin with vigorous shaking at 37 °C. When the culture reached an A_{600} of 0.6-0.8, 1,10-phenanthroline (100 mM dissolved in 100 mM HCl) was added to a final concentration of 100 μ M (102). The culture was allowed to grow for an additional 15 minutes after which the expression of CDO was induced with 0.4 mM IPTG. The culture was incubated at 22 °C for an additional 6 hours.

Cells were harvested by centrifugation at 5000 rpm at 4 °C and the cell paste was resuspended in 100 mL of 25 mM HEPES, pH 7.5, and 10% glycerol supplemented with 2 μ g/mL lysozyme. The cell slurry was lysed by sonication followed by centrifugation at 10 000 rpm at 4 °C for 20 min. Streptomycin sulfate (1.5% w/v) was added to the resulting supernatant to precipitate nucleic acids and the solution was stirred for 1 h at 4 °C. The precipitated nucleic acids were removed by centrifugation at 10 000 rpm at 4 °C for 20 min. Ammonium sulfate (20% w/v) was added to the supernatant and the solution was stirred briefly in the cold room prior to loading onto a Phenyl SepharoseTM Fast Flow column equilibrated in 25 mM HEPES

buffer, pH 7.5, 20% ammonium sulfate, and 10% glycerol. Following a column wash, the protein was eluted using a linear gradient of 20-15% ammonium sulfate in 25 mM HEPES, pH 7.5, and 10% glycerol. The purest fractions as assessed by SDS-PAGE were pooled and concentrated by precipitating with 70% ammonium sulfate. The pellet was resuspended in the desired volume of 25 mM HEPES, pH 7.5, 100 mM NaCl and 10% glycerol. The resulting solution was dialyzed twice against 2 L of the resuspension buffer to remove residual 1,10-phenanthroline, and the protein concentration determined by UV-visible absorption spectroscopy at 280 nm using a molar extinction coefficient of $25\,440\text{ M}^{-1}\text{cm}^{-1}$ (101). The purified CDO enzyme was iron reconstituted with a molar ratio of 1.2:1 ferrous ammonium sulfate to protein, and dialyzed twice against one liter of 25 mM HEPES, pH 7.5, 100 mM NaCl and 10% glycerol. Aliquots of the protein samples were flash frozen in liquid nitrogen and stored at $-80\text{ }^{\circ}\text{C}$. For clarity, the enzyme isoform lacking the crosslink will be referred to as non crosslinked CDO, and the enzyme isoform with the C93-Tyr157 crosslink will be referred to as crosslinked CDO.

2.2.4 *Quantitation of iron*

The total iron content in all enzyme preparations was determined using inductively-coupled plasma-atomic emission spectroscopy (ICP-AES). Samples of CDO (10 μM) prepared in 25 mM HEPES, pH 7.5 at a final volume of 600 μL were analyzed using a Perkin-Elmer Optima 7300 DV ICP-AES (Perkin-Elmer Life Sciences, Fremont, CA). Commercial iron standards for ICP-AES were used to generate the standard curve and the concentration of iron in each of the prepared protein samples relative to the protein concentration was determined. Distilled and deionized water and 25 mM HEPES buffer, pH 7.5 were used as controls. The results are an average of three separate experiments.

2.2.5 *Correlating crosslink formation with non crosslinked CDO activity*

The specific activity of non crosslinked CDO enzyme was measured by the rate of dioxygen utilization with a Clark-type oxygen electrode (Hansatech, Inc., Norfolk, United Kingdom). The reactions consisted of 2 μ M CDO and 1 mM ascorbic acid in 25 mM HEPES buffer, pH 7.5. Reactions were initiated by the addition of varying concentrations of cysteine (0-100 mM) to the reaction mixture in a final volume of 1 mL. Reactions monitored the decrease in the concentration of dioxygen in the reaction chamber over a period of 10 minutes after which one of the substrates became limiting and the kinetic traces leveled off. Samples used in the kinetic investigations were immediately ultrafiltered using Amicon Ultrafree-MC centrifugal filter devices (10 kDa MWCO). Protein samples retained in the filtration devices were further analyzed for crosslink formation by SDS-PAGE.

2.2.6 *Generation of homogenously crosslinked form of CDO*

The crosslinked form of CDO was generated by incubating non crosslinked CDO (5 μ M) in the presence of 100 mM cysteine and 25 mM HEPES buffer, pH 7.5 to a final volume of 500 μ L. The reactions were incubated at 37 °C for a period of 15 minutes with moderate shaking at 100 rpm after which all the reactions were combined and ultrafiltered using Amicon Ultra-4 Centrifugal Filter Units (10 kDa MWCO). The flow through was discarded and the protein samples retained in the filtration devices were washed three times with 25 mM HEPES buffer, pH 7.5 and 10% glycerol. Complete formation of the crosslinked enzyme was confirmed by SDS-PAGE and the crosslinked protein was assayed for activity and used in EPR analysis.

2.2.7 *Steady-state kinetic analyses of homogenously crosslinked CDO*

Steady-state kinetic investigations of homogenously crosslinked CDO were determined using an oxygen electrode where the rate of dioxygen utilization was monitored. The standard

assay contained 1 μM crosslinked CDO protein incubated in the presence and in the absence of 1 mM ascorbate in 25 mM HEPES buffer, pH 7.5 at 37 °C. Reactions were initiated by the addition of cysteine (10 μM -10 mM). Initial velocities were obtained within the first 10 s of the reaction and plotted against substrate concentration. The steady-state kinetic parameters of wild-type, C93S, and Y157F CDO proteins were determined using 2 μM protein in the presence of 1 mM ascorbate. The data were fit to the Michaelis-Menten equation using KaleidaGraphTM software to obtain the steady-state kinetic parameters which were calculated as the average of three separate experiments.

2.2.8 *Analysis of the cysteine sulfinic acid product*

The rate of dioxygen consumption was correlated with the rate of cysteine sulfinic acid (CSA) formation using LC-MS. The reaction conditions for dioxygen utilization were similar to the steady-state kinetic experiments. Samples were analyzed for the concentration of dioxygen consumed within one minute, and the reactions were terminated by the addition of 1 μL of formic acid (90% v/v). Mass analysis was performed using an Ultra Performance LC System (ACQUITY, Waters Corp., Milford, MA, USA) coupled with a quadrupole time-of-flight mass spectrometer (Q-ToF Premier, Waters) with electrospray ionization (ESI) in ESI⁺-MS mode. Each sample was initially applied to a C18 column (ACQUITY UPLC® BEH C18, 1.7 μm , 2.1 x 50 mm, Waters) for separation with a linear gradient prior to mass analysis. Solution A contained 5% acetonitrile and 0.1% formic acid, and solution B contained 95% acetonitrile and 0.1% formic acid. After a 10 min wash with 95% solution A, the applied samples were separated with a linear gradient of 95% A to 5% A over 6 min (flow rate 150 $\mu\text{L}/\text{min}$). Ions of interest were analyzed for mass accuracy and elemental composition and the respective ions were quantified by computing the intensity of the chromatograms. The concentration of CSA formed was

determined by comparison to a standard curve constructed with known quantities of CSA (10 μ M-5 mM). All the values obtained are an average of three separate experiments.

2.2.9 EPR spectroscopy

Electron paramagnetic resonance (EPR) spectra at X-band frequency (9.38 GHz) were recorded on a Bruker EMX spectrometer (Bruker Biospin Corporation, Billerica, MA). Cooling was performed with an Oxford Instruments ESR 900 flow cryostat and an ITC4 temperature controller. Samples were prepared for EPR analysis by diluting respective protein samples to a final concentration of 80-100 μ M in 25 mM HEPES buffer, pH 7.5, 100 mM NaCl, and 10% glycerol in a final volume of 300 μ L. For samples where cysteine was included, 10 mM cysteine was added to diluted protein samples in a final volume of 300 μ L. For anaerobic studies, protein samples were first prepared in crimp top vials and sealed with an aluminum cover with a rubber septum. The protein was deoxygenated with 20 min of alternate vacuuming and equilibration with high purity argon on an ice slurry. The samples were then transferred into a glovebox maintained under an atmosphere of 95% nitrogen gas and 5% hydrogen gas. Deoxygenated buffer was used to prepare samples for EPR measurements prior to being transferred to an EPR tube. All spectra were recorded using the following instrument settings: microwave frequency, 9.38 GHz; microwave power, 1.99 mW; receiver gain, 2×10^4 ; modulation frequency, 100 kHz; modulation amplitude, 6 G; time constant, 327.68 ms; sweep time, 335.5 s. The EPR spectra were recorded as the sum of two accumulations and were normalized by subtracting the spectrum of buffer used to prepare the samples. Spin quantitation was performed using 10 mM copper perchlorate as the standard (10 mM CuSO_4 , 2 mM NaClO_4 , 10 mM HCl) and the concentration of iron was calculated relative to the amount of iron bound as determined by ICP-AES.

2.3 Results

2.3.1 Preparation of homogenously non crosslinked CDO

The similar physical properties between the crosslinked and non crosslinked isoforms of CDO make it difficult to isolate each isoform for independent study. Prior attempts to obtain the homogenous isoforms have proven unsuccessful. In order to understand the role of the crosslink in the active site of CDO, a procedure for isolating the homogenously non crosslinked form of CDO was developed which required that the enzyme was not exposed to free iron during the expression and purification processes. This method involved addition of 1, 10-phenanthroline to the cell culture shortly before inducing the cells for protein expression (102). The purified CDO enzyme resolved as a single band on SDS-PAGE, which correlated with the slower migrating isoform in CDO that lacks the Cys93-Tyr157 crosslink (Fig. 2.1). The catalytic activity of CDO depends on the availability of iron bound in the active site. The amount of iron in non crosslinked CDO samples was < 0.1% following purification. It was therefore necessary to reconstitute purified non crosslinked CDO with iron. Ferrous ammonium sulfate was added to the purified non crosslinked enzyme in a 1.2:1 (Fe:protein) molar ratio. The iron loaded protein was then dialyzed twice against an iron free buffer to remove any unbound iron. Results from ICP-AES experiments revealed that the iron reconstituted purified non crosslinked CDO isoform contained ~50% iron. The amount of bound iron in non crosslinked CDO was similar to the amount of bound iron in CDO containing both isoforms.

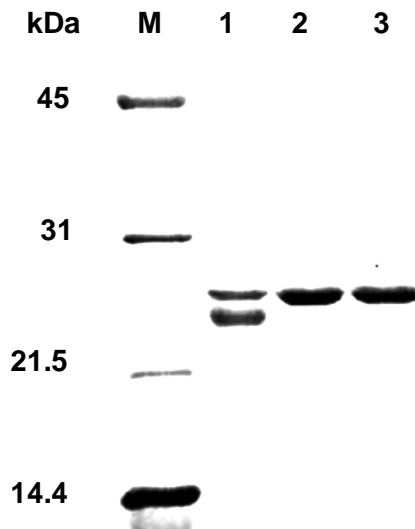


Figure 2.1: Analysis of non crosslinked and wild-type CDO by SDS-PAGE. (M) Molecular weight marker, (1) Purified wild-type CDO, (2) Purified non crosslinked CDO reconstituted with iron, (3) Purified iron free non crosslinked CDO. Acrylamide gels (12%) were run with samples pretreated by boiling for 3 min in sample buffer containing 2% SDS and 5% 2-mercaptoethanol.

2.3.2 Activity of non crosslinked CDO

Enzymatic activity of the non crosslinked CDO isoform was investigated using a Clark-type oxygen electrode and the rate of dioxygen consumption at varying cysteine concentrations (0-100 mM) was monitored. The concentration of dioxygen in the reaction chamber was recorded as a function of time (Fig. 2.2). Interestingly, at relatively high cysteine concentrations (> 20 mM) the rate of dioxygen consumption occurred in two phases. A slow phase was observed within the first two minutes of the reaction and a fast phase was observed after approximately five minutes. Protein samples from the activity assays analyzed on SDS-PAGE showed an observable increase in the amount of crosslink formed with increasing cysteine concentration (Fig. 2.3). At 100 mM cysteine, the homogenously non crosslinked CDO isoform in the reaction had been converted to the homogenously crosslinked isoform in less than ten minutes. The initial slow phase corresponded with the utilization of dioxygen during formation of the crosslink, and the second fast phase represented oxidation of the cysteine substrate by CDO. Similar results were observed with CDO containing both isoforms (data not shown). ICP-AES experiments were performed to investigate the amount of iron present following formation of the crosslinked CDO isoform. Homogenously crosslinked CDO contained $48 \pm 1.9\%$ iron suggesting that complete conversion to the non crosslinked isoform occurred with substoichiometric amounts of iron. However, iron was required for crosslink formation as non crosslinked CDO that had not been reconstituted with iron was unable to form the crosslink.

2.3.3 Steady-state kinetic parameters of crosslinked CDO

Following the observation that formation of the Cys93-Tyr157 crosslink correlated with increased catalytic activity of CDO, the steady-state kinetic parameters of the homogeneously crosslinked enzyme were evaluated. Crosslinked CDO was generated by incubating samples containing non crosslinked CDO with 100 mM cysteine. SDS-PAGE analysis confirmed the formation of the crosslink in the prepared protein samples. Enzymatic activity of the crosslinked CDO enzyme was determined by monitoring the rate of dioxygen utilization in the absence and in the presence of 1 mM ascorbate at pH 7.5 (Fig.2.4). Including an external reductant in kinetic investigations of CDO containing both isoforms improved the catalytic activity of the enzyme(101). However, crosslinked CDO was active even in the absence of an external reductant (Table 2.1). Similar results were obtained with crosslinked CDO formed from CDO containing both isoforms. Therefore the external reductant was only necessary when both crosslinked and non crosslinked CDO isoforms were present. The kinetic parameters were corrected for the amount of iron bound and the k_{cat}/K_m value in the absence of ascorbate was $10882 \pm 276 \text{ mM}^{-1} \cdot \text{min}^{-1}$, which is an ~40-fold increase compared to the k_{cat}/K_m value previously reported for CDO containing both isoforms with the addition of ascorbate to the reaction. We were unable to obtain accurate kinetic parameters for non crosslinked CDO as the reaction is partitioned between crosslink formation and cysteine oxidation.

The reaction catalyzed by CDO requires that one equivalent of molecular oxygen reacts with cysteine to generate cysteine sulfinic acid (CSA). Samples analyzed for dioxygen utilization were also analyzed for CSA production by mass spectrometry to confirm that the concentration of dioxygen consumed was coupled with CSA formation. The specific activity of crosslinked CDO enzyme was $5043 \pm 241 \text{ nmol of dioxygen consumed min}^{-1} \cdot \text{mg}^{-1}$ of enzyme which

corresponded with the production of 4783 ± 798 nmol of CSA $\text{min}^{-1} \cdot \text{mg}^{-1}$ of enzyme (Table 2.2). The ~1:1 ratio for the coupling of dioxygen utilization and CSA product formation suggest that the increased activity observed for crosslinked CDO is due to oxidation of the cysteine substrate. Similar specific activities for dioxygen utilization and CSA production were also observed for CDO containing both isoforms, but the overall values were lower than those obtained for crosslinked CDO (Table 2.2).

2.3.4 Contribution of Cys93 and Tyr157 residues to the catalytic activity of CDO

In order to further evaluate the role of the crosslink in cysteine substrate oxidation, steady-state kinetic investigations were performed with the Cys93 and Tyr157 CDO variants for comparison with crosslinked CDO and CDO containing both isoforms. Substitution of Cys93 to serine and Tyr157 to phenylalanine yielded one isoform of CDO, which correlated with non crosslinked CDO when analyzed by SDS-PAGE. The C93S CDO variant contained $39 \pm 1\%$ iron bound similar to wild-type CDO, while Y157F CDO contained lower levels of iron bound at $23 \pm 1\%$. The kinetic parameters for C93S and Y157F CDO were corrected for the amount of iron bound (Table 3.3). The C93S CDO enzyme still possessed activity although the k_{cat}/K_m value was ~5-fold lower than CDO containing both isoforms, and 27-fold lower than crosslinked CDO in the absence of ascorbate. A comparable decrease in the k_{cat}/K_m value was also observed for the Y157F CDO variant with an ~3.5-fold decrease in the k_{cat}/K_m value compared to CDO containing both isoforms and a 19-fold reduction in the k_{cat}/K_m value compared to crosslinked CDO.

2.3.5 EPR analysis of non crosslinked and crosslinked CDO

The coordinated iron in the resting form of CDO containing both isoforms was previously shown to exist in the high spin ferric state with an EPR signal observed at $g = 4.3$ (101). The addition of cysteine to oxidized CDO leads to an increase in the signal intensity, and

was attributed to the formation of cysteine-bound Fe(III)-CDO (91). Interestingly, the redox state of the iron in non crosslinked CDO was found to exist primarily in the EPR-silent ferrous form as there was no observable EPR signal (Fig. 2.5, black trace). Addition of cysteine under aerobic conditions resulted in an increase in intensity in the EPR signal at $g = 4.3$ arising from a high spin ferric iron ($S = 5/2$) (Fig. 2.5, red trace). The change in the observed spectrum suggests that the ferrous iron is oxidized to the ferric form through formation of the crosslink and/or cysteine oxidation as catalysis could still occur in the presence of dioxygen. Analysis of crosslinked CDO revealed a sharp EPR signal at $g = 4.3$ arising from an $S = 5/2$ spin system (Fig. 2.6, black trace). This signal was assigned to high spin ferric iron bound in the active site of crosslinked CDO. Results from double integration of the EPR signal suggested that the concentration of the high-spin ferric species accounted for more than 90% of the total iron. Contrary to what is observed for CDO containing both isoforms, addition of cysteine under aerobic conditions did not lead to significant changes in the signal intensity. The EPR signal intensity at $g = 4.3$ for crosslinked CDO in the presence of cysteine was also observed under anaerobic conditions. The results suggest that the increase in the signal intensity observed with the addition of cysteine in CDO containing both isoforms may be due to formation of the crosslink.

Table 2.1: Steady-state kinetic parameters of crosslinked and wild-type CDO^a

	crosslinked CDO		wild-type CDO ^b
	(+) ascorbate	(-) ascorbate	(+) ascorbate
k_{cat} (min^{-1})	1697 ± 39	2449 ± 3.5	128 ± 4
K_{m} (mM)	0.22 ± 0.02	0.23 ± 0.01	0.06 ± 0.01
$k_{\text{cat}}/K_{\text{m}}$ ($\text{mM}^{-1}\text{min}^{-1}$)	7714 ± 656	10882 ± 276	1995 ± 324

^a The reported kinetic parameters were adjusted for iron content.

^b Wild-type CDO containing non crosslinked and crosslinked isoforms.

Table 2.2: Specific activity of dioxygen utilization and cysteine sulfinic acid production of crosslinked and wild-type CDO

	dioxygen utilization (nmol/min/mg)	cysteine sulfinic acid production (nmol/min/mg)
Crosslinked CDO	5043 ± 242.1	4783 ± 798.3
Wild-type CDO ^a	1007 ± 50	1200 ± 15

^a Wild-type CDO containing non crosslinked and crosslinked isoforms.

Table 2.3: Steady-state kinetic parameters and percent iron content of wild-type, C93S, and Y157F CDO^a

	k_{cat} (min^{-1})	K_{m} (mM)	$k_{\text{cat}}/K_{\text{m}}$ ($\text{mM}^{-1} \cdot \text{min}^{-1}$)	% iron bound
wild-type CDO ^b	128 ± 5.6	0.064 ± 0.010	1995 ± 324	$39 \pm 1\%$
C93S CDO	45.9 ± 2.4	0.12 ± 0.02	399 ± 89	$39 \pm 2\%$
Y157F CDO	28.7 ± 1.5	0.053 ± 0.005	574 ± 64	$23 \pm 1\%$

^a The reported kinetic parameters were adjusted for iron content.

^b Wild-type CDO containing non crosslinked and crosslinked isoforms.

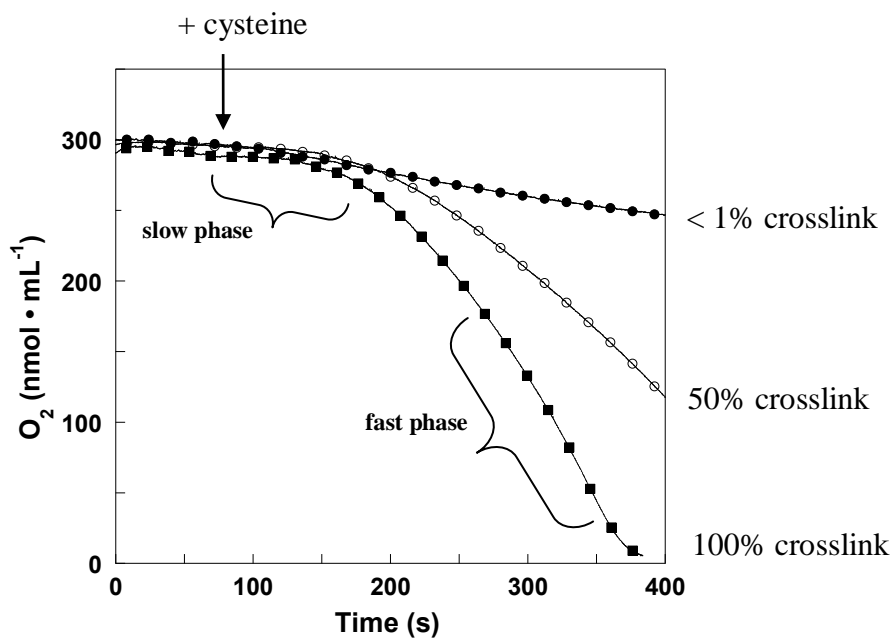


Figure 2.2: Dioxygen utilization of non crosslinked CDO. The plot represents the decrease in dioxygen concentration with time at different cysteine concentrations. The slow phase and fast phase of the reactions have been highlighted in the graph. The kinetic traces show dioxygen utilization at 1 mM (●), 40 mM (○), and 100 mM (■) cysteine. Reaction mixtures contained CDO (2 μM) and ascorbate (1 mM) in 25 mM HEPES, pH 7.5 at 37 °C. Assays were initiated by the addition of a range of cysteine concentrations (0-100 mM).

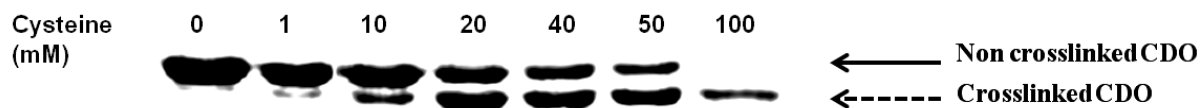


Figure 2.3: Analysis of crosslink formation during catalysis by SDS-PAGE. Protein samples used in the activity analysis of the non crosslinked CDO enzyme were ultrafiltered with Amicon Ultrafree-MC centrifugal filter devices (10 kDa MWCO). Acrylamide gels (12%) were run with samples pretreated by boiling for 3 min in sample buffer containing 2% SDS and 5% 2-mercaptoethanol.

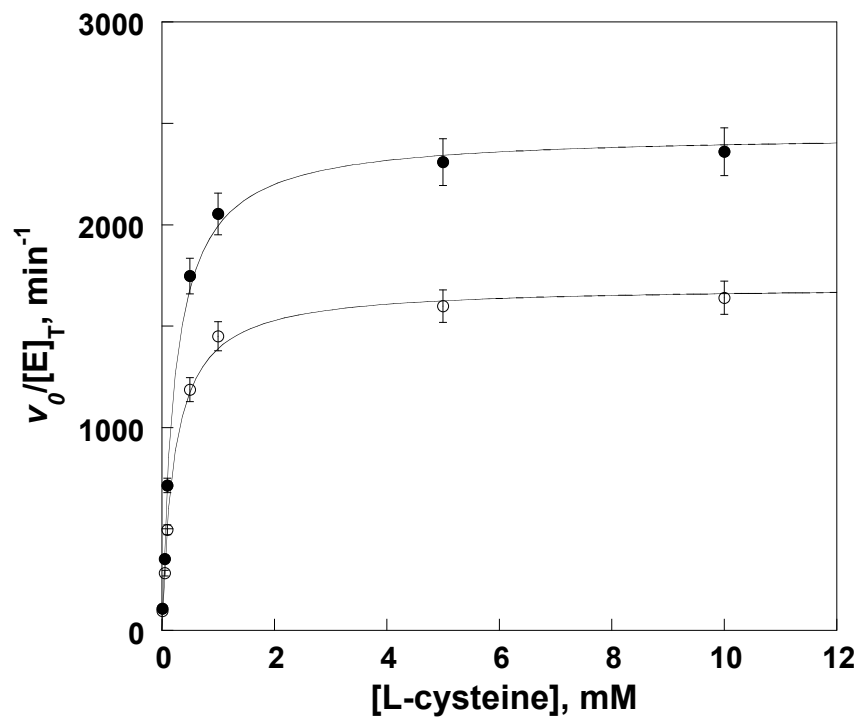


Figure 2.4: Steady-state kinetic traces of crosslinked CDO enzyme. The steady-state kinetic traces were obtained by measuring the consumption of dioxygen with a Clark-type oxygen electrode. Reaction mixtures contained CDO (1 μM) in 25 mM HEPES, pH 7.5 at 37 $^\circ\text{C}$ in the absence (●) and presence (○) of ascorbate (1 mM). Assays were initiated by the addition of a range of cysteine concentrations (10 μM -10 mM). Each point is the average of at least three separate experiments.

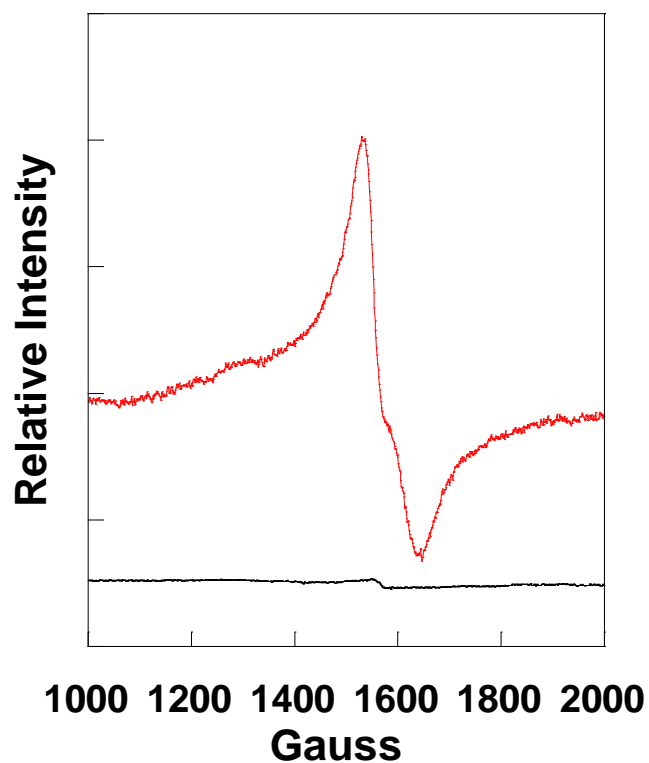


Figure 2.5: X-band EPR spectra of non crosslinked CDO. non crosslinked CDO (—); non crosslinked CDO with 10 mM cysteine added under aerobic conditions (—). Spectra were taken with 100 μ M protein in 25 mM HEPES buffer, pH 7.5, 100 mM NaCl, and 10% glycerol. All spectra were recorded at 9.38 GHz, with a field modulation frequency of 100 kHz and modulation amplitude of 6 G. All spectra were recorded at 8-10 K.

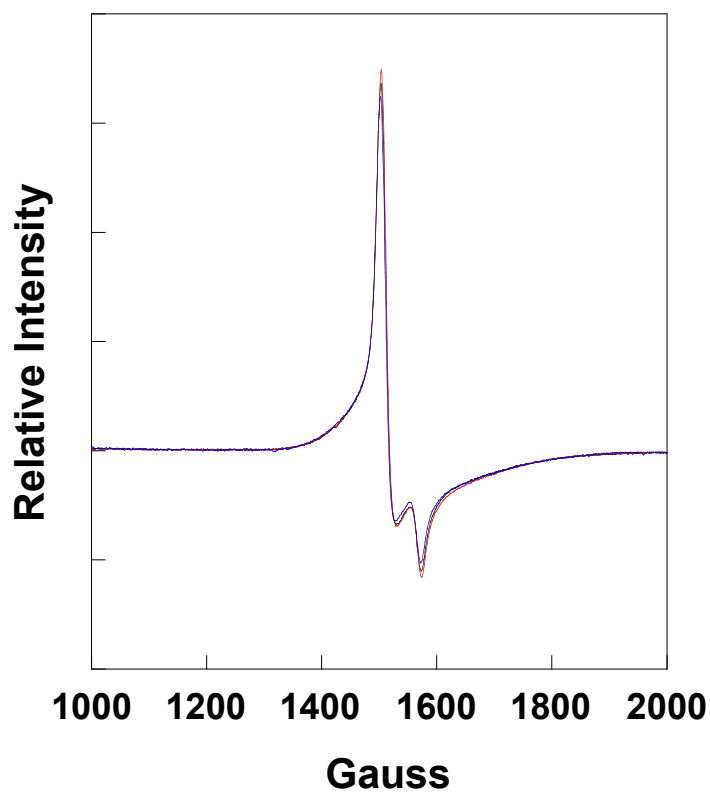


Figure 2.6: X-band EPR spectra of crosslinked CDO samples. crosslinked CDO (—); crosslinked CDO with 10 mM cysteine added under aerobic conditions (—); crosslinked CDO with 10 mM cysteine added under anaerobic conditions (—). Spectra were taken with ~80 μ M protein in 25 mM HEPES buffer, pH 7.5, 100 mM NaCl, and 10% glycerol. All spectra were recorded at 9.38 GHz, with a field modulation frequency of 100 kHz and modulation amplitude of 6 G. All spectra were recorded at 8-10 K.

2.4 Discussion

Prior to this study, probes to evaluate the role of the Cys93-Tyr157 crosslink in CDO have involved the comparative analysis of variants of CDO unable to form the crosslink and CDO containing a heterogenous mixture of both the crosslinked and non crosslinked CDO isoforms. Experiments to separate the crosslinked and non crosslinked isoforms of CDO have been marginally successful. Consistent with previous results, substitution of Cys93 to serine and Tyr157 to phenylalanine diminished but did not abolish the catalytic activity of CDO (1, 90). Evaluating the role of the crosslink through substitution of the amino acids involved in crosslink formation could be problematic since these residues are located in the active site and likely play an integral role in the catalytic mechanism of CDO. To fully characterize the crosslinked and non crosslinked isoforms, the two isoforms needed to be evaluated independently. It was previously reported that formation of the crosslink in CDO requires the presence of ferrous iron, L-cysteine, and dioxygen (90). Because iron is required for crosslink formation, the Fe²⁺-chelator 1, 10-phenanthroline was added to the cell culture shortly before induction. SDS-PAGE analysis of the purified protein revealed the presence of a single isoform of CDO correlating with protein lacking the crosslink. This is the first time that CDO devoid of the Cys93-Tyr157 crosslink has been isolated and purified to homogeneity. Reconstitution of the apo non crosslinked enzyme with ferrous iron yielded a protein with ~50 % iron, which is comparable to the value obtained for CDO containing both isoforms. The amount of iron bound in the active site of CDO ranges from 10–68 %, which implies that the 3-His binding site does not bind iron as tightly as the 3-His/1-carboxylate binding site present in some cupin metalloproteins (1, 63).

There was no EPR signal observed for purified non crosslinked CDO suggesting that non crosslinked CDO stabilizes the ferrous redox state. With the addition of cysteine, the EPR

spectrum gave a sharp signal at $g = 4.3$ indicative of high spin ferric iron. The EPR studies were performed in the presence of both cysteine and dioxygen leading to the oxidation of the iron center. The iron center of CDO containing both isoforms was previously shown to exist in the high-spin ferric state, and a sharp EPR signal was observed with the addition of cysteine. The increase in the signal intensity was associated with cysteine coordinating to the metal center (91). The change in the EPR signal may suggest direct coordination of the substrate to the active site iron or a structural rearrangement of the active site either due to substrate binding or the presence of the crosslink. Taken together, the non crosslinked CDO enzyme stabilizes the ferrous redox state, but the iron is oxidized to Fe^{3+} upon exposure to cysteine and dioxygen during crosslink formation. The requirement that reduced iron is needed for crosslink formation, may explain why CDO containing both isoforms purified in the ferric redox state requires ascorbate in the reaction (101).

Oxygen electrode measurements revealed an unusual biphasic activity at relatively high concentrations of cysteine, which was associated with two chemical events taking place. The rate of the two phases was dependent on increasing cysteine concentrations. To distinguish between the two chemical processes, we investigated whether formation of the Cys93-Tyr157 crosslink was responsible for the occurrence of one of the two phases. Indeed, SDS-PAGE analysis of the samples used in activity measurements showed that increasing the concentration of cysteine in the assay correlated with increased crosslink formation. The initial slow phase observed can be explained as the time taken to process the Cys-Tyr crosslink which consequently leads to activation of the enzyme as seen in the fast phase. Dioxygen consumption in the fast phase correlated with cysteine sulfinic acid formation suggesting that the rate increase represents the second chemical process which is cysteine oxidation. A biphasic response to cysteine oxidation

was recently reported in which an increase in CDO crosslink formation correlated with an increase in the rate of cysteine sulfinic acid formation after one hour incubation with cysteine in the presence of dioxygen (99). However, formation of the Cys93-Tyr157 crosslink in CDO is complete in less than 10 min and therefore does not require lengthy incubation times.

Steady-state kinetic evaluation of crosslinked CDO gave comparable results in the presence and absence of ascorbate. The active redox state of CDO has been reported to be Fe^{2+} , and CDO containing both isoforms was shown to have enhanced activity with the addition of a reductant (101). Surprisingly, results from EPR analysis of crosslinked CDO showed that the active site iron was entirely in the ferric redox state. Furthermore, there was no observable change in signal intensity when cysteine was added under aerobic or anaerobic conditions. This data suggests that the active site geometry of crosslinked CDO may not be altered upon addition of cysteine either under anaerobic or aerobic conditions. This fixed geometry is also associated with an ~5-fold increase in the $k_{\text{cat}}/K_{\text{m}}$ value over CDO containing both isoforms. It can be rationalized that the active site of crosslinked CDO may be in an entatic state in which formation of the crosslink constrains the metal coordination environment to adopt a geometry which closely resembles the reactive intermediate species formed during the course of the reaction (103). This would enhance the activity of CDO by lowering the energy required to reorganize the active site during catalysis (103). A similar mechanistic feature is observed in blue copper proteins in which Cu^{1+} geometry is imposed on the Cu^{2+} active site which enhances electron transfer (104). Since most of the proposed mechanisms for cysteine oxidation by CDO posit the initial formation of Fe^{3+} superoxo species upon binding of dioxygen to the enzyme-substrate complex, our results suggest that the active site of crosslinked CDO with a ferric iron structurally resembles the proposed Cys-bound Fe^{3+} intermediate. The substrate therefore enters a

preorganized active site, which would explain the increased catalytic efficiency observed in crosslinked CDO.

The presence of Fe^{3+} in the active site of crosslinked CDO poses the question whether cysteine oxidation is initiated by activating dioxygen or activating the substrate for reaction with dioxygen. Mononuclear iron enzymes that utilize dioxygen as a cosubstrate are divided into two generalized groups: (1) dioxygen activating and (2) substrate activating enzymes (105). Dioxygen activating enzymes utilize a ferrous site, which binds dioxygen to generate iron-oxygen compounds that react with the substrate to form the product, while substrate-activating enzymes utilize a high spin ferric site to activate the substrate for reaction with dioxygen. If oxidation of cysteine in CDO follows the first mechanistic strategy, then there would need to be an electron donor to generate Fe^{2+} for activation of dioxygen and reaction with cysteine. The Cys93-Tyr157 crosslink could be viewed as a source of the electron required to reduce the bound ferric iron to the ferrous form similar to galactose oxidase whose Cys-Tyr crosslink has been extensively characterized as a free radical site (67, 86, 88). However, we did not observe any stable tyrosyl radical species by UV-visible or EPR spectroscopy suggesting that a tyrosyl radical may not be involved in the catalytic mechanism of crosslinked CDO. If cysteine oxidation occurs through a substrate activation mechanism, the ferric iron of crosslinked CDO is already primed to initiate the reaction. In this regard, spectroscopic characterization of CDO by MCD spectroscopy showed that cysteine binds directly to high spin Fe^{3+} in a similar manner as it binds Fe^{2+} via its S atom (65). Analogous to the intradiol-cleaving catechol dioxygenases that utilize Fe^{3+} site to activate the catecholate substrate, the Fe^{3+} center in crosslinked CDO may activate the cysteine-thiolate ligand for reaction with dioxygen. Binding of cysteine and dioxygen to the iron center simultaneously may promote the transfer of electron density from

cysteine sulfur to dioxygen via the metal center resulting in a sulfur ligand with a cation radical character and Fe^{3+} superoxo species (106).

As previously shown, iron, dioxygen, and cysteine are requirements for crosslink formation. In galactose oxidase, galactose and dioxygen are not essential for crosslink formation suggesting that the mechanisms for CDO and galactose oxidase crosslink formation are different (67). An anomaly from these studies is that there is complete crosslink formation at high cysteine concentrations even though there are substoichiometric amounts of iron bound. If iron is required for crosslink formation, then the iron would either have to transfer between active sites or an activated cysteine substrate is directly involved and transferred between active sites. Although there are several mechanisms proposed for crosslink formation, the question of how the crosslink is formed to completion with substoichiometric amounts of iron in recombinant CDO has not been addressed (90, 99). However, it is evident from the steady-state kinetic studies that formation of the crosslink and oxidation of the bound iron to the ferric form are two critical events that markedly enhance the catalytic efficiency of CDO. The slow phase observed in the kinetic assays with homogeneously non crosslinked CDO may be attributed to the processes of crosslink formation and oxidation of Fe^{2+} to Fe^{3+} . Lipoygenases have been shown to exhibit an analogous mechanistic strategy where the as-isolated enzyme is found in the Fe^{2+} form which is activated by oxidation with the fatty acid hydroperoxide product generating the catalytically active Fe^{3+} -containing enzyme (107). The catalytic cycle in CDO therefore could proceed with an oxidized iron center as outlined in figure 2.7 with cysteine coordinating Fe^{3+} . Binding of cysteine to the Fe^{3+} center increases the affinity of the metal center for dioxygen binding at an adjacent coordination site (108). Coordination of cysteine to Fe^{3+} (Fig. 2.7, II) leads to electron transfer from the thiolate to Fe^{3+} to form the thiyl radical and Fe^{2+} . The Fe^{2+} is then able to

activate dioxygen forming an iron superoxo intermediate (Fig. 2.7, III). Activation of the two substrates would promote radical coupling between the thiyl sulfur and the distal oxygen forming the cyclic iron peroxo complex (Fig. 2.7, IV). Homolytic cleavage of the O-O bond would lead to the formation of a sulfoxy-cation and a single oxygen atom bound to the metal center (Fig. 2.7, V). Recombination of the sulfoxy-cation and the oxygen atom would generate the Fe³⁺-bound cysteine sulfinic acid product which is subsequently released from the active site by hydrolysis (Fig. 2.7, VI). The iron was not reduced to the ferrous state when cysteine was added to crosslinked CDO under either anaerobic or aerobic conditions. Therefore, it is likely that electron transfer from the cysteine thiolate occurs once dioxygen coordinates the iron center forming a ternary complex that promotes electron transfer. This mechanism differs from the intradiol dioxygenase enzymes where dioxygen reacts directly with the activated catechol substrate. For the intradiol dioxygenase enzymes, the oxygen-surrogate NO is unable to coordinate the metal center unless the iron center has been reduced (109-110). However, the oxygen-surrogate KCN was shown to coordinate the Fe³⁺ center of CDO in the presence of Cys, suggesting that oxygen is able to coordinate the ferric redox form (100).

It was previously shown that CDO present in the cellular lysate exists primarily in the non crosslinked ferrous form(101). Exposure of the enzyme to dioxygen during the purification process consequently leads to formation of the Cys93-Tyr157 crosslink and oxidation of the iron center. On the basis of this observation, it can be inferred that within the cell, the predominant CDO isoform is non crosslinked CDO and the crosslink is generated as a consequence of exposing the enzyme to increasing concentrations of cysteine. Indeed, *in vivo* studies demonstrated formation of the crosslink in rats exposed to high cysteine concentrations (90). Thus, formation of the crosslink appears to be a regulatory mechanism, which enhances the

catalytic efficiency of CDO when the cell is exposed to high cysteine concentrations. Differentiation between crosslink formation or catalysis lies in the oxidation state of the bound iron. The presence of Fe^{2+} in non crosslinked CDO favors formation of the crosslink while presence of Fe^{3+} in crosslinked CDO favors oxidation of cysteine to cysteine sulfinic acid. The observation that complete crosslink formation is achieved in an enzyme with substoichiometric amounts of iron bound has interesting mechanistic implications. Further investigations are planned to investigate how the iron free active sites acquire the crosslink.

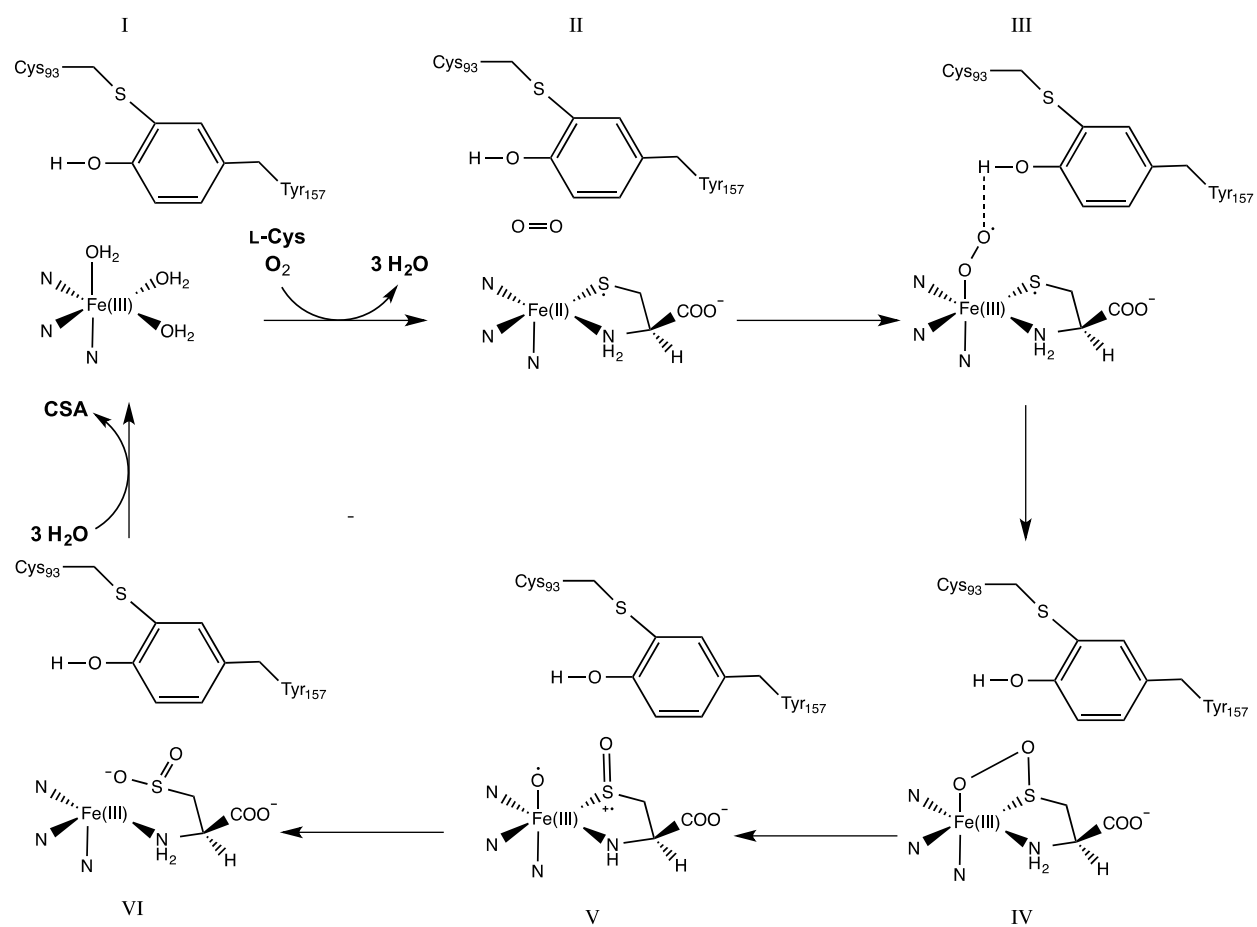


Figure 2.7: Proposed mechanism for cysteine oxidation.

Chapter 3

Investigating the Enzyme-Substrate Interactions within the Active Site of Cysteine Dioxygenase

3.1 Introduction

Intracellular concentrations of free cysteine in mammalian organisms are regulated by cysteine dioxygenase (CDO), an enzyme that catalyzes the irreversible oxidation of L-cysteine to L-cysteine sulfinic acid (6). CDO is a mononuclear iron dependent enzyme that incorporates molecular oxygen into the thiol group of L-cysteine forming the L-cysteine sulfinic acid product (62, 94). The reaction catalyzed by CDO marks the initial step in the biosynthesis of important metabolites including pyruvate, sulfate, and taurine (5). Several high resolution three-dimensional structures of mammalian CDO have been determined, allowing multiple mechanisms of L-cysteine oxidation to be proposed from a structural point of view. As illustrated in Figure 3.1, the active site of CDO is comprised of Fe^{2+} ion that is coordinated by His86, His88, and His140 (1). The 3-His metal binding ligand set is an unusual feature of CDO because it deviates from the more common 3-His/1-Glu set of ligands that coordinate the active site metal in most cupin metalloproteins. In addition to the iron coordinating ligands, the active site of mammalian CDO contains a novel covalent crosslink between Cys93 and Tyr157. The hydroxyl group of Tyr157 forms a short (2.6 Å) hydrogen bond with an iron coordinating water molecule in the resting enzyme (3). Therefore, it has been proposed that the Cys-Tyr crosslink suitably positions Tyr157 to participate in hydrogen bonding interactions with intermediates formed

during catalysis. Additionally, the active site of CDO contains several highly conserved residues including Tyr58, whose position is fixed through weak π -orbital stacking interactions with Trp77 (2). The hydroxyl group of Tyr58 points directly into the active site cavity of CDO where it is proposed to participate in hydrogen bonding interactions with the bound cysteine substrate. The other conserved amino acid in the active site of CDO is Arg60, and based on the three dimensional structure, this residue is well positioned to interact electrostatically with the bound cysteine substrate (2). The three dimensional structure of human CDO in complex with L-cysteine revealed a chelating mode of substrate binding, where the thiol and amino groups directly coordinate the active site iron (Fig. 3.1) (1). Although data from XAS studies provided no evidence of cysteine sulfur ligation to the iron center, results from MCD spectroscopy supported direct cysteine sulfur and active site iron interactions (65, 111). The order of substrate binding to the active site iron was investigated using nitric oxide (NO) which was used as a surrogate for dioxygen binding. In these experiments, CDO was shown to be unreactive towards NO in the absence of L-cysteine, demonstrating that this enzyme utilizes an ordered substrate binding mechanism in which L-cysteine binds first, followed by dioxygen (66).

CDO has been shown to be highly specific for L-cysteine and it has been suggested that the bidentate mode of substrate binding potentially contributes to the high substrate specificity exhibited by this enzyme (1). The proposed mode of substrate binding requires initial deprotonation of the thiol and amino groups of L-cysteine. With the available three dimensional structures, there has been proposals that deprotonation of L-cysteine may be facilitated either by a catalytic triad of Ser153-His155-Tyr157, a water molecule, or a nearby hydroxide molecule (2). Experimentally, information regarding the participation of an active site base in substrate deprotonation is still lacking.

There are key amino acid residues within an enzyme's active site that play active roles during the catalytic process. Based on the available three-dimensional structures of CDO, Tyr58 and Arg60 are suitably positioned to interact with the bound cysteine substrate during catalysis (1-2). However, limited experimental evidence is available to support this hypothesis. In the current study, site directed mutagenesis of the two residues, accompanied by detailed kinetic and spectroscopic investigations of the respective CDO variants were employed to provide additional information on the participation of Tyr58 and Arg60 in catalysis. To probe substrate specificity, molecules that are structurally analogous to L-cysteine were utilized in kinetic and spectroscopic characterization of wild-type CDO and the variants of Tyr58 and Arg60. The protonation states of key functional groups that are relevant to CDO catalysis were investigated through an in depth analysis of the dependence of the kinetic parameters of wild-type CDO on pH. Our current results provide invaluable insights into the nature of enzyme-substrate interactions, and the protonation states of functional groups involved in catalytic events.

3.2 Materials and methods

3.2.1 Materials:

Pfu Turbo DNA polymerase was purchased from Agilent (La Jolla, CA). DNA primers were purchased from Invitrogen (Carlsbad, CA). 4-(2-Hydroxyethyl)piperazine-1-ethanesulfonic acid (HEPES), Bis-Tris, 2-(cyclohexylamino)ethanesulfonic acid (CHES), L-cysteine, cysteamine, D-cysteine, 3-mercaptopropionate, L-ascorbic acid, ammonium sulfate, ampicillin, streptomycin sulfate, lysozyme, sodium dithionite, potassium chloride (KCl), Isopropyl- β -D-thiogalactoside (IPTG), N,N,N',N'-tetramethylethylenediamine and brilliant blue R were purchased from Sigma (St. Louis, MO). Sodium dodecyl sulfate (SDS), 30% acrylamide Bis solution, 1.5M Tris-HCl buffer pH 8.8, and 0.5M Tris-HCl buffer pH 6.8 were purchased from Biorad (Hercules, CA). Glycerol and sodium chloride were purchased from Macron Fine Chemicals (Center valley, PA). Phenyl SepharoseTM 6 Fast Flow (high sub) was purchased from GE Healthcare Biosciences, (Uppsala, Sweden). Amicon Ultrafree-MC Centrifugal Filter Devices (10 kD MWCO) and Amicon Ultra-4 Centrifugal Filter Devices (10 kD MWCO) were purchased from Millipore (Billerica, MA). Difco-brand Luria-Bertani (LB) media was purchased from Becton, Dickinson and company (Sparks, MD).

3.2.2 Construction of expression vectors

The pET21a plasmid containing the rat CDO gene was used to construct the respective CDO variants. All primers were designed as 29 base oligonucleotides with the desired substitution. The wild-type Tyr58 codon was replaced with CGC and TTT for Y58A and Y58F respectively, and the wild-type Arg60 codon was replaced with CGC and AAA for R60A and R60K, respectively. The constructs were confirmed by DNA sequence analysis at Davis

Sequencing (University of California, Davis). Successful constructs were transformed into *E. coli* BL21 (DE3) competent cells and stored as glycerol stocks at -80°C for further analysis.

3.2.3 *Expression and purification of wild-type CDO and CDO variants*

Expression and purification of the wild-type CDO was carried out as previously described with minor modifications (101). To obtain purified CDO variants, cells from the stored glycerol stocks containing the respective plasmid were isolated on LB-agar plates containing 0.1 mg/mL ampicillin. A single colony was selected from the plates and was used to inoculate 5 mL LB broth containing 0.1 mg/mL ampicillin which was grown for 6 h at 37°C. A 1% inoculum from the 5 mL culture was used to inoculate a 100 mL LB-amp media which was grown overnight at 37°C. 20 mL of the overnight culture was used to inoculate each of four 1 L cultures of LB broth containing 0.1 mg/mL ampicillin. The cultures were incubated at 37°C until the A_{600} reached 0.6-0.8 after which IPTG was added to a final concentration of 0.4 mM. The cells were incubated for an additional 6 h at 22°C. Cells were harvested by centrifugation at 5000 rpm for 20 min at 4°C. The cell pellet was resuspended in 25 mM HEPES, pH 7.5, and 10% glycerol (v/v) supplemented with 2 µg/mL lysozyme. The supernatant following the nucleic acid precipitation step was supplemented with 20% ammonium sulfate (w/v) and applied onto a Phenyl SepharoseTM 6 Fast Flow column. Protein was eluted using a linear gradient from 20-15% ammonium sulfate in 25 mM HEPES buffer, pH 7.5, and 10% glycerol. Pure protein fractions as assessed by SDS-PAGE were pooled and concentrated by precipitation with 70% ammonium sulfate (w/v). The protein pellet was resuspended in the desired volume of 25 mM HEPES buffer, pH 7.5, 100 mM NaCl, and 10% glycerol. The iron loading and dialysis steps were carried out as previously reported (101). Protein samples were divided into 500 µL aliquots, flash frozen in liquid nitrogen and stored at -80°C.

3.2.4 *Quantitation of iron*

The total iron content in the variants and wild-type CDO was determined using inductively-coupled plasma-atomic emission spectroscopy (ICP-AES). Enzyme samples (10 μ M) prepared in 25 mM HEPES, pH 7.5 at a final volume of 600 μ L were analyzed using a Perkin-Elmer Optima 7300 DV ICP-AES (Perkin-Elmer Life Sciences, Fremont, CA). Commercial iron standards for ICP-AES were used to generate the standard curve and the concentration of iron in each of the prepared protein samples relative to the protein concentration was determined. Distilled and deionized water and 25 mM HEPES buffer, pH 7.5 were used as controls. The results are an average of three separate experiments.

3.2.5 *Circular dichroism spectroscopy*

Circular dichroism (CD) spectra of the variants and wild-type CDO were obtained using 10 μ M of enzyme in 5 mM potassium phosphate buffer, pH 7.5. Spectra were measured using a Jasco J-810 spectropolarimeter (Easton, MD). Measurements were taken in 0.1 nm increments from 300 to 185 nm in a 0.1 cm path length cuvette with a bandwidth of 1 nm and a scanning speed of 50 nm/min. All spectra were corrected by subtracting the CD spectra of the buffer obtained under similar conditions. Each spectrum is the average of 8 accumulations.

3.2.6 *Steady state kinetic analyses of the variants and wild-type CDO*

Steady-state kinetic investigations of the variants and wild-type CDO were determined by measuring the rate of dioxygen utilization using a Clark-type oxygen electrode (Hansatech, Inc., Norfolk, United Kingdom). The standard assay consisted of 2 μ M CDO and 1 mM L-ascorbic acid in 25 mM HEPES buffer, pH 7.5 incubated at 37°C. Reactions were initiated by the addition of varying concentrations of L-cysteine (0.1-50 mM). Initial velocities were obtained within the first 10 s of the reaction and plotted against substrate concentration. The data were fit to the

Michaelis-Menten equation using KaleidaGraph™ software to obtain the steady state kinetic parameters which were calculated as the average of three separate experiments. In reactions where structural analogs of L-cysteine were utilized, reactions were initiated by the addition of varying concentrations of the respective analog (0.1-50 mM) and the initial rates of the reaction were used to determine the respective kinetic parameters.

3.2.7 Dependence of kinetic parameters of wild-type CDO on pH

The dependence of wild-type CDO kinetic parameters on pH was determined by measuring the initial rates of dioxygen consumption at varying concentrations of L-cysteine (10 μM-20 mM) and 1 mM ascorbate, at 37°C using an oxygen electrode. The buffer system utilized in these studies consisted of 25 mM Bis Tris (pH range of 5.8-7.2), 25 mM HEPES (pH range of 7.2-8.5) and 25 mM CHES (pH range of 8.5-10.0). The buffer system was prepared with no additional salt because preliminary studies revealed an inhibitory response when salt was included. Overlapping assays were performed in Bis Tris and HEPES at pH 7.2, and in HEPES and CHES at pH 8.5 to ensure that the activities observed were not affected by the buffers utilized. The initial reaction rates were fit to the Michaelis-Menten equation using KaleidaGraph™ software to determine the steady state kinetic parameters. The $\log(k_{\text{cat}})$ and $\log(k_{\text{cat}}/K_{\text{m}})$ were plotted against pH and the data were best fit to a double ionization model (eq 1) using KaleidaGraph™ software.

$$\log y = \log \left[C / \left(1 + \frac{H}{K_1} + \frac{K_2}{H} \right) \right] \quad (1)$$

In equation 1, H is $[\text{H}^+]$, y is k_{cat} or $k_{\text{cat}}/K_{\text{m}}$, C is the pH independent value of y , and K_1 and K_2 are the dissociation constants for ionizable groups on L-cysteine bound-CDO complex. All assays were performed in triplicate. Stability of CDO with pH was determined by two methods. First, wild-type CDO (20 μM) was preincubated in the appropriate buffer (pH 5.8-10.0)

at 25°C for 30 min. Then the catalytic activity of the respective preincubated enzyme preparations was determined in 25 mM HEPES buffer, pH 7.5. The second method involved obtaining the circular dichroism spectra of the enzyme preparations that had been preincubated at 25°C for 30 min in the appropriate buffers (pH 5.8-10.0). Each spectra was obtained using 10 µM CDO in 5 mM potassium phosphate buffer pH 7.5.

3.2.8 EPR spectroscopy

Electron paramagnetic resonance (EPR) spectra at X-band frequency (9.38 GHz) were recorded on a Bruker EMX spectrometer (Bruker Biospin Corporation, Billerica, MA). Cooling was performed with an Oxford Instruments ESR 900 flow cryostat and an ITC4 temperature controller. Samples were prepared for EPR analysis by diluting the variants and wild-type CDO to a final concentration of 100 µM in 25 mM HEPES buffer, pH 7.5, 100 mM NaCl, and 10% glycerol in a final volume of 300 µL. In samples where L-cysteine and structural analogs of L-cysteine were included, 10 mM L-cysteine or the respective analog was added to diluted protein samples in a final volume of 300 µL. Each protein sample was transferred into EPR tubes and frozen in liquid nitrogen. All spectra were recorded using the following instrument settings: microwave frequency, 9.38 GHz; microwave power, 1.99 mW; receiver gain, 2×10^4 ; modulation frequency, 100 kHz; modulation amplitude, 6 G; time constant, 327.68 ms; sweep time, 335.5 s. The EPR spectra were recorded as the sum of 2 accumulations and were normalized by subtracting the spectrum of buffer that was used to prepare the samples.

3.3 Results

3.3.1 Structural characterization of the CDO variants

The three-dimensional structures of CDO have revealed the presence of some highly conserved amino acid residues that line the active site cavity. Among these residues, are Tyr58 and Arg60 which based on their location within the active site, have been proposed to play a role in cysteine substrate coordination during catalysis (Fig. 3.1) (1-3). The three-dimensional structure of human CDO in complex with cysteine revealed that cysteine coordinates the active site iron via the thiol and amino groups allowing the carboxyl group to participate in hydrogen bonding and electrostatic interactions with Tyr58 and Arg60 (1). To evaluate experimentally the roles of Tyr58 and Arg60 in catalysis, we isolated and purified Tyr58 and Arg60 CDO variants. It was previously shown that CDO contains a heterogenous mixture of non crosslinked and crosslinked species which are identified by their different migration patterns on SDS-PAGE. Mass spectroscopic and mutational analyses have revealed that the slower migrating isoform lacks the Cys-Tyr crosslink while the faster migrating isoform contains the Cys-Tyr crosslink (90, 98). Interestingly, analysis of the variant proteins on SDS-PAGE revealed that Y58A CDO existed primarily as a single isoform corresponding to the slower migrating isoform of wild-type CDO (upper band, Fig. 3.2). Conversely, the R60A CDO variant existed primarily as a single isoform corresponding to the faster migrating isoform of wild-type CDO (lower band, Fig. 3.2). The Y58F and R60K CDO variants showed equal proportions of the slower and faster migrating isoforms. Circular dichroism (CD) spectra of the variant proteins were obtained to investigate any changes in the overall secondary structure of CDO as a result of the respective substitutions. The overlaid CD spectra of Y58A and Y58F CDO variants were comparable to the spectrum of wild-type CDO, suggesting that substituting Tyr58 with Ala or Phe did not disrupt the gross

secondary structure of CDO (Fig. 3.3). The CD spectra of R60A and R60K CDO were also comparable to the spectrum of wild-type CDO, suggesting that the overall secondary structure of CDO was not disrupted upon substitution of Arg60 with Ala or Lys (Fig. 3.4). Since the catalytic activity of CDO depends on the presence of iron bound within the active site, the total iron content in the CDO variants was investigated and compared with wild-type CDO. Results from ICP-AES experiments established that the iron content in the CDO variants under investigation was comparable to that in wild-type CDO (Table 3.1).

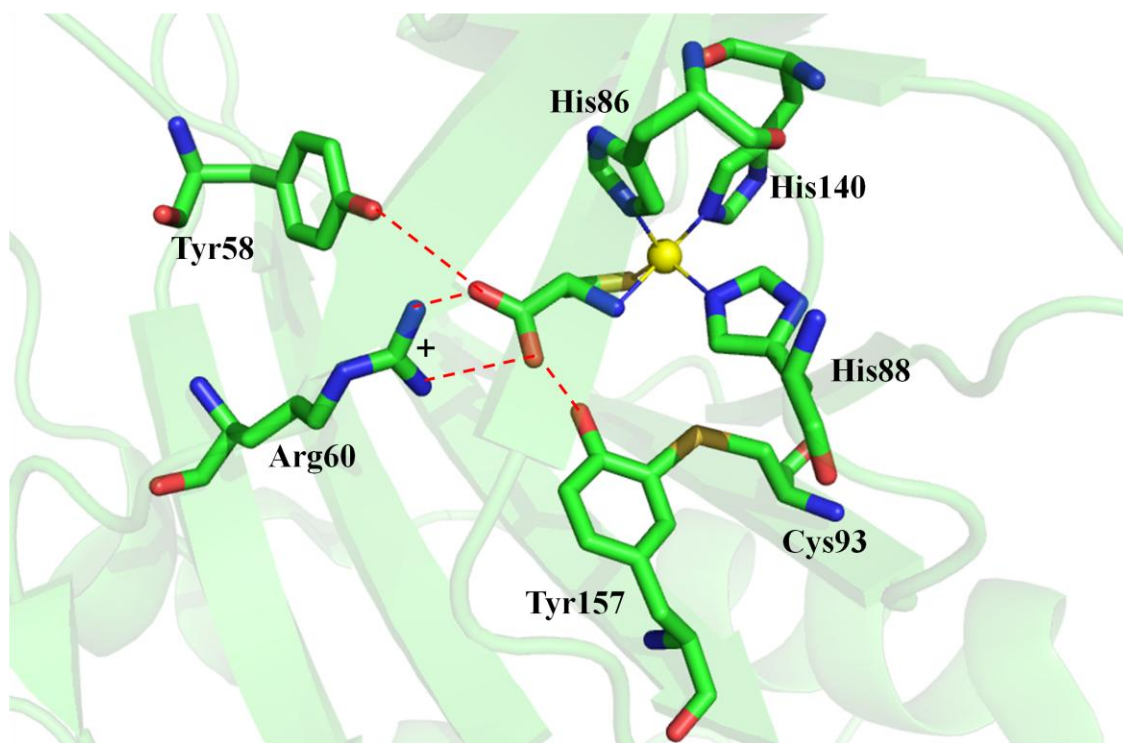


Figure 3.1: Active site of cysteine dioxygenase with bound L-cysteine showing the 3-His metal binding residues and the Cys93-Tyr157 crosslink. Substrate stabilization through non covalent interactions provided by Arg60 and Tyr58 are highlighted with red dashed lines. The structure was taken from PDB entry 2IC1.

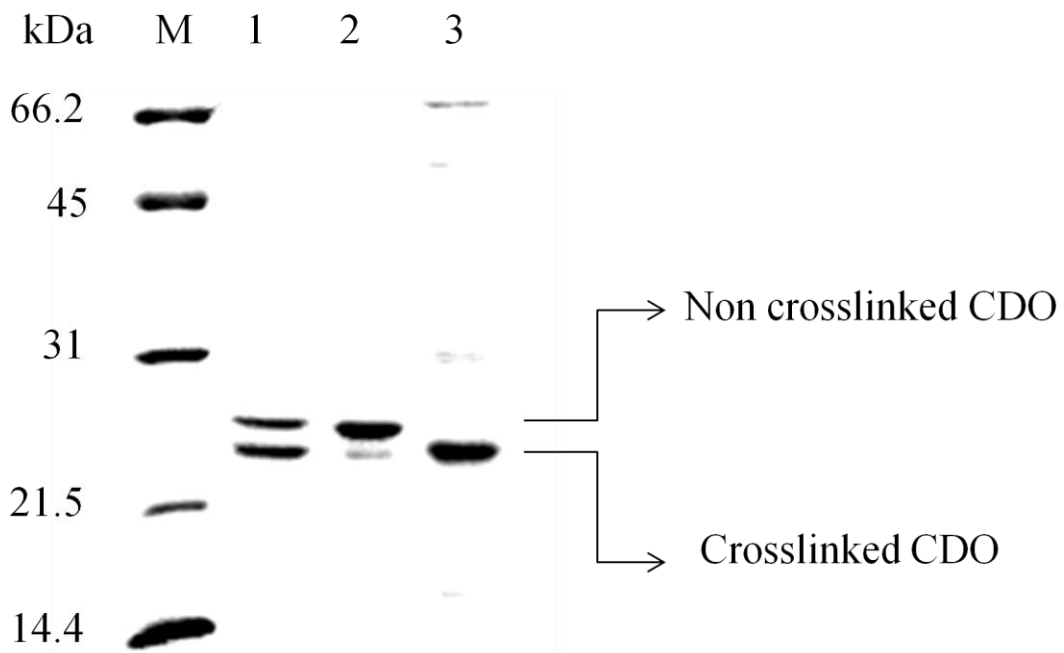


Figure 3.2: SDS-PAGE analysis of wild-type CDO, Y58A and R60A CDO variants. (M) Molecular weight marker, (1) wild-type CDO, (2) Y58A CDO (3) R60A CDO. Acrylamide gels (12%) were run with samples pretreated by boiling for 3 min in sample buffer containing 2% SDS and 5% 2-mercaptoethanol.

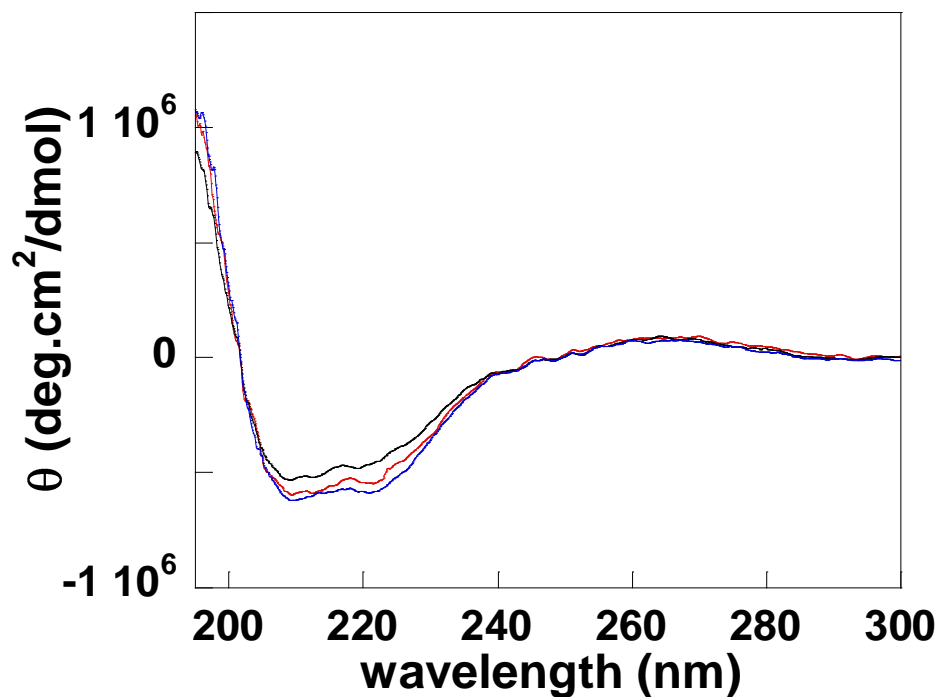


Figure 3.3: Circular dichroism spectra of wild-type CDO (—), Y58A CDO (—), and Y58F CDO (—) variants. Measurements were taken in 0.1 nm increments from 300 to 185 nm in a 0.1 cm path length cuvette with a bandwidth of 1 nm and a scanning speed of 50 nm/min. Each spectrum is the average of 8 accumulations.

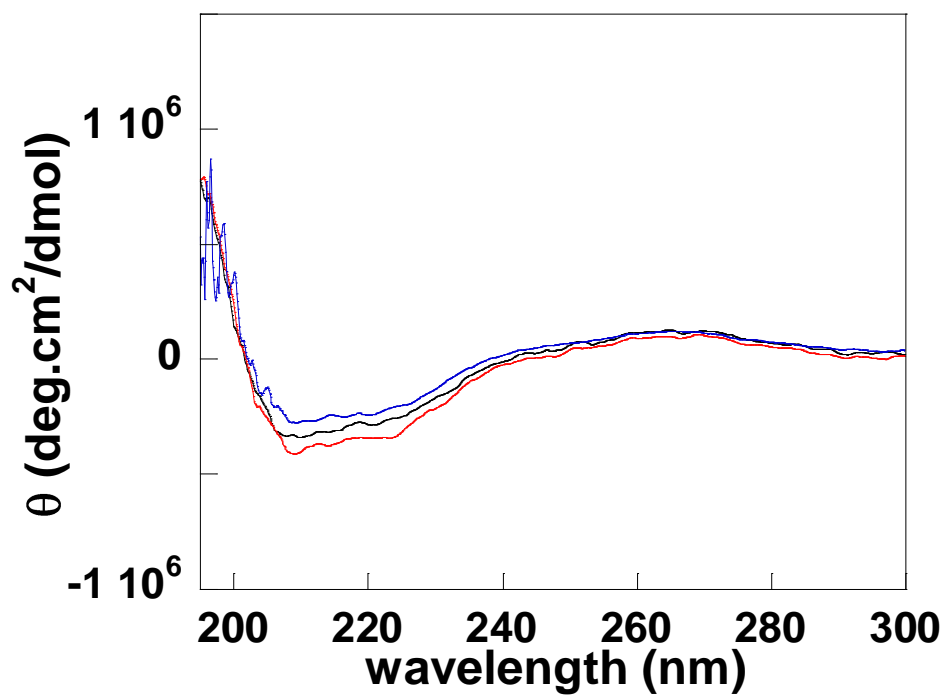


Figure 3.4: Circular dichroism spectra of wild-type CDO (—), R60A CDO (—), and R60K CDO (—) variants. Measurements were taken in 0.1 nm increments from 300 to 185 nm in a 0.1 cm path length cuvette with a bandwidth of 1 nm and a scanning speed of 50 nm/min. Each spectrum is the average of 8 accumulations.

Table 3.1: Iron incorporation in wild-type, Y58A, Y58F, R60A, and R60K CDO

Enzyme	% iron Bound ^a
wild-type CDO	39 ± 1
Y58A CDO	30 ± 0.9
Y58F CDO	28 ± 0.6
R60A CDO	31 ± 2
R60K CDO	31 ± 0.7

^a Total iron content relative to protein concentration

3.3.2 Activity analyses of the CDO variants with L-cysteine

The three-dimensional structure of CDO suggests that, based on their position within the active site, Tyr58 and Arg60 residues may be involved in substrate coordination during catalysis. In order to evaluate the involvement of Tyr58 and Arg60 in catalysis, steady state kinetic investigations were performed with Tyr58 and Arg60 CDO variants for comparison with the wild-type enzyme. The Tyr58 CDO variants (Y58A and Y58F) exhibited a 6-fold decrease in the k_{cat}/K_m value compared to the wild-type enzyme (Table 3.2). The kinetic parameters obtained with the Arg60 CDO variants (R60A and R60K) revealed a 20-fold decrease in the k_{cat}/K_m value relative to the wild-type protein (Table 3.3).

3.3.3 Activity analyses of the variants and wild-type CDO with substrate analogs

Previous studies investigating substrate specificity report that CDO is highly specific for L-cysteine (64). To evaluate the relevance of the functional groups of L-cysteine in catalysis, the catalytic activity of wild-type CDO and the variants was investigated using compounds that are structurally similar to L-cysteine (Fig 3.5). These compounds included cysteamine, (lacks the carboxyl group), 3-mercaptopropionate (lacks the amino group), and D-cysteine (the D-stereoisomer of cysteine). The kinetic parameters were determined by monitoring the rate of dioxygen consumption while varying the concentrations of the respective substrates (0.1-50 mM) (Table 3.2 and 3.3). Changing the stereochemistry of the substrate from L-cysteine to D-cysteine resulted in a 30-fold decrease in the k_{cat}/K_m value of wild-type CDO. The k_{cat}/K_m values of the Tyr58 and Arg60 CDO variants when D-cysteine was utilized as the substrate were comparable to the k_{cat}/K_m value of wild-type CDO with the same substrate. These results are in agreement with a recent report where the catalytic efficiency for wild-type CDO with D-cysteine was found to be lower compared to that with L-cysteine (100). From our results, it is apparent that CDO

demonstrates a stronger preference for L-cysteine relative to D-cysteine. The kinetic parameters for the variants and wild-type CDO with D-cysteine are similar suggesting that D-cysteine binds to the active sites of the respective proteins in a similar conformation which may not be optimal for catalysis.

The catalytic relevance of the carboxyl group of L-cysteine was investigated by utilizing cysteamine as a substrate in steady state kinetic analysis of wild-type CDO and the variants. Interestingly, the k_{cat} value of wild-type CDO with cysteamine was analogous to the value obtained with the L-cysteine substrate (Table 3.2). However, a pronounced (33-fold) increase in the apparent K_m value for cysteamine was observed which consequently led to a 32-fold decrease in the k_{cat}/K_m value. All the CDO variants under investigation exhibited k_{cat}/K_m values with cysteamine that were comparable the k_{cat}/K_m value of wild-type CDO with the same substrate (Table 3.2 and 3.3). The reduced catalytic activity observed in the respective enzymes with cysteamine clearly demonstrates that the carboxyl group of L-cysteine is of crucial importance for optimal catalysis. Experiments measuring hypotaurine formation revealed impaired cysteamine oxidation in which more oxygen was utilized compared to the amount of hypotaurine produced in wild-type CDO (data not shown). None of the respective enzymes displayed any activity with 3-mercaptopropionate which lacks the amino group. The lack of detectable catalytic activity with 3-mercaptopropionate suggests a key role for the amino group of L-cysteine in substrate coordination.

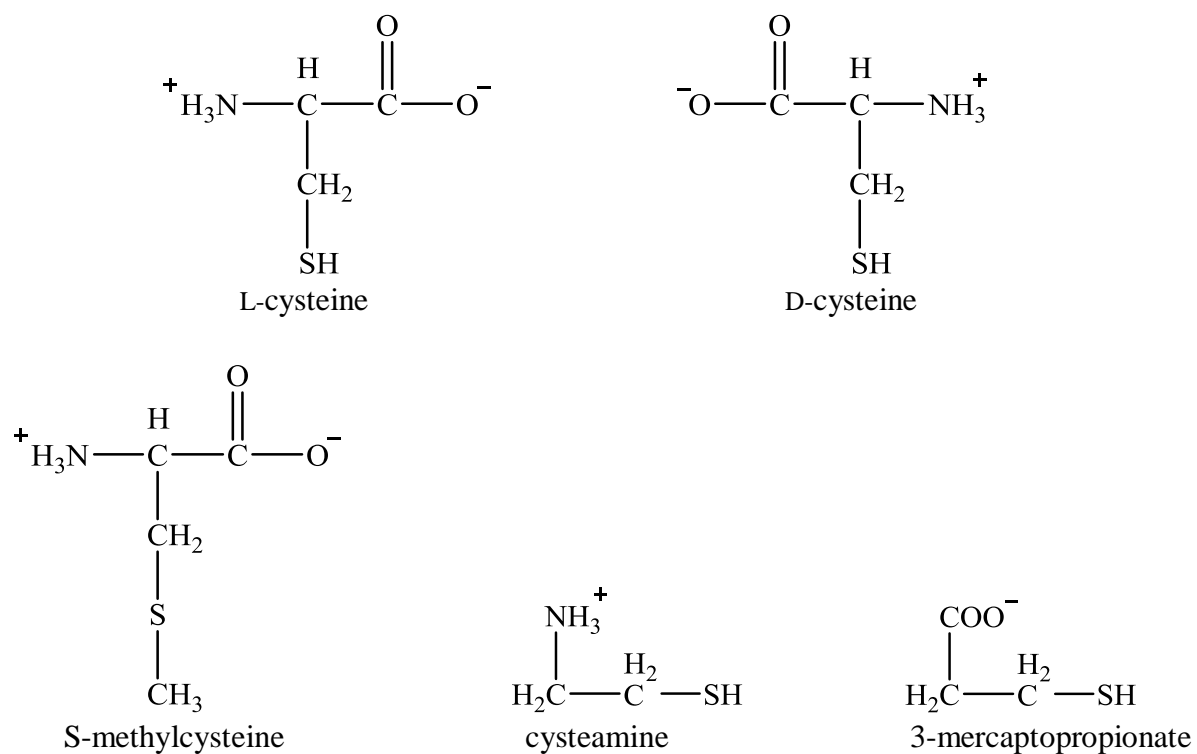


Figure 3.5: Substrates utilized in kinetic and spectroscopic investigations.

Table 3.2: Steady-state kinetic parameters of wild-type, Y58A, and Y58F CDO ^a

substrate	parameter	Enzyme		
		WT-CDO	Y58A CDO	Y58F CDO
L-cysteine	k_{cat} (min^{-1})	55 ± 1.0	85 ± 10	48 ± 1.0
	K_{m} (mM)	0.3 ± 0.1	3.0 ± 0.5	2.0 ± 0.3
	$k_{\text{cat}}/K_{\text{m}}$ ($\text{mM}^{-1}\cdot\text{min}^{-1}$)	180 ± 40	30 ± 6	28 ± 5.0
D-cysteine	k_{cat} (min^{-1})	15 ± 0.6	10 ± 1	21 ± 1.0
	K_{m} (mM)	2.0 ± 0.6	2 ± 1	3.0 ± 0.4
	$k_{\text{cat}}/K_{\text{m}}$ ($\text{mM}^{-1}\cdot\text{min}^{-1}$)	6.4 ± 2.0	4.2 ± 2.0	6.5 ± 1.0
cysteamine	k_{cat} (min^{-1})	63 ± 3.0	61 ± 5.0	41 ± 2.0
	K_{m} (mM)	10 ± 1	10 ± 2	6 ± 1
	$k_{\text{cat}}/K_{\text{m}}$ ($\text{mM}^{-1}\cdot\text{min}^{-1}$)	5.6 ± 0.6	6.3 ± 1.0	6.9 ± 0.7
3-mercaptopropionate	k_{cat} (min^{-1})	ND ^b	ND	ND
	K_{m} (mM)			
	$k_{\text{cat}}/K_{\text{m}}$ ($\text{mM}^{-1}\cdot\text{min}^{-1}$)			

^a Initial rates investigated rate of dioxygen consumption at varying concentrations of the respective substrates (0.1-50 mM) in 25 mM HEPES buffer, pH 7.5

^b No activity detected at all substrate concentrations

Table 3.3: Steady-state kinetic parameters for wild-type, R60A, and R60K CDO ^a

substrate	parameter	Enzyme		
		WT-CDO	R60A CDO	R60K CDO
L-cysteine	k_{cat} (min^{-1})	55 ± 1.0	13 ± 2.0	56 ± 0.4
	K_{m} (mM)	0.3 ± 0.1	2.0 ± 0.6	4.7 ± 0.3
	$k_{\text{cat}}/K_{\text{m}}$ ($\text{mM}^{-1}\cdot\text{min}^{-1}$)	180 ± 40	8.6 ± 4.0	12 ± 0.8
D-cysteine	k_{cat} (min^{-1})	15 ± 0.6	13 ± 0.2	11 ± 0.3
	K_{m} (mM)	2.0 ± 0.6	3.0 ± 0.7	2.9 ± 0.6
	$k_{\text{cat}}/K_{\text{m}}$ ($\text{mM}^{-1}\cdot\text{min}^{-1}$)	6.4 ± 2.0	4.1 ± 0.9	3.6 ± 0.7
cysteamine	k_{cat} (min^{-1})	63 ± 3.0	36 ± 2.0	39 ± 1.0
	K_{m} (mM)	10 ± 1	17 ± 2.0	10 ± 0.8
	$k_{\text{cat}}/K_{\text{m}}$ ($\text{mM}^{-1}\cdot\text{min}^{-1}$)	5.6 ± 0.6	2.2 ± 0.3	3.8 ± 0.3
3-mercaptopropionate	k_{cat} (min^{-1})	ND ^b	ND	ND
	K_{m} (mM)			
	$k_{\text{cat}}/K_{\text{m}}$ ($\text{mM}^{-1}\cdot\text{min}^{-1}$)			

^a Initial rates investigated rate of dioxygen consumption at varying concentrations of the respective substrates (0.1-50 mM) in 25 mM HEPES buffer, pH 7.5

^b No activity detected at all substrate concentrations

3.3.4 Probing the effect of L-cysteine and cysteine analogs on the metal coordination site of wild-type CDO

It was previously shown that in the absence of substrate, purified wild-type CDO exhibits a characteristic EPR signal at $g = 4.3$, typical of high spin ferric iron (Fig. 3.6A, green trace) (101). Upon addition of L-cysteine, the intensity of the ferric EPR signal increases sharply indicating the direct coordination of the substrate to the active site iron (Fig. 3.6A, dark blue trace). To probe the contribution of the various functional groups of L-cysteine in the formation of the intensified EPR signal, the L-cysteine substrate was substituted with D-cysteine, cysteamine, 3-mercaptopropionate, and S-methylcysteine. Interestingly, addition of D-cysteine to wild-type CDO yielded an identical spectrum as that of wild-type CDO with L-cysteine (Fig. 3.6A, light blue trace). The striking spectra similarity of wild-type CDO with D-cysteine and with L-cysteine possibly indicates that the mode of coordination of the two substrates to the active site iron may be the same, since they both have the same functional groups but are isomers. The effect of the carboxyl group of L-cysteine on the metal coordination environment was investigated using cysteamine. Addition of cysteamine to wild-type CDO also resulted in an increased EPR signal intensity at $g = 4.3$ (Fig. 3.6A, red trace). However, the EPR signal observed with cysteamine was considerably smaller than that observed with L-cysteine. Although, there was no activity with 3-mercaptopropionate, the effect of the amino group on the metal coordination environment was investigated. Addition of 3-mercaptopropionate to wild-type CDO also resulted in an increase in the intensity of the ferric EPR signal (Fig. 3.6A, black trace). The EPR spectra of wild-type CDO with cysteamine and 3-mercaptopropionate were more axial compared to the rhombic spectra of wild-type CDO with D-cysteine and with L-cysteine. All the substrates analyzed thus far have a thiol group. To evaluate whether the presence of the thiol group was essential for substrate coordination to the iron center, S-

methylcysteine was utilized in the EPR investigations. Interestingly, addition of S-methylcysteine to wild-type CDO did not alter the EPR signal of the enzyme (Fig. 3.6B, dark blue trace). The effect of the product of L-cysteine oxidation on the iron coordination environment was also investigated by obtaining the spectrum of wild-type CDO in the presence of L-cysteine sulfinic acid (Fig. 3.6B, light blue trace). There was no observable change in the spectrum of wild-type CDO with and without L-cysteine sulfinic acid. The lack of observable changes in the EPR of wild-type CDO in the presence of S-methylcysteine and L-cysteine sulfinic acid demonstrates that the thiol group of L-cysteine is essential in substrate coordination.

3.3.5 Evaluating the effect of L-cysteine and cysteine analogs on the metal coordination site of the CDO variants

To further investigate the role of second sphere interactions with the bound cysteine substrate, L-cysteine and cysteine analogs were utilized in the EPR analyses of the Tyr58 and Arg60 CDO variants. The hydroxyl group of Tyr58 points directly into the active site as shown in figure 3.1, where it is proposed to participate in hydrogen bonding interactions with the carboxyl group of the bound cysteine substrate. Substitution of Tyr58 with either Phe or Ala may disrupt these interactions and consequently alter the metal binding site when L-cysteine is coordinated. The green EPR traces represent the EPR spectra of the Y58F and Y58A CDO variants (Fig. 3.7A and B, respectively). The characteristic EPR signal at $g = 4.3$ was also observed in these CDO variants, indicating that the two enzymes also contain the high spin ferric species observed in wild-type CDO. The changes observed in the EPR signal intensities upon addition of either L-cysteine, D-cysteine, cysteamine, 3-mercaptopropionate, or S-methylcysteine to Y58F CDO were similar to those observed with wild-type CDO (Fig. 3.7A). The similarity between the EPR spectra of Y58F and wild-type CDO may indicate that the respective substrates had similar effects on the metal coordination environments of the two enzymes. The changes

observed in the EPR spectra of Y58A CDO in the presence of the respective substrates were also comparable to those observed with the wild-type enzyme, with some slight variations with some substrates. For example, the EPR signal of Y58A CDO with 3-mercaptopropionate was notably smaller, (Fig. 3.7B, black trace), compared to the signal of wild-type CDO with the same substrate. The variations observed in the EPR spectra of Y58A CDO demonstrate that the metal binding site may have been altered upon the less conservative substitution of Tyr58 to Ala.

One of the charged amino acid residues in the active site of CDO is Arg60. It has been proposed from the three-dimensional structure of CDO that Arg60 stabilizes the bound substrate through hydrogen bonding and electrostatic interactions (2). The EPR spectra of R60K and R60A CDO variants revealed that the active site iron in these variants was also in the ferric redox state (Fig. 3.8A and 3.8B, respectively). Since substitution of Arg60 with Lys is a conservative substitution, the changes observed in the EPR signal intensities upon addition of L-cysteine and the respective cysteine analogs to R60K CDO were essentially similar to those observed with the wild-type enzyme (Fig. 3.8A). However, some slight variations were observed in the EPR spectra of R60A CDO in the presence of the respective substrates. Some of the more notable variations were observed with cysteamine and 3-mercaptopropionate (Fig. 3.8B, red and black traces respectively). The EPR signal intensity of R60A CDO with cysteamine was considerably smaller compared to the signal of wild-type CDO with the same substrate, and even more minimal was the EPR signal of R60A CDO in the presence of 3-mercaptopropionate. The observed variations in the EPR spectra of R60A with the respective analogs indicate that the metal binding site had been disrupted upon substitution of Arg60 with Ala.

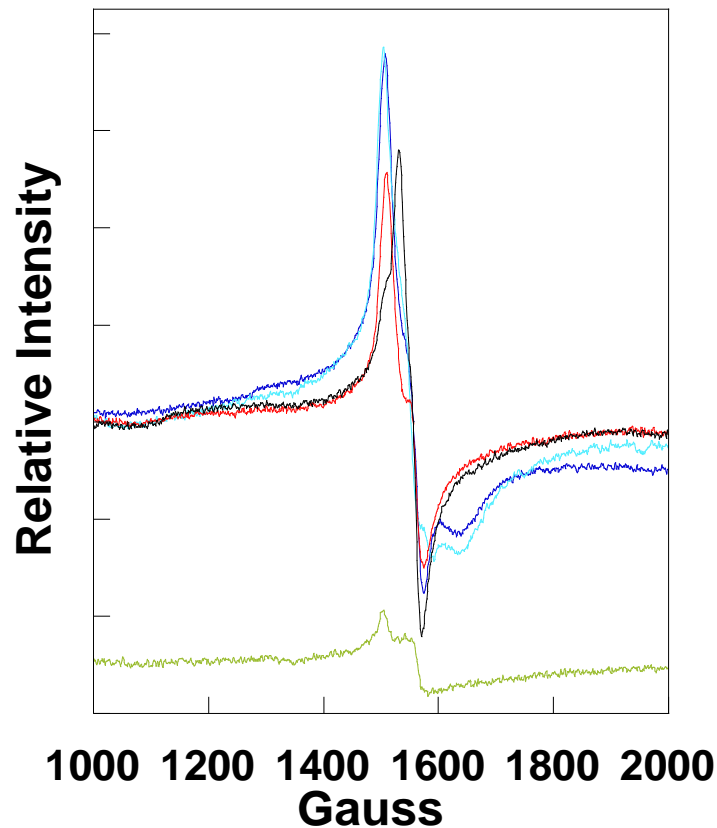


Figure 3.6A: X-band EPR spectra of wild-type CDO showing the effects of various substrates on the metal coordination environment. Substrate free wild-type CDO (—); wild-type CDO with 10 mM L-cysteine (—); wild-type CDO with 10 mM D-cysteine (—); wild-type CDO with 10 mM cysteamine (—); wild-type CDO with 10 mM 3-mercaptopropionate (—). Spectra were taken with 100 μ M protein in 25 mM HEPES buffer, pH 7.5, 100 mM NaCl, and 10% glycerol. All spectra were recorded at 9.38 GHz, with a field modulation frequency of 100 kHz and modulation amplitude of 6 G. All spectra were recorded at 8-10 K.

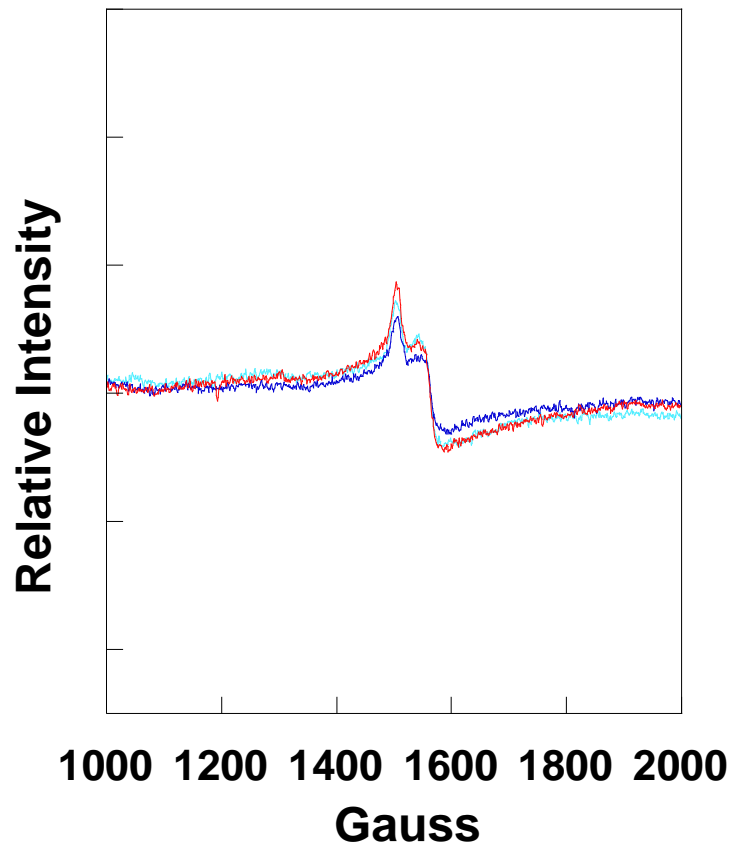


Figure 3.6B: X-band EPR spectra of wild-type CDO showing the effects of S-methylcysteine and L-cysteine sulfinic acid on the metal coordination environment. Substrate free wild-type CDO (—); wild-type CDO with 10 mM S-methylcysteine (—); wild-type CDO with 10 mM L-cysteine sulfinic acid (—). Spectra were taken with 100 μ M protein in 25 mM HEPES buffer, pH 7.5, 100 mM NaCl, and 10% glycerol. All spectra were recorded at 9.38 GHz, with a field modulation frequency of 100 kHz and modulation amplitude of 6 G. All spectra were recorded at 8-10 K.

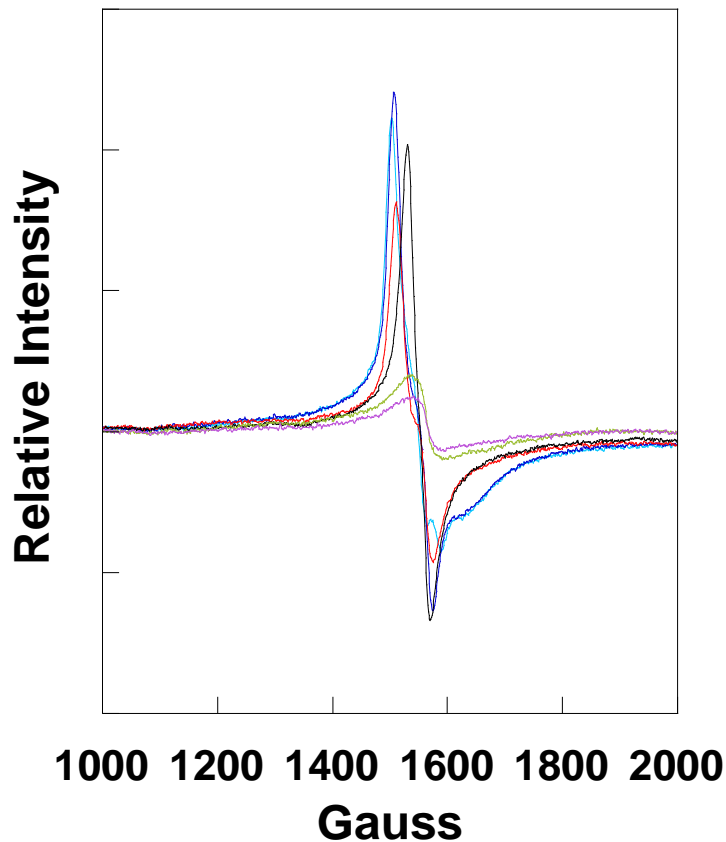


Figure 3.7A: X-band EPR spectra of Y58F CDO variant showing the effects of various substrates on the metal coordination environment. Y58F CDO without substrate (—); Y58F CDO with 10 mM L-cysteine (—); Y58F CDO with 10 mM D-cysteine (—); Y58F CDO with 10 mM cysteamine (—); Y58F CDO with 10 mM 3-mercaptopropionate (—); Y58F CDO with 10 mM S-methylcysteine (—). Spectra were taken with 100 μ M protein in 25 mM HEPES buffer, pH 7.5, 100 mM NaCl, and 10% glycerol. All spectra were recorded at 9.38 GHz, with a field modulation frequency of 100 kHz and modulation amplitude of 6 G. All spectra were recorded at 8-10 K.

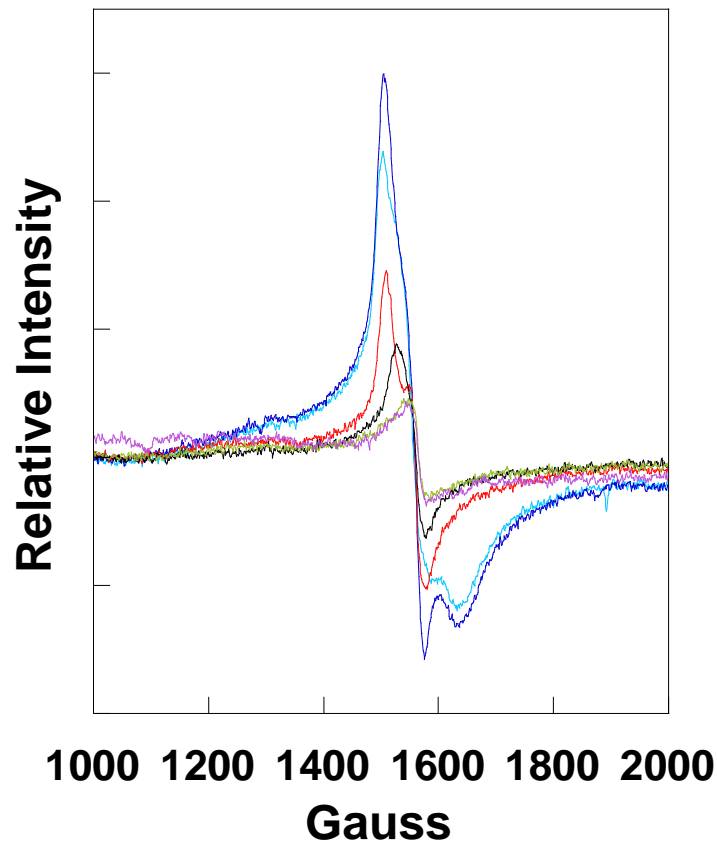


Figure 3.7B: X-band EPR spectra of Y58A CDO variant showing the effects of various substrates on the metal coordination environment. Y58A CDO without substrate (—); Y58A CDO with 10 mM L-cysteine (—); Y58A CDO with 10 mM D-cysteine (—); Y58A CDO with 10 mM cysteamine (—); Y58A CDO with 10 mM 3-mercaptopropionate (—); Y58A CDO with 10 mM S-methylcysteine (—). Spectra were taken with 100 μ M protein in 25 mM HEPES buffer, pH 7.5, 100 mM NaCl, and 10% glycerol. All spectra were recorded at 9.38 GHz, with a field modulation frequency of 100 kHz and modulation amplitude of 6 G. All spectra were recorded at 8-10 K.

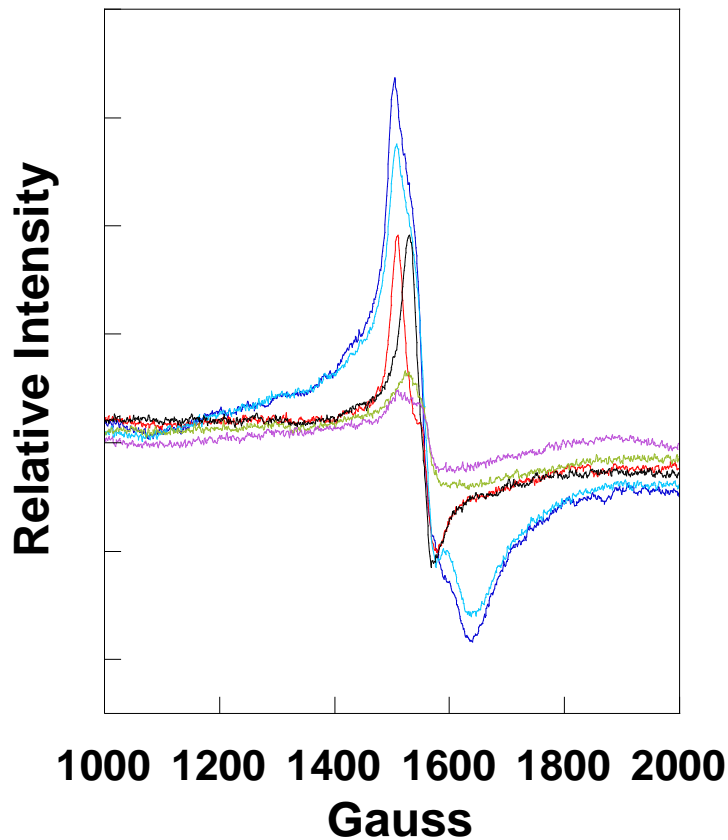


Figure 3.8A: X-band EPR spectra of R60K CDO variant showing the effects of various substrates on the metal coordination environment. R60K CDO without substrate (—); R60K CDO with 10 mM L-cysteine (—); R60K CDO with 10 mM D-cysteine (—); R60K CDO with 10 mM cysteamine (—); R60K CDO with 10 mM 3-mercaptopropionate (—); R60K CDO with 10 mM S-methylcysteine (—). Spectra were taken with 100 μ M protein in 25 mM HEPES buffer, pH 7.5, 100 mM NaCl, and 10% glycerol. All spectra were recorded at 9.38 GHz, with a field modulation frequency of 100 kHz and modulation amplitude of 6 G. All spectra were recorded at 8-10 K.

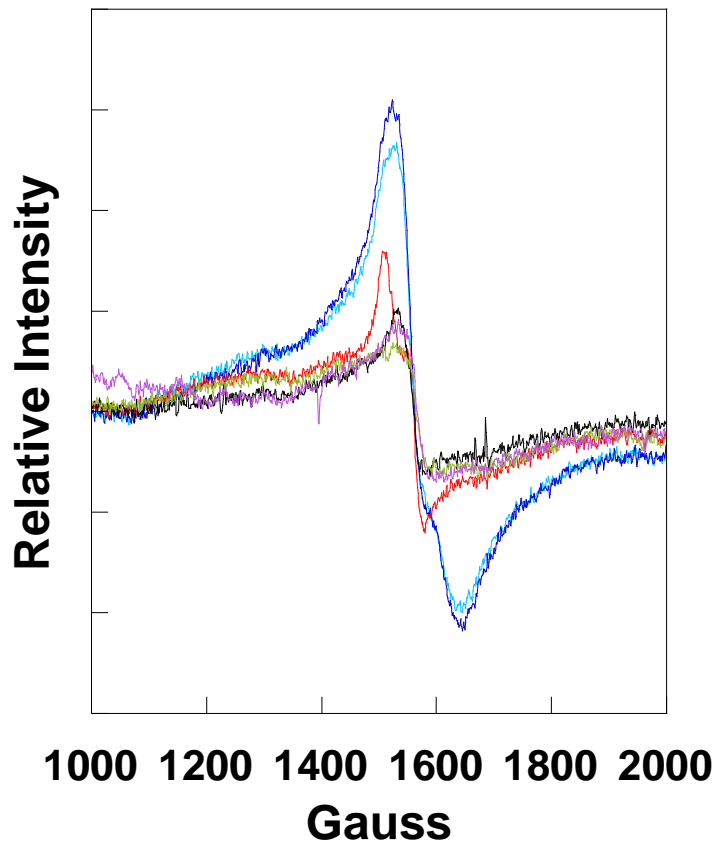


Figure 3.8B: X-band EPR spectra of R60A CDO variant showing the effects of various substrates on the metal coordination environment. R60A CDO without substrate (—); R60A CDO with 10 mM L-cysteine (—); R60A CDO with 10 mM D-cysteine (—); R60A CDO with 10 mM cysteamine (—); R60A CDO with 10 mM 3-mercaptopropionate (—); R60A CDO with 10 mM S-methylcysteine (—). Spectra were taken with 100 μ M protein in 25 mM HEPES buffer, pH 7.5, 100 mM NaCl, and 10% glycerol. All spectra were recorded at 9.38 GHz, with a field modulation frequency of 100 kHz and modulation amplitude of 6 G. All spectra were recorded at 8-10 K.

3.3.6 Dependence of wild-type CDO kinetic parameters on pH

To evaluate the ionization states of groups participating in the dioxygenation reaction of CDO, steady state kinetic parameters of wild-type CDO as a function of pH were determined. Analysis of the stability of wild-type CDO with pH using circular dichroism spectroscopy revealed that the enzyme was stable over the entire experimental pH range (5.8-9.5). This was demonstrated by the unperturbed overall secondary structure of CDO that had been preincubated in the respective pH values (Fig. 3.9). Additionally, the catalytic activity of CDO preincubated at the various pH values was restored when the enzyme was assayed at pH 7.5. The pH dependence of k_{cat} as a function of pH is illustrated in figure 3.10A. Two ionizable groups are apparent in the k_{cat} pH profile, one with a $\text{p}K_{\text{a}}$ value of 6.60 ± 0.02 and the other one with a $\text{p}K_{\text{a}}$ value of 8.6 ± 0.1 . The observed $\text{p}K_{\text{a}}$ values in the k_{cat} pH profile indicate that in the enzyme substrate complex, a group with a $\text{p}K_{\text{a}}$ value of 6.6 should be in the unprotonated state and another group with a $\text{p}K_{\text{a}}$ value of 8.6 should be protonated for catalysis to take place through product release. The pH profile of $k_{\text{cat}}/K_{\text{m}}$ which is illustrated in figure 3.10B, also revealed two ionizable groups with $\text{p}K_{\text{a}}$ values of 7.60 ± 0.02 and 9.3 ± 0.3 . This suggests that two groups in the free enzyme or in the free substrate, one with a $\text{p}K_{\text{a}}$ value of 7.6 must be unprotonated and another group with a $\text{p}K_{\text{a}}$ value of 9.3 must be in the protonated form to commit the reaction through the first irreversible step.

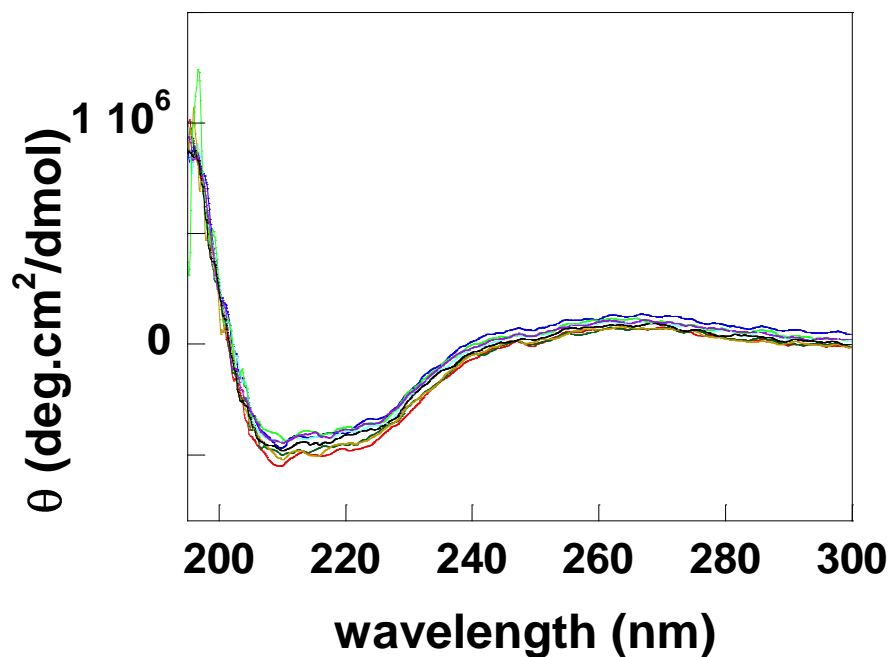


Figure 3.9: Circular dichroism spectra showing the stability of wild-type CDO with varying pH. Wild-type CDO before preincubation (—); preincubation at pH 5.8 (—); at pH 6.0 (—); at pH 7.5 (—); at pH 8.0 (—); at pH 9.0 (—); at pH 10.0 (—); Measurements were taken in 0.1 nm increments from 300 to 185 nm in a 0.1 cm path length cuvette with a bandwidth of 1 nm and a scanning speed of 50 nm/min. Each spectrum is the average of 8 accumulations.

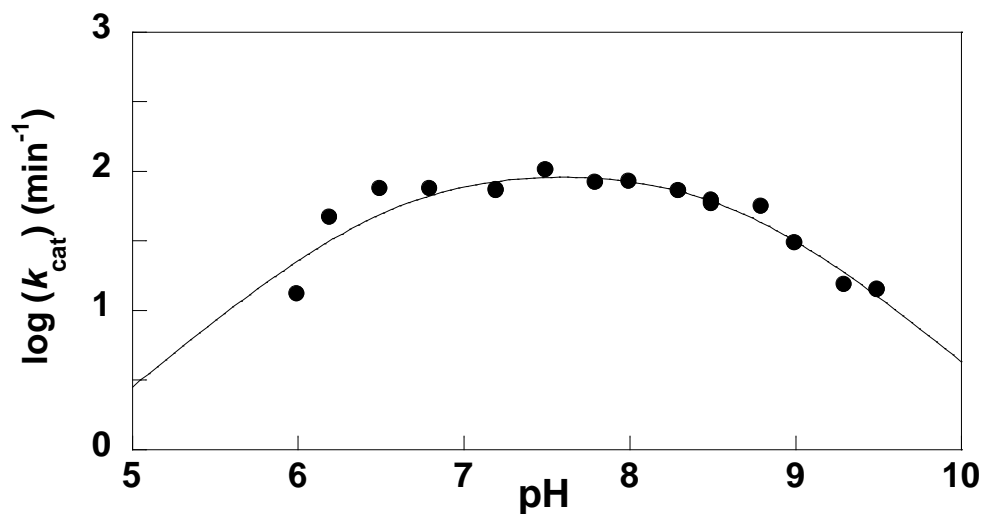


Figure 3.10A: Dependence of k_{cat} values of wild-type CDO on pH. Initial rates investigated the rate of dioxygen utilization at varying concentrations of L-cysteine (0.01-20 mM) in either 25 mM Bis Tris (pH range of 5.8-7.2), 25 mM HEPES (pH range of 7.2-8.5), or 25 mM CHES (pH range of 8.5-10.0). All assays contained 1 mM L-ascorbate. Each point is an average of 3 separate experiments. The solid line is a theoretical curve generated by a fit to eq 1.

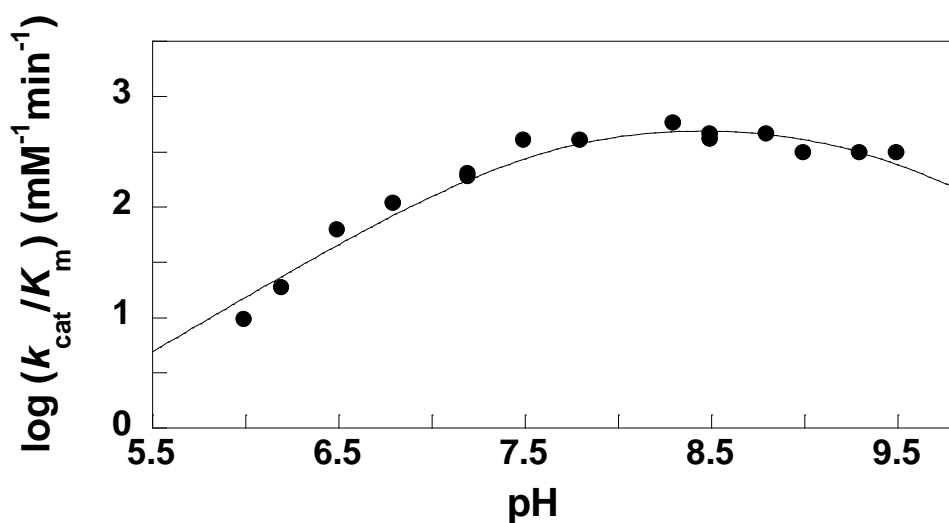


Figure 3.10B: Dependence of k_{cat}/K_m values of wild-type CDO on pH. Initial rates investigated the rate of dioxygen utilization at varying concentrations of L-cysteine (0.01-20 mM) in either 25 mM Bis Tris (pH range of 5.8-7.2), 25 mM HEPES (pH range of 7.2-8.5), or 25 mM CHES (pH range of 8.5-10.0). All assays contained 1 mM L-ascorbate. Each point is an average of 3 separate experiments. The solid line is a theoretical curve generated by a fit to eq 1.

3.4 Discussion

The available three dimensional structures of CDO have provided invaluable information regarding the active site which is poised for the dioxygenation reaction. The active site iron is coordinated by only 3-His residues which is a deviation from the more common 3-His/1-Glu coordination pattern observed in cupin metalloproteins (*1-3*). The three-dimensional structure of human CDO in complex with L-cysteine showed that the 3-His metal binding site is important for coordinating L-cysteine in a bidentate fashion through the thiol and amino groups (*1*). This mode of L-cysteine coordination is a smart strategy that opens up a coordination site for the dioxygen substrate to bind leading to the subsequent oxidation of L-cysteine. Substrate coordination via the amino and thiol groups places the carboxyl group of L-cysteine at a favorable distance for electrostatic and H-bonding interactions with Tyr58 and Arg60. The three dimensional structures of CDO have therefore provided insight into the mechanistic roles of Tyr58 and Arg60 in substrate coordination. However, the roles of these two residues have not been evaluated experimentally. We sought to address this issue through the detailed comparative analysis of the variants of Tyr58 and Arg60 with the wild-type enzyme. Structural characterization of the respective variants using circular dichroism spectroscopy showed that the overall secondary structure of CDO was not disrupted with the respective substitutions. Additionally, iron incorporation in all the variants was comparable with wild-type CDO indicating that Tyr58 and Arg60 are not directly involved in the stability of the active site iron.

Our results revealed that recombinant Y58A CDO exists primarily in the non crosslinked isoform. Previous studies have shown that formation of the Cys-Tyr crosslink in CDO requires the presence of the substrate, L-cysteine (*90, 100*). Substitution of Tyr58 with Ala may disrupt substrate coordination within the active site which prevents formation of the crosslink during

protein expression in Y58A CDO. Additionally, steady state kinetic investigations of Y58A and Y58F CDO variants revealed a 6-fold decrease in the k_{cat}/K_m value relative to that of wild-type CDO, suggesting that Tyr58 plays an essential role in catalysis. The conservative substitution of Arg60 with Lys had no effect on the k_{cat} value but the K_m value for L-cysteine was increased by ~15-fold suggesting that Arg60 plays an important role in catalysis. The observation that R60A CDO exists primarily in the crosslinked form was quite intriguing, especially because previous studies have shown that the presence of the Cys-Tyr crosslink enhances the catalytic activity of CDO. On the contrary, a ~20-fold decrease in the k_{cat}/K_m value for R60A CDO was observed. Based on the three-dimensional structure of CDO, Arg60 has been proposed to interact with the hydroxyl group of Tyr157 through a hydrogen bond network involving Arg60, His155, and Tyr58 (1). It can be rationalized that the disruption of these interactions through substitution of Arg60 with Ala could move Tyr157 closer to Cys93 leading to crosslink formation. Therefore, formation of the crosslink in R60A does not correlate with activation of the enzyme. The reduced activity observed with the Arg60 CDO variants provides experimental evidence that Arg60 plays an integral role in catalysis, by possibly stabilizing the bound cysteine substrate through electrostatic interactions.

Steady state kinetic investigations of the variants and wild-type CDO with substrates that are structurally analogous to L-cysteine have provided useful information regarding the relevance of the various functional groups of L-cysteine in binding and catalysis. The active site of CDO displays remarkable catalytic stereospecificity which is evidenced by the reduced catalytic activity with D-cysteine. The kinetic parameters of the variants and wild-type CDO with D-cysteine were similar, suggesting that the mode of interaction of D-cysteine with the active sites of the respective proteins may be identical. The observation that D-cysteine does not discriminate

between the active sites of the variants and wild-type CDO provides additional evidence that D-cysteine is not a preferred substrate for CDO.

Cysteamine was previously shown to enhance the catalytic activity of CDO but it was not a substrate in that particular study (63). However, in our current studies with cysteamine, the k_{cat} values of the variants and wild-type CDO were comparable to those observed with L-cysteine. In addition, R60A CDO actually exhibited higher k_{cat} values with cysteamine than with L-cysteine, but the overall catalytic efficiency was decreased. It is likely that cysteamine binds the active sites of the respective enzymes in a similar manner as L-cysteine, via the thiol and amino groups. Unlike L-cysteine, cysteamine may not be optimally coordinated because it lacks the carboxyl group which provides additional stability in the active site. Cysteamine is a product of coenzyme A degradation and is oxidized by cysteamine dioxygenase (ADO) to hypotaurine which is subsequently oxidized to taurine. Sequence analysis suggests that ADO is also a member of the cupin superfamily and the enzyme utilizes a similar active site metal coordinating ligand set as that observed in CDO (112). Additionally, it has been reported that mammalian ADO migrates as two or three bands on SDS-PAGE, suggesting a possible post translational modification as that observed in CDO, although further studies are required to verify such a possibility (112). ADO is highly specific for cysteamine and does not oxidize cysteine (39). While CDO contains substoichiometric amounts of iron bound in the active site, ADO contains stoichiometric amounts of iron suggesting that the active sites of the two thiol dioxygenases may be different and selective towards their respective reactions (39).

Previous studies have shown that 3-mercaptopropionate inhibits CDO (63). In our kinetic investigations, there was no detectable activity with 3-mercaptopropionate. Oxidation of 3-mercaptopropionate is catalyzed by 3-mercaptopropionate dioxygenase which also can not use

either cysteine or cysteamine as a substrate, further demonstrating the specificity exhibited by thiol dioxygenases for their respective reactions.

Additional insights into the nature of enzyme-substrate interactions were provided by EPR analyses of the variants and wild-type CDO in the presence of alternative substrates. The similarity between the EPR spectra of wild-type CDO with L-cysteine and with D-cysteine was indeed striking, suggesting that altering the stereochemistry from L-cysteine to D-cysteine does not affect binding of the two substrates in the active site of CDO. As illustrated in figure 3.1, the bidentate coordination of L-cysteine to the active site iron places the carboxyl group in a favorable position for additional stabilizing interactions with Arg60 and Tyr58. These substrate stabilizing interactions may be disrupted by a change in stereochemistry from L-cysteine to D-cysteine. Therefore, the reduced catalytic efficiency observed with D-cysteine may not be due to compromised binding, but can be attributed to the disruption of important substrate stabilizing interactions as a result of a misplaced functional group. The EPR spectra of wild-type CDO in the presence of L-cysteine and D-cysteine were more rhombic compared to the spectra of CDO with cysteamine and 3-mercaptopropionate, which were more axial. It is worth noting that among the substrate analogs utilized; only L-cysteine and D-cysteine could induce formation of the Cys-Tyr crosslink within the active site of CDO. Therefore, the differences in anisotropy could be attributed to the presence of the Cys-Tyr crosslink which has been proposed to fix the position of Tyr157 for stabilization of reaction intermediates during catalysis.

The EPR signal observed in wild-type CDO with cysteamine was considerably smaller compared to that with L-cysteine. The carboxyl group of L-cysteine may anchor the substrate optimally within the active site for catalysis to take place. This additional stability of the enzyme-substrate complex offered by the carboxyl group is missing in cysteamine leading to the

reduced signal intensity with cysteamine relative to that with L-cysteine. Addition of 3-mercaptopropionate to wild-type CDO displayed a comparable signal as that with cysteamine. It can be argued that 3-mercaptopropionate coordinates the active site iron via the thiol group alone, such that the carboxyl group interacts favorably with the guanidinium group of Arg60. The minimal change in the EPR signal intensity observed in R60A CDO in the presence of 3-mercaptopropionate provides evidence to support monodentate coordination through the thiol group. Regardless of the mode of binding, 3-mercaptopropionate is not a catalytically viable substrate for CDO.

In addition to structural data, results from MCD and resonance Raman spectroscopies were also consistent with the bidentate mode of substrate coordination via the thiol and amino groups of L-cysteine (65). However, data from XAS studies provided no evidence for sulfur ligation to the iron center (111). To investigate whether the thiol group of L-cysteine coordinates the active site iron, S-methylcysteine and L-cysteine sulfinic acid were utilized in the EPR investigations. There were no observable changes in the EPR spectra of wild-type CDO in the absence and in the presence of the two compounds. The terminal methyl group of S-methylcysteine blocks the thiol group from coordinating with the active site iron. The lack of observable changes in the EPR spectra of wild-type CDO in the presence of S-methylcysteine and L-cysteine sulfinic acid demonstrates that a free thiol group is required in order for the substrate to coordinate the active site iron. Additional insights regarding the metal binding site of CDO were obtained through the EPR analyses of Tyr58 and Arg60 CDO variants, in the presence of L-cysteine and cysteine analogs. The EPR spectral features observed with the conservative substitutions (Y58F and R60K) were comparable to those of the wild-type enzyme, indicating that the metal coordination environment of these variants was similar to that of wild-

type CDO. However, slight variations were observed with Y58A and R60A CDO variants in the presence of cysteamine and 3-mercaptopropionate where the EPR signals were notably smaller. The variations observed with the non conservative substitutions demonstrate that substrate coordination may be altered in these variants.

The effective and productive interaction of an enzyme with the substrate often requires that some functional groups be in their protonated state and other functional groups be in their deprotonated state for catalysis to take place. To investigate the required protonation states of groups involved in CDO catalysis/crosslink formation, the pH dependence of k_{cat} and k_{cat}/K_m values of wild-type CDO was determined. The pH dependence on k_{cat} values revealed two ionizable groups with $\text{p}K_a$ values of 6.60 ± 0.02 and 8.60 ± 0.06 . Because the $\text{p}K_a$ values observed in the k_{cat} pH profile represent ionizable groups on the enzyme-substrate complex that are required for catalysis up through product release, the lower $\text{p}K_a$ value of 6.6 may represent an active site His residue which is important in catalysis. The His155 residue is located 5.9 Å away from the catalytic iron and participates in a hydrogen bond network involving Tyr58, Arg60, and Tyr157 (1). It is likely that His155 functions as an active site base in proton abstraction from the cysteine substrate. However, additional experiments are necessary in order to positively assign His155 as the active site base. The higher $\text{p}K_a$ value of 8.6 may possibly represent either Tyr157 ($\text{p}K_a = 10.46$) or Arg60 ($\text{p}K_a = 12.48$). These amino acid residues require being in their protonated state for catalysis to take place. In the proposed mechanism for formation of the Cys-Tyr crosslink which precedes oxidation of L-cysteine, a proton coupled electron transfer (PCET) process has been proposed in which iron bound superoxo intermediate is further reduced to a peroxo species. The proton donor in this step has been proposed to be Tyr157 but further work is required in order to assign Tyr157 the role of an active site acid. A $\text{p}K_a$ value of 8.6 is slightly

displaced relative to the pK_a values of Tyr157 and Arg60 but it is not unusual for pK_a values to be perturbed depending on the micro environment of the amino acids and as a result of formation of the enzyme-substrate complex (113). The pH dependence on k_{cat}/K_m values revealed two ionizable groups with pK_a values of 7.60 ± 0.02 and 9.3 ± 0.3 . The pK_a values observed in the pH profile of k_{cat}/K_m represent the required protonation states for binding and catalysis of groups on the free enzyme and the free substrate in order for the reaction to commit through the first irreversible step (113). It is likely that the low pK_a value of 7.6 represents the ionization of L-cysteine substrate which requires being deprotonated so that it can bind the active site iron. It is also possible that the pK_a of 7.6 represents the same residue (His155) observed in the k_{cat} profile that requires being in the deprotonated form, and is probably the active site base. Further experimental work is required in order to deduce which functional group contains the observed pK_a value. The higher pK_a value of 9.3 may possibly represent the same group observed in the k_{cat} profile, which is Arg60 or Try157. The Arg60 residue is in close proximity to the metal center and participates in the hydrogen bond network involving Tyr157, Tyr58, and His155 (1). In the crystal structure of human CDO in complex with L-cysteine, the guanidinium group of Arg60 is at a favorable distance (2.3 and 2.9 Å) to interact electrostatically with the carboxyl group of L-cysteine (1). Deprotonation of Arg60 may interfere with this interaction and consequently destabilize the bound substrate, hence the decrease in catalytic activity of wild-type CDO at higher pH values.

In summary, our results demonstrate that Arg60 and Tyr58 are strategically positioned within the active site of CDO to stabilize the bound substrate through hydrogen bonding and electrostatic interactions. This stabilization is facilitated by the bidentate coordination of L-cysteine to the active site iron through the thiol and amino groups, effectively placing the

carboxyl group of the substrate at a favorable position to interact with Arg60 and Tyr58. The bidentate mode of substrate coordination is also responsible for the remarkable substrate specificity exhibited by CDO. The pH studies have provided invaluable insights into the relevant protonation states of groups participating in binding and catalysis and our results have identified potential amino acid residues involved in acid/base catalysis. Additional work is planned in order to positively assign the observed pK_a values to the proposed amino acids.

Chapter Four

Summary

Regulation of intracellular concentration of cysteine is an important physiological process that is dependent on the mononuclear non-heme iron enzyme, cysteine dioxygenase (CDO). CDO catalyzes the oxidation of L-cysteine to form L-cysteine sulfinic acid. The product of this reaction is a branchpoint between two metabolic pathways. In one pathway, L-cysteine sulfinic acid may undergo a decarboxylation reaction catalyzed by cysteine sulfinate decarboxylase, (CSD) to form hypotaurine. Further oxidation of hypotaurine leads to formation of taurine, a metabolite with a broad range of physiological functions. The potential role of taurine in protection against cardiovascular diseases has attracted considerable attention in recent years. In addition to lowering the level of low density lipoproteins (LDL) which contribute to plaque buildup on the arterial walls, taurine plays a key role in the detoxification of cholesterol through conjugation into bile acids, a process that vastly increases the solubility of cholesterol and facilitates its excretion (26). Taurine has been described as a potent antioxidant although it is incapable of scavenging the common oxidants like superoxide, hydrogen peroxide, and hydroxyl radical. The antioxidant benefits of taurine arise from its ability to neutralize hypochlorous acid, which is a very powerful oxidant produced by neutrophils, and it is converted to a less toxic form, *N*-chlorotaurine (28, 114). The alternate pathway of L-cysteine sulfinic acid catabolism involves a transamination reaction with α -ketoglutarate to form β -sulfinylpyruvate in a reaction catalyzed by aspartate amino transferase. Further catabolism of β -sulfinylpyruvate may lead to

formation of pyruvate and sulfite. Subsequent oxidation of sulfite by sulfite oxidase generates sulfate which may either be excreted or used in other sulfur dependent transformations. The rate limiting step towards formation of either taurine or pyruvate and sulfite is the reaction catalyzed by CDO. Therefore, in addition to playing a central role in maintaining appropriate concentrations of cellular cysteine, CDO initiates the formation of metabolites with important physiological roles.

The available three-dimensional structures of CDO have revealed two interesting features within the active site. First, the catalytic site is comprised of a mononuclear iron ligated by 3-His residues (His86, His88, and His140). This is a deviation from the 3-His/1-Glu ligand set that is commonly observed in most cupin metalloproteins. The rationale for such a variation in metal coordination is still unclear. However, the current evidence points towards the possibility that this variation might be a mechanistically driven strategy, in order to carry out the dioxygenation reaction more efficiently. Second, in close proximity to the active site iron is a covalent crosslink between Cys93 and Tyr157. The presence of this crosslink has triggered considerable attention regarding its physiological relevance and the factors that lead to its biogenesis. Purified wild-type CDO exists as a heterogenous mixture of two isoforms, in which one isoform contains the Cys-Tyr crosslink while the other isoform lacks the crosslink. Because of their identical physical properties, efforts to separate the two isoforms have not been successful. In fact, previous characterization of CDO has involved a heterogenous mixture of both the crosslinked and non crosslinked isoforms. The studies presented in this dissertation have focused on understanding the mechanistic strategies employed by CDO towards L-cysteine oxidation. This objective was achieved using two main approaches: First, to investigate the role of the Cys-Tyr crosslink in the active site of CDO, a protocol was developed to separate the crosslinked and non crosslinked

CDO isoforms. Characterization of the individual isoforms has provided a more thorough kinetic and spectroscopic evaluation of the crosslinked and non crosslinked forms of CDO. The second approach investigated the key enzyme-substrate interactions that are relevant to CDO catalysis. The role of outer sphere residues in catalysis was evaluated through mutational analysis of Tyr58 and Arg60 residues which have been proposed to interact with the bound cysteine substrate. Additionally, substrates which are structurally similar to L-cysteine were utilized to probe the relevance of the functional groups of L-cysteine in substrate coordination.

4.1 Analysis of non crosslinked and crosslinked CDO

Previous investigations suggested that cysteine, iron and dioxygen are a prerequisite for the biosynthesis of the Cys-Tyr crosslink in CDO (90). On this basis, an expression protocol was designed that required CDO to be expressed and purified under iron depleted conditions. The protocol involved the addition of 1,10-phenanthroline to the cell culture shortly before induction. Analysis of the purified protein revealed the presence of a single isoform that correlated with the non crosslinked form of CDO. Because the catalytic activity of CDO is dependent on the presence of iron within the active site, purified non crosslinked CDO was reconstituted with ferrous iron and the reconstituted enzyme contained ~50 % iron. The oxidation state of the bound iron in non crosslinked CDO was probed using EPR spectroscopy and the results indicate that the homogenously non crosslinked CDO stabilizes the EPR silent ferrous redox state. A sharp EPR signal was observed at $g = 4.3$ upon addition of L-cysteine to non crosslinked CDO, suggesting the direct coordination of L-cysteine to the metal center. One striking feature regarding the work presented in this dissertation is the unusual biphasic activity observed with non crosslinked CDO at relatively high concentrations of L-cysteine. There was an initial slow phase which was attributed to the process of Cys-Tyr crosslink formation which consequently

led to activation of the enzyme in the fast phase, which corresponded with L-cysteine oxidation. The observation that formation of the Cys-Tyr crosslink correlated with enzyme activation was quite intriguing and required the steady state kinetic parameters of the homogeneously crosslinked enzyme to be obtained. Interestingly, steady state kinetic evaluation of homogeneously crosslinked CDO revealed an ~5-fold increase in the k_{cat}/K_m value over the wild-type enzyme that contained a heterogeneous mixture of the non crosslinked and crosslinked CDO isoforms. Further evaluation of homogeneously crosslinked CDO using EPR spectroscopy revealed that the active site iron was purely in the ferric redox state, characterized by the sharp EPR signal at $g = 4.3$. Additionally, there was no observable change in the EPR signal intensity upon addition of L-cysteine to crosslinked CDO under anaerobic or aerobic conditions, suggesting that the active site geometry was not altered in the presence of the substrate. The observation that crosslinked CDO exists in the oxidized Fe^{3+} form was indeed surprising because the reported oxidation state of active site iron in CDO containing a heterogeneous mixture of crosslinked and non crosslinked isoforms is Fe^{2+} (115). It is likely that the reports on the redox state of CDO only consider the oxidation state of the non crosslinked population of CDO. The current studies have unequivocally demonstrated that the two isoforms have distinct oxidation states which commit CDO towards either crosslink formation or cysteine oxidation.

4.2 Physiological relevance

CDO that is present in the cell lysate exists primarily in the non crosslinked ferrous form, and the crosslink is generated during the process of aerobic expression and purification of the enzyme (101). On this basis, it can safely be concluded that within the cell, the predominant form of CDO is the non crosslinked isoform. Given the observation that non crosslinked CDO is readily converted to the crosslinked form on exposure to high concentrations of cysteine under

aerobic conditions, it can also be concluded that the Cys-Tyr crosslink in CDO is formed when the enzyme is subjected to high concentrations of cysteine within the cell. The dependence of crosslink formation on cysteine can be viewed as a regulatory mechanism in which CDO achieves maximum catalytic competence at high cysteine concentrations, facilitating the removal of excess cysteine from the cell which could otherwise be potentially toxic. When cellular concentrations of cysteine become limiting, the Cys-Tyr crosslink is not formed. Subsequently, CDO is not activated and in fact, studies have shown that at low concentrations of cysteine, CDO is ubiquitinated and degraded by the 26S proteasome (7). The overall effect is the conservation of the available cysteine which is then channeled to other biosynthetic pathways such as protein synthesis, formation of coenzyme A, and glutathione biosynthesis. The data presented in this dissertation is in good agreement with *in vivo* studies, where it was demonstrated that CDO that was isolated from the liver of rats fed a low protein (cysteine) containing diet was mainly in the non crosslinked form. Conversely, the enzyme that was isolated from the liver of rats fed a high protein (cysteine) containing diet was mainly in the crosslinked form (6, 90, 116). The tight cysteine dependent regulation of CDO activity/concentration in mammalian organisms clearly demonstrates that cysteine homeostasis is indeed an essential physiological process.

4.3 Enzyme-substrate interactions within the active site of CDO

Based on the available three-dimensional structures of CDO, it is apparent that the active site of CDO is uniquely designed for the efficient oxidation of L-cysteine. The 3-His binding site is ideal for the bidentate coordination of L-cysteine via the thiol and amino groups. Binding of L-cysteine consequently facilitates the binding of dioxygen to the free coordination site on the active site iron. In addition to structural evidence, the current studies implicate a role for Tyr58 and Arg60 which are in close proximity to the active site iron, in stabilizing the bound L-cysteine

substrate. The substrate stabilization effect arises from the bidentate mode of substrate coordination to the active site iron, which places the carboxyl group of L-cysteine at a favorable position to interact with Tyr58 and Arg60 through hydrogen bonding and electrostatic interactions. Additionally, the remarkable substrate specificity exhibited by CDO is attributed to the bidentate mode of L-cysteine binding. The relevance of the functional groups of L-cysteine in catalysis was evaluated using molecules that are structurally analogous to L-cysteine and the results lend support to the hypothesis that the thiol group of the L-cysteine coordinates the active site iron.

The required protonation states of groups participating in catalysis were evaluated by determining the pH dependence of k_{cat} and $k_{\text{cat}}/K_{\text{m}}$ values of wild-type CDO. The pH profile of k_{cat} values revealed two ionizable groups with $\text{p}K_{\text{a}}$ values of 6.60 ± 0.02 and 8.60 ± 0.06 . These results demonstrate that a group in the enzyme-substrate complex with a $\text{p}K_{\text{a}}$ value of 6.6 should be in the unprotonated form and another group with a $\text{p}K_{\text{a}}$ value of 8.6 should be in the protonated form in order to commit the reaction through product release. The lower $\text{p}K_{\text{a}}$ value of 6.6 possibly represents His155 which is conserved among all known forms of mammalian CDO enzymes. Because coordination of the L-cysteine substrate requires initial deprotonation of the thiol and amino groups, it is likely that His155 functions as an active site base in proton abstraction from the cysteine substrate. The higher $\text{p}K_{\text{a}}$ value of 8.6 may represent either Tyr157 or Arg60 which are also conserved among all known forms of mammalian CDO enzymes and play essential roles in catalysis. In the proposed mechanism for formation of the Cys-Tyr crosslink which precedes oxidation of L-cysteine, a proton coupled electron transfer (PCET) process has been proposed in which iron bound superoxo intermediate is further reduced to a peroxo species. The proton donor in this step has been proposed to be Tyr157 but further work is required in order to assign Tyr157 the role of an active site acid. The pH profile of $k_{\text{cat}}/K_{\text{m}}$

revealed two ionizable groups with pK_a values of 7.60 ± 0.02 and 9.3 ± 0.3 . These results demonstrate that two groups present in the free enzyme or in the free substrate, one with a pK_a value of 7.6 must be in the unprotonated form, and another group with a pK_a value of 9.3 must be in the protonated form in order to commit the reaction through the first irreversible step. It is likely that the low pK_a value of 7.6 represents the ionization of L-cysteine substrate which requires being deprotonated so that it can bind the active site iron. It can also be argued that the pK_a value of 7.6 observed on the k_{cat}/K_m profile could also represent the same group observed in the k_{cat} profile (His155) which possibly deprotonates the L-cysteine substrate. The higher pK_a value of 9.3 may possibly represent the same group observed in the k_{cat} profile, which is Arg60 or Try157. The mutational studies presented in this dissertation have demonstrated that Arg60 plays an essential role in catalysis and this was evidenced by the 20-fold decrease in the k_{cat}/K_m value of R60A compared to the wild-type enzyme that contains a mixture of both the crosslinked and non crosslinked CDO isoforms. Although SDS-PAGE analysis of R60A CDO revealed that this variant existed primarily in the crosslinked form, the k_{cat}/K_m value of R60A CDO was ~400-fold lower compared to the homogeneously crosslinked wild-type CDO enzyme. These observations clearly demonstrate that the presence of Arg60 in the active site of CDO is of utmost importance. In the three-dimensional structure of human CDO in complex with L-cysteine, the guanidinium group of Arg60 is at a favorable distance (2.3 and 2.9 Å) to interact electrostatically with the carboxyl group of L-cysteine (1). Therefore, the drop in the activity of wild-type CDO at higher pH values could be the consequence of deprotonating Arg60 which requires being in the protonated and charged form in order to interact electrostatically with the carboxyl group of the bound L-cysteine substrate.

In conclusion, the separation of the non crosslinked and crosslinked isoforms of CDO and the initial characterization of the two isoforms provide a good groundwork for future mechanistic investigations. The presented results from the pH profile studies also provide a good starting point for an in depth characterization of groups participating in acid/base catalysis.

References

1. Ye, S., Wu, X., Wei, L., Tang, D., Sun, P., Bartlam, M., and Rao, Z. (2007) An insight into the mechanism of human cysteine dioxygenase. Key roles of the thioether-bonded tyrosine-cysteine cofactor, *J Biol Chem* 282, 3391-3402.
2. McCoy, J. G., Bailey, L. J., Bitto, E., Bingman, C. A., Aceti, D. J., Fox, B. G., and Phillips, G. N., Jr. (2006) Structure and mechanism of mouse cysteine dioxygenase, *Proc Natl Acad Sci U S A* 103, 3084-3089.
3. Simmons, C. R., Liu, Q., Huang, Q., Hao, Q., Begley, T. P., Karplus, P. A., and Stipanuk, M. H. (2006) Crystal structure of mammalian cysteine dioxygenase. A novel mononuclear iron center for cysteine thiol oxidation, *J Biol Chem* 281, 18723-18733.
4. Stipanuk, M. H. (2004) Sulfur amino acid metabolism: pathways for production and removal of homocysteine and cysteine, *Annu Rev Nutr* 24, 539-577.
5. Stipanuk, M. H., and Ueki, I. (2011) Dealing with methionine/homocysteine sulfur: cysteine metabolism to taurine and inorganic sulfur, *J Inherit Metab Dis* 34, 17-32.
6. Stipanuk, M. H., Dominy, J. E., Jr., Lee, J. I., and Coloso, R. M. (2006) Mammalian cysteine metabolism: new insights into regulation of cysteine metabolism, *J Nutr* 136, 1652S-1659S.
7. Dominy, J. E., Jr., Hirschberger, L. L., Coloso, R. M., and Stipanuk, M. H. (2006) Regulation of cysteine dioxygenase degradation is mediated by intracellular cysteine levels and the ubiquitin-26 S proteasome system in the living rat, *Biochem J* 394, 267-273.
8. Stipanuk, M. H., Coloso, R. M., Garcia, R. A., and Banks, M. F. (1992) Cysteine concentration regulates cysteine metabolism to glutathione, sulfate and taurine in rat hepatocytes, *J Nutr* 122, 420-427.
9. Kalinina, E. V., Chernov, N. N., and Saprin, A. N. (2008) Involvement of thio-, peroxi-, and glutaredoxins in cellular redox-dependent processes, *Biochemistry (Mosc)* 73, 1493-1510.
10. Jacob, C., Knight, I., and Winyard, P. G. Aspects of the biological redox chemistry of cysteine: from simple redox responses to sophisticated signalling pathways.

11. Nordberg, J., and Arner, E. S. (2001) Reactive oxygen species, antioxidants, and the mammalian thioredoxin system, *Free Radic Biol Med* 31, 1287-1312.
12. Arner, E. S., and Holmgren, A. (2000) Physiological functions of thioredoxin and thioredoxin reductase, *Eur J Biochem* 267, 6102-6109.
13. Rhee, S. G., Kang, S. W., Jeong, W., Chang, T. S., Yang, K. S., and Woo, H. A. (2005) Intracellular messenger function of hydrogen peroxide and its regulation by peroxiredoxins, *Curr Opin Cell Biol* 17, 183-189.
14. Wood, Z. A., Schroder, E., Robin Harris, J., and Poole, L. B. (2003) Structure, mechanism and regulation of peroxiredoxins, *Trends Biochem Sci* 28, 32-40.
15. Ellis, H. R., and Poole, L. B. (1997) Novel application of 7-chloro-4-nitrobenzo-2-oxa-1,3-diazole to identify cysteine sulfenic acid in the AhpC component of alkyl hydroperoxide reductase, *Biochemistry* 36, 15013-15018.
16. Ellis, H. R., and Poole, L. B. (1997) Roles for the two cysteine residues of AhpC in catalysis of peroxide reduction by alkyl hydroperoxide reductase from *Salmonella typhimurium*, *Biochemistry* 36, 13349-13356.
17. Maher, P. (2005) The effects of stress and aging on glutathione metabolism, *Ageing Res Rev* 4, 288-314.
18. Schafer, F. Q., and Buettner, G. R. (2001) Redox environment of the cell as viewed through the redox state of the glutathione disulfide/glutathione couple, *Free Radic Biol Med* 30, 1191-1212.
19. Robishaw, J. D., and Neely, J. R. (1985) Coenzyme A metabolism, *Am J Physiol* 248, E1-9.
20. Leonardi, R., Zhang, Y. M., Rock, C. O., and Jackowski, S. (2005) Coenzyme A: back in action, *Prog Lipid Res* 44, 125-153.
21. Zhou, B., Westaway, S. K., Levinson, B., Johnson, M. A., Gitschier, J., and Hayflick, S. J. (2001) A novel pantothenate kinase gene (*PANK2*) is defective in Hallervorden-Spatz syndrome, *Nat Genet* 28, 345-349.
22. Perry, T. L., Norman, M. G., Yong, V. W., Whiting, S., Crichton, J. U., Hansen, S., and Kish, S. J. (1985) Hallervorden-Spatz disease: cysteine accumulation and cysteine dioxygenase deficiency in the globus pallidus, *Ann Neurol* 18, 482-489.
23. Chen, C. Q., Xin, H., and Zhu, Y. Z. (2007) Hydrogen sulfide: third gaseous transmitter, but with great pharmacological potential, *Acta Pharmacol Sin* 28, 1709-1716.

24. Fiorucci, S., Distrutti, E., Cirino, G., and Wallace, J. L. (2006) The emerging roles of hydrogen sulfide in the gastrointestinal tract and liver, *Gastroenterology* 131, 259-271.
25. Xu, Y. J., Arneja, A. S., Tappia, P. S., and Dhalla, N. S. (2008) The potential health benefits of taurine in cardiovascular disease, *Exp Clin Cardiol* 13, 57-65.
26. Wojcik, O. P., Koenig, K. L., Zeleniuch-Jacquotte, A., Costa, M., and Chen, Y. (2010) The potential protective effects of taurine on coronary heart disease, *Atherosclerosis* 208, 19-25.
27. Yamamoto, J., Akabane, S., Yoshimi, H., Nakai, M., and Ikeda, M. (1985) Effects of taurine on stress-evoked hemodynamic and plasma catecholamine changes in spontaneously hypertensive rats, *Hypertension* 7, 913-922.
28. Birdsall, T. C. (1998) Therapeutic applications of taurine, *Altern Med Rev* 3, 128-136.
29. Guion-Rain, M. C., Portemer, C., and Chatagner, F. (1975) Rat liver cysteine sulfinatase decarboxylase: purification, new appraisal of the molecular weight and determination of catalytic properties, *Biochim Biophys Acta* 384, 265-276.
30. Recasens, M., Benezra, R., Basset, P., and Mandel, P. (1980) Cysteine sulfinatase aminotransferase and aspartate aminotransferase isoenzymes of rat brain. Purification, characterization, and further evidence for identity, *Biochemistry* 19, 4583-4589.
31. Bella, D. L., Hirschberger, L. L., Hosokawa, Y., and Stipanuk, M. H. (1999) Mechanisms involved in the regulation of key enzymes of cysteine metabolism in rat liver *in vivo*, *Am J Physiol* 276, E326-335.
32. Hirschberger, L. L., Daval, S., Stover, P. J., and Stipanuk, M. H. (2001) Murine cysteine dioxygenase gene: structural organization, tissue-specific expression and promoter identification, *Gene* 277, 153-161.
33. Bella, D. L., Hirschberger, L. L., Kwon, Y. H., and Stipanuk, M. H. (2002) Cysteine metabolism in periportal and perivenous hepatocytes: perivenous cells have greater capacity for glutathione production and taurine synthesis but not for cysteine catabolism, *Amino Acids* 23, 453-458.
34. Lee, J. I., Londono, M., Hirschberger, L. L., and Stipanuk, M. H. (2004) Regulation of cysteine dioxygenase and gamma-glutamylcysteine synthetase is associated with hepatic cysteine level, *J Nutr Biochem* 15, 112-122.
35. Stipanuk, M. H., Londono, M., Lee, J. I., Hu, M., and Yu, A. F. (2002) Enzymes and metabolites of cysteine metabolism in nonhepatic tissues of rats show little response to changes in dietary protein or sulfur amino acid levels, *J Nutr* 132, 3369-3378.

36. Bella, D. L., Hahn, C., and Stipanuk, M. H. (1999) Effects of nonsulfur and sulfur amino acids on the regulation of hepatic enzymes of cysteine metabolism, *Am J Physiol* 277, E144-153.
37. Bella, D. L., Kwon, Y. H., Hirschberger, L. L., and Stipanuk, M. H. (2000) Post-transcriptional regulation of cysteine dioxygenase in rat liver, *Adv Exp Med Biol* 483, 71-85.
38. Stipanuk, M. H., Hirschberger, L. L., Londono, M. P., Cresenzi, C. L., and Yu, A. F. (2004) The ubiquitin-proteasome system is responsible for cysteine-responsive regulation of cysteine dioxygenase concentration in liver, *Am J Physiol Endocrinol Metab* 286, E439-448.
39. Stipanuk, M. H., Simmons, C. R., Karplus, P. A., and Dominy, J. E., Jr. (2011) Thiol dioxygenases: unique families of cupin proteins, *Amino Acids* 41, 91-102.
40. Dunwell, J. M., Khuri, S., and Gane, P. J. (2000) Microbial relatives of the seed storage proteins of higher plants: conservation of structure and diversification of function during evolution of the cupin superfamily, *Microbiol Mol Biol Rev* 64, 153-179.
41. Straganz, G. D., and Nidetzky, B. (2006) Variations of the 2-His-1-carboxylate theme in mononuclear non-heme Fe²⁺ oxygenases, *Chembiochem* 7, 1536-1548.
42. Opaleye, O., Rose, R. S., Whittaker, M. M., Woo, E. J., Whittaker, J. W., and Pickersgill, R. W. (2006) Structural and spectroscopic studies shed light on the mechanism of oxalate oxidase, *J Biol Chem* 281, 6428-6433.
43. Woo, E. J., Dunwell, J. M., Goodenough, P. W., Marvier, A. C., and Pickersgill, R. W. (2000) Germin is a manganese containing homohexamer with oxalate oxidase and superoxide dismutase activities, *Nat Struct Biol* 7, 1036-1040.
44. Gane, P. J., Dunwell, J. M., and Warwicker, J. (1998) Modeling based on the structure of vicilins predicts a histidine cluster in the active site of oxalate oxidase, *J Mol Evol* 46, 488-493.
45. Tanner, A., Bowater, L., Fairhurst, S. A., and Bornemann, S. (2001) Oxalate decarboxylase requires manganese and dioxygen for activity. Overexpression and characterization of *Bacillus subtilis* YvrK and YoaN, *J Biol Chem* 276, 43627-43634.
46. Schaab, M. R., Barney, B. M., and Francisco, W. A. (2006) Kinetic and spectroscopic studies on the quercetin 2,3-dioxygenase from *Bacillus subtilis*, *Biochemistry* 45, 1009-1016.
47. Fusetti, F., Schroter, K. H., Steiner, R. A., van Noort, P. I., Pijning, T., Rozeboom, H. J., Kalk, K. H., Egmond, M. R., and Dijkstra, B. W. (2002) Crystal structure of the copper-containing quercetin 2,3-dioxygenase from *Aspergillus japonicus*, *Structure* 10, 259-268.

48. Gopal, B., Madan, L. L., Betz, S. F., and Kossiakoff, A. A. (2005) The crystal structure of a quercetin 2,3-dioxygenase from *Bacillus subtilis* suggests modulation of enzyme activity by a change in the metal ion at the active site(s), *Biochemistry* 44, 193-201.
49. Hund, H. K., Breuer, J., Lingens, F., Huttermann, J., Kappl, R., and Fetzner, S. (1999) Flavonol 2,4-dioxygenase from *Aspergillus niger* DSM 821, a type 2 Cu²⁺-containing glycoprotein, *Eur J Biochem* 263, 871-878.
50. Kooter, I. M., Steiner, R. A., Dijkstra, B. W., van Noort, P. I., Egmond, M. R., and Huber, M. (2002) EPR characterization of the mononuclear Cu-containing *Aspergillus japonicus* quercetin 2,3-dioxygenase reveals dramatic changes upon anaerobic binding of substrates, *Eur J Biochem* 269, 2971-2979.
51. Costas, M., Mehn, M. P., Jensen, M. P., and Que, L. (2004) Dioxygen Activation at Mononuclear Nonheme Iron Active Sites: Enzymes, Models, and Intermediates, *Chemical Reviews* 104, 939-986.
52. Dai, Y., Pochapsky, T. C., and Abeles, R. H. (2001) Mechanistic studies of two dioxygenases in the methionine salvage pathway of *Klebsiella pneumoniae*, *Biochemistry* 40, 6379-6387.
53. Al-Mjeni, F., Ju, T., Pochapsky, T. C., and Maroney, M. J. (2002) XAS investigation of the structure and function of Ni in acireductone dioxygenase, *Biochemistry* 41, 6761-6769.
54. Ju, T., Goldsmith, R. B., Chai, S. C., Maroney, M. J., Pochapsky, S. S., and Pochapsky, T. C. (2006) One protein, two enzymes revisited: a structural entropy switch interconverts the two isoforms of acireductone dioxygenase, *J Mol Biol* 363, 823-834.
55. Dai, Y., Wensink, P. C., and Abeles, R. H. (1999) One protein, two enzymes, *J Biol Chem* 274, 1193-1195.
56. Ballantyne, B., and Cawley, T. J. (2001) 2,4-Pentanedione, *J Appl Toxicol* 21, 165-171.
57. Straganz, G. D., Glieder, A., Brecker, L., Ribbons, D. W., and Steiner, W. (2003) Acetylacetone-cleaving enzyme Dke1: a novel C-C-bond-cleaving enzyme from *Acinetobacter johnsonii*, *Biochem J* 369, 573-581.
58. Leitgeb, S., Straganz, G. D., and Nidetzky, B. (2009) Biochemical characterization and mutational analysis of the mononuclear non-haem Fe²⁺ site in Dke1, a cupin-type dioxygenase from *Acinetobacter johnsonii*, *Biochem J* 418, 403-411.
59. Straganz, G. D., Egger, S., Aquino, G., D'Auria, S., and Nidetzky, B. (2006) Exploring the cupin-type metal-coordinating signature of acetylacetone dioxygenase Dke1 with site-directed mutagenesis: Catalytic reaction profile and Fe²⁺ binding stability of Glu-69→Gln mutant, *Journal of Molecular Catalysis B: Enzymatic* 39, 171-178.

60. Straganz, G. D., and Nidetzky, B. (2005) Reaction coordinate analysis for beta-diketone cleavage by the non-heme Fe²⁺-dependent dioxygenase Dke1, *J Am Chem Soc* 127, 12306-12314.
61. Straganz, G. D., Hofer, H., Steiner, W., and Nidetzky, B. (2004) Electronic substituent effects on the cleavage specificity of a non-heme Fe²⁺-dependent beta-diketone dioxygenase and their mechanistic implications, *J Am Chem Soc* 126, 12202-12203.
62. Yamaguchi, K., Hosokawa, Y., Kohashi, N., Kori, Y., Sakakibara, S., and Ueda, I. (1978) Rat liver cysteine dioxygenase (cysteine oxidase). Further purification, characterization, and analysis of the activation and inactivation, *J Biochem* 83, 479-491.
63. Chai, S. C., Jerkins, A. A., Banik, J. J., Shalev, I., Pinkham, J. L., Uden, P. C., and Maroney, M. J. (2005) Heterologous expression, purification, and characterization of recombinant rat cysteine dioxygenase, *J Biol Chem* 280, 9865-9869.
64. Ewetz, L., and Sorbo, B. (1966) Characteristics of the cysteinesulfinate-forming enzyme system in rat liver, *Biochim Biophys Acta* 128, 296-305.
65. Gardner, J. D., Pierce, B. S., Fox, B. G., and Brunold, T. C. (2010) Spectroscopic and computational characterization of substrate-bound mouse cysteine dioxygenase: nature of the ferrous and ferric cysteine adducts and mechanistic implications, *Biochemistry* 49, 6033-6041.
66. Pierce, B. S., Gardner, J. D., Bailey, L. J., Brunold, T. C., and Fox, B. G. (2007) Characterization of the nitrosyl adduct of substrate-bound mouse cysteine dioxygenase by electron paramagnetic resonance: electronic structure of the active site and mechanistic implications, *Biochemistry* 46, 8569-8578.
67. Rogers, M. S., Hurtado-Guerrero, R., Firbank, S. J., Halcrow, M. A., Dooley, D. M., Phillips, S. E., Knowles, P. F., and McPherson, M. J. (2008) Cross-link formation of the cysteine 228-tyrosine 272 catalytic cofactor of galactose oxidase does not require dioxygen, *Biochemistry* 47, 10428-10439.
68. Davidson, V. L. (2005) Structure and mechanism of tryptophylquinone enzymes, *Bioorg Chem* 33, 159-170.
69. Davidson, V. L. (2007) Protein-derived cofactors. Expanding the scope of post-translational modifications, *Biochemistry* 46, 5283-5292.
70. Davidson, V. L. (2011) Generation of protein-derived redox cofactors by posttranslational modification, *Mol Biosyst* 7, 29-37.
71. Pearson, A. R., De La Mora-Rey, T., Graichen, M. E., Wang, Y., Jones, L. H., Marimanikkupam, S., Agger, S. A., Grimsrud, P. A., Davidson, V. L., and Wilmot, C. M.

- (2004) Further insights into quinone cofactor biogenesis: probing the role of mauG in methylamine dehydrogenase tryptophan tryptophylquinone formation, *Biochemistry* 43, 5494-5502.
72. Wang, Y., Li, X., Jones, L. H., Pearson, A. R., Wilmot, C. M., and Davidson, V. L. (2005) MauG-dependent *in vitro* biosynthesis of tryptophan tryptophylquinone in methylamine dehydrogenase, *J Am Chem Soc* 127, 8258-8259.
73. Datta, S., Mori, Y., Takagi, K., Kawaguchi, K., Chen, Z. W., Okajima, T., Kuroda, S., Ikeda, T., Kano, K., Tanizawa, K., and Mathews, F. S. (2001) Structure of a quinohemoprotein amine dehydrogenase with an uncommon redox cofactor and highly unusual crosslinking, *Proc Natl Acad Sci U S A* 98, 14268-14273.
74. Sun, D., Ono, K., Okajima, T., Tanizawa, K., Uchida, M., Yamamoto, Y., Mathews, F. S., and Davidson, V. L. (2003) Chemical and kinetic reaction mechanisms of quinohemoprotein amine dehydrogenase from *Paracoccus denitrificans*, *Biochemistry* 42, 10896-10903.
75. Ndontsa, E. N., Moore, R. L., and Goodwin, D. C. (2012) Stimulation of KatG catalase activity by peroxidatic electron donors, *Arch Biochem Biophys* 525, 215-222.
76. Ghiladi, R. A., Medzihradzky, K. F., and Ortiz de Montellano, P. R. (2005) Role of the Met-Tyr-Trp cross-link in *Mycobacterium tuberculosis* catalase-peroxidase (KatG) as revealed by KatG(M255I), *Biochemistry* 44, 15093-15105.
77. Ghiladi, R. A., Knudsen, G. M., Medzihradzky, K. F., and Ortiz de Montellano, P. R. (2005) The Met-Tyr-Trp cross-link in *Mycobacterium tuberculosis* catalase-peroxidase (KatG): autocatalytic formation and effect on enzyme catalysis and spectroscopic properties, *J Biol Chem* 280, 22651-22663.
78. Yamada, Y., Fujiwara, T., Sato, T., Igarashi, N., and Tanaka, N. (2002) The 2.0 Å crystal structure of catalase-peroxidase from *Haloarcula marismortui*, *Nat Struct Biol* 9, 691-695.
79. Bertrand, T., Eady, N. A., Jones, J. N., Jesmin, Nagy, J. M., Jamart-Gregoire, B., Raven, E. L., and Brown, K. A. (2004) Crystal structure of *Mycobacterium tuberculosis* catalase-peroxidase, *J Biol Chem* 279, 38991-38999.
80. Njuma, O. J., Ndontsa, E. N., and Goodwin, D. C. (2013) Catalase in peroxidase clothing: Interdependent cooperation of two cofactors in the catalytic versatility of KatG, *Arch Biochem Biophys*.
81. Jakopitsch, C., Auer, M., Ivancich, A., Ruker, F., Furtmuller, P. G., and Obinger, C. (2003) Total conversion of bifunctional catalase-peroxidase (KatG) to monofunctional peroxidase by exchange of a conserved distal side tyrosine, *J Biol Chem* 278, 20185-20191.

82. Klema, V. J., and Wilmot, C. M. (2012) The role of protein crystallography in defining the mechanisms of biogenesis and catalysis in copper amine oxidase, *Int J Mol Sci* 13, 5375-5405.
83. Maintz, L., and Novak, N. (2007) Histamine and histamine intolerance, *Am J Clin Nutr* 85, 1185-1196.
84. Samuels, N. M., and Klinman, J. P. (2006) Investigation of Cu¹⁺-dependent 2,4,5-trihydroxyphenylalanine quinone biogenesis in *Hansenula polymorpha* amine oxidase, *J Biol Chem* 281, 21114-21118.
85. Firbank, S. J., Rogers, M. S., Wilmot, C. M., Dooley, D. M., Halcrow, M. A., Knowles, P. F., McPherson, M. J., and Phillips, S. E. V. (2001) Crystal structure of the precursor of galactose oxidase: An unusual self-processing enzyme, *Proceedings of the National Academy of Sciences* 98, 12932-12937.
86. Whittaker, M. M., and Whittaker, J. W. (2003) Cu¹⁺-dependent biogenesis of the galactose oxidase redox cofactor, *J Biol Chem* 278, 22090-22101.
87. Firbank, S., Rogers, M., Guerrero, R. H., Dooley, D. M., Halcrow, M. A., Phillips, S. E., Knowles, P. F., and McPherson, M. J. (2004) Cofactor processing in galactose oxidase, *Biochem Soc Symp*, 15-25.
88. Whittaker, J. W. (2005) The radical chemistry of galactose oxidase, *Arch Biochem Biophys* 433, 227-239.
89. Whittaker, M. M., Ballou, D. P., and Whittaker, J. W. (1998) Kinetic isotope effects as probes of the mechanism of galactose oxidase, *Biochemistry* 37, 8426-8436.
90. Dominy, J. E., Jr., Hwang, J., Guo, S., Hirschberger, L. L., Zhang, S., and Stipanuk, M. H. (2008) Synthesis of amino acid cofactor in cysteine dioxygenase is regulated by substrate and represents a novel post-translational regulation of activity, *J Biol Chem* 283, 12188-12201.
91. Crawford, J. A., Li, W., and Pierce, B. S. (2011) Single turnover of substrate-bound ferric cysteine dioxygenase with superoxide anion: enzymatic reactivation, product formation, and a transient intermediate, *Biochemistry* 50, 10241-10253.
92. Soerbo, B., and Ewetz, L. (1965) The enzymatic oxidation of cysteine to cysteinesulfinate in rat liver, *Biochem Biophys Res Commun* 18, 359-363.
93. Wainer, A. (1965) The production of cysteinesulfinic acid from cysteine *in vitro*, *Biochim Biophys Acta* 104, 405-412.
94. Lombardini, J. B., Singer, T. P., and Boyer, P. D. (1969) Cystein oxygenase. II. Studies on the mechanism of the reaction with 18oxygen, *J Biol Chem* 244, 1172-1175.

95. Simmons, C. R., Krishnamoorthy, K., Granett, S. L., Schuller, D. J., Dominy, J. E., Jr., Begley, T. P., Stipanuk, M. H., and Karplus, P. A. (2008) A putative Fe²⁺-bound persulfenate intermediate in cysteine dioxygenase, *Biochemistry* 47, 11390-11392.
96. Whittaker, M. M., Kersten, P. J., Nakamura, N., Sanders-Loehr, J., Schweizer, E. S., and Whittaker, J. W. (1996) Glyoxal oxidase from *Phanerochaete chrysosporium* is a new radical-copper oxidase, *J Biol Chem* 271, 681-687.
97. Schnell, R., Sandalova, T., Hellman, U., Lindqvist, Y., and Schneider, G. (2005) Siroheme- and [Fe4-S4]-dependent NirA from Mycobacterium tuberculosis is a sulfite reductase with a covalent Cys-Tyr bond in the active site, *J Biol Chem* 280, 27319-27328.
98. Kleffmann, T., Jongkees, S. A., Fairweather, G., Wilbanks, S. M., and Jameson, G. N. (2009) Mass-spectrometric characterization of two posttranslational modifications of cysteine dioxygenase, *J Biol Inorg Chem* 14, 913-921.
99. Siakkou, E., Rutledge, M. T., Wilbanks, S. M., and Jameson, G. N. (2011) Correlating crosslink formation with enzymatic activity in cysteine dioxygenase, *Biochim Biophys Acta* 1814, 2003-2009.
100. Li, W., Blaesi, E. J., Pecore, M. D., Crowell, J. K., and Pierce, B. S. (2013) Second-Sphere Interactions between the C93-Y157 Cross-Link and the Substrate-Bound Fe Site Influence the O₂ Coupling Efficiency in Mouse Cysteine Dioxygenase, *Biochemistry* 52, 9104-9119.
101. Imsand, E. M., Njeri, C. W., and Ellis, H. R. (2012) Addition of an external electron donor to *in vitro* assays of cysteine dioxygenase precludes the need for exogenous iron, *Arch Biochem Biophys* 521, 10-17.
102. Parkin, S. E., Chen, S., Ley, B. A., Mangravite, L., Edmondson, D. E., Huynh, B. H., and Bollinger, J. M., Jr. (1998) Electron injection through a specific pathway determines the outcome of oxygen activation at the diiron cluster in the F208Y mutant of *Escherichia coli* ribonucleotide reductase protein R2, *Biochemistry* 37, 1124-1130.
103. Chaka, G., Sonnenberg, J. L., Schlegel, H. B., Heeg, M. J., Jaeger, G., Nelson, T. J., Ochrymowycz, L. A., and Rorabacher, D. B. (2007) A definitive example of a geometric "entatic state" effect: electron-transfer kinetics for a copper(II/I) complex involving A quinquedentate macrocyclic trithiaether-bipyridine ligand, *J Am Chem Soc* 129, 5217-5227.
104. Church, W. B., Guss, J. M., Potter, J. J., and Freeman, H. C. (1986) The crystal structure of mercury-substituted poplar plastocyanin at 1.9-Å resolution, *J Biol Chem* 261, 234-237.

105. Neidig, M. L., Wecksler, A. T., Schenk, G., Holman, T. R., and Solomon, E. I. (2007) Kinetic and spectroscopic studies of N694C lipoxygenase: a probe of the substrate activation mechanism of a nonheme ferric enzyme, *J Am Chem Soc* 129, 7531-7537.
106. Kovaleva, E. G., and Lipscomb, J. D. (2007) Crystal structures of Fe²⁺-dioxygenase superoxo, alkylperoxo, and bound product intermediates, *Science* 316, 453-457.
107. Tomchick, D. R., Phan, P., Cymborowski, M., Minor, W., and Holman, T. R. (2001) Structural and functional characterization of second-coordination sphere mutants of soybean lipoxygenase-1, *Biochemistry* 40, 7509-7517.
108. Fetzner, S. (2012) Ring-cleaving dioxygenases with a cupin fold, *Appl Environ Microbiol* 78, 2505-2514.
109. Wasinger, E. C., Davis, M. I., Pau, M. Y., Orville, A. M., Zaleski, J. M., Hedman, B., Lipscomb, J. D., Hodgson, K. O., and Solomon, E. I. (2003) Spectroscopic studies of the effect of ligand donor strength on the Fe-NO bond intradiol dioxygenases, *Inorg Chem* 42, 365-376.
110. Orville, A. M., and Lipscomb, J. D. (1993) Simultaneous binding of nitric oxide and isotopically labeled substrates or inhibitors by reduced protocatechuate 3,4-dioxygenase, *J Biol Chem* 268, 8596-8607.
111. Chai, S. C., Bruyere, J. R., and Maroney, M. J. (2006) Probes of the catalytic site of cysteine dioxygenase, *J Biol Chem* 281, 15774-15779.
112. Dominy, J. E., Jr., Simmons, C. R., Hirschberger, L. L., Hwang, J., Coloso, R. M., and Stipanuk, M. H. (2007) Discovery and characterization of a second mammalian thiol dioxygenase, cysteamine dioxygenase, *J Biol Chem* 282, 25189-25198.
113. Cleland, W. W. (1982) The use of pH studies to determine chemical mechanisms of enzyme-catalyzed reactions, *Methods Enzymol* 87, 390-405.
114. Schaffer, S. W., Jong, C. J., Ramila, K. C., and Azuma, J. (2010) Physiological roles of taurine in heart and muscle, *J Biomed Sci* 17 Suppl 1, S2.
115. Tchesnokov, E. P., Wilbanks, S. M., and Jameson, G. N. (2012) A strongly bound high-spin Fe²⁺ coordinates cysteine and homocysteine in cysteine dioxygenase, *Biochemistry* 51, 257-264.
116. Stipanuk, M. H., Ueki, I., Dominy, J. E., Jr., Simmons, C. R., and Hirschberger, L. L. (2009) Cysteine dioxygenase: a robust system for regulation of cellular cysteine levels, *Amino Acids* 37, 55-63.
117. Papanikolaou, G., Pantopoulos, K. (2005) Iron metabolism and toxicity, *Toxicology and Applied Pharmacology* 202, 199-211.